

2020-09-01

Testing models of linear dune formation by provenance analysis with composite sediment fingerprints

Telfer, Matt

<http://hdl.handle.net/10026.1/16026>

10.1016/j.geomorph.2020.107208

Geomorphology

Elsevier BV

All content in PEARL is protected by copyright law. Author manuscripts are made available in accordance with publisher policies. Please cite only the published version using the details provided on the item record or document. In the absence of an open licence (e.g. Creative Commons), permissions for further reuse of content should be sought from the publisher or author.

Manuscript Number: GEOMOR-9211R2

Title: Testing models of linear dune formation by provenance analysis with composite sediment fingerprints

Article Type: Research Paper

Keywords: Linear dunes; Dune extension; Sediment provenance; Monte Carlo simulation.

Corresponding Author: Dr. Matt Telfer,

Corresponding Author's Institution: Plymouth University

First Author: Matt Telfer

Order of Authors: Matt Telfer; Hamid Gholami; Paul P Hesse; Andrew Fisher; Richard Hartley

Abstract: The formative mechanisms of linear (longitudinal) dunes and dunefields remain uncertain, and multiple hypotheses have been proposed. A central debate is the degree to which dunes act as along-dune sediment transport corridors, implying that dunes grow primarily by extension, or whether they are comprised of locally-derived sands moved from adjacent interdunes (the 'wind-rift' model). Sediment fingerprinting studies, with origins in fluvial science, have been shown to offer the possibility to trace the provenance of aeolian sands, and thus elucidate transport pathways.

Two models (a Monte Carlo framework and a Generalized Likelihood Uncertainty Estimate framework) are used here to provide quantitative estimates of the sediment sources that have supplied a linear dune in the central Simpson Desert of central Australia. Four possible sources are identified that may have supplied the dune; two adjacent interdunes, one upwind low ridge of sand, and a merging upwind dune. Two sites near the dune's crest are used as the target, and provided twenty surface samples for analysis. Following geochemical assay, stepwise discriminant function analysis identified optimum elemental sediment fingerprints for a variety of possible sediment pathway configurations.

Results suggest that the sands of the dune are sourced predominantly from upwind dunes and sand sources, and that likely contributions from neighbouring dune swales are typically <20%. As such, wind-rift mechanisms of linear dune formation are not supported by these data. More complex sediment pathway configurations (i.e. other than a binary approach: interdune vs. along-dune), whilst confirming the initial findings, had reduced discriminatory power. Further separation of source pathways (e.g. identifying the relative roles of different upwind sources) was not possible with any confidence.

The findings suggest recent sediment accretion of a linear dune dominated by along-dune sand flux, and thus support an extensional component for the development of such dunes. Whilst it is noted that at a point-by-point basis this might not exclude accretion by vertical growth, as some have observed, there is no clear support for a substantive contribution to the dune sands from adjacent interdunes. Moreover, the use of

contemporary sediment fingerprinting methods to question hypotheses of aeolian geomorphology suggests that such methods have great potential for addressing other terrestrial geomorphological questions where identifying sediment pathways can provide vital insight.

Research Data Related to this Submission

Title: Data for: Testing models of linear dune formation by provenance analysis with composite sediment fingerprints

Repository: Mendeley Data

<https://data.mendeley.com/datasets/f6n4rkxhx7/draft?a=947f7067-3a11-4916-adb5-9225310ef503>

Title: Data for: Testing models of linear dune formation by provenance analysis with composite sediment fingerprints

Repository: Mendeley Data

<https://data.mendeley.com/datasets/rb5676cxsw/draft?a=0aaa36d1-2e76-487c-b2ba-d3bf6044d73e>

Reviewer #1

The manuscript is very strong on the analysis but lacks information on (1) local geomorphology to provide context; (2) the sand sampling and analytical methods; and (3) a proper description of the sediment analysis results

These are now added, and discussed in appropriate places below.

The discussion section is rather lengthy, but the conclusions appear sound.

For this reason, we go only halfway with the suggestion of the second reviewer to move the content of the intro to the discussion.

Specific Comments

1.1 (Mis labeled-should be 1.2) Models for linear dune formation –

Now corrected

Need to include the Courrech du Pont (2014) model in the discussion.

We agree that this is an important development, which merits discussion. This is now mentioned, albeit it briefly as it is less directly relevant to the aims of this study, in the discussion of linear dune models.

Suggest merging Experimental Set up with this section

This section is now moved to open materials and methods, as suggested

include a better description of the field sampling strategy - e.g. explain "ten locations", so that they can be reconciled with the figures that describe the modeling results. I had to look back to Figure 1 to remind myself that X and Y are dune crest samples

Moving Figure 1 into this section hopefully clarifies this. We have also clarified the nature of the sampling.

Analytical Methods - which elements were analyzed using the ICP.

The full suite of elements analysed, and the methods used, are now included in the methods.

The particle size analysis and geochemical tracers need to be clearly described and tabulated in this section. Describe PS and geochemical patterns on dune and interdune and explain Table 1. I would move the particle size information (section 3.3) to the start of the section and provide some information on the significance of these data - how do they compare to studies such as Folk (1970)?

We agree that clearer basic description is needed here, as well as greater clarity on the organisation of the results section. We now begin this section with an overview of the structure of this section. The particle size data are brought forward as suggested, and Folk (1971) and Lancaster (1982) cited here. The grain size data are very much in line with what is well established, and on their own are little new. We retain the geochemical data ahead of the particle size data, though, as that is very much the focus of the interpretation of the paper.

Table 1 - what are the units?

This is now corrected, with apologies.

In addition, table 2 is amended to correct significance rounding to a more consistent and meaningful figure – This includes, where relevant, substitution of zero values; whilst 0.000 may be correct to four significant figures, the true value is not zero, and thus <0.001 has been substituted.

Discussion - Tracer elements - also cite Muhs (2017) for a discussion of the significance of these and other elements

This highly relevant paper is now mentioned, especially with regard to origins of variance in K and Ba concentrations, and the relative weathering resistance of K-feldspars.

Courrech du Pont, S., Narteau, C., Gao, X., 2014. Two modes for dune orientation. *Geology* 42, 743-746.

Folk, R., 1970. Longitudinal dunes of the northwestern edge of the Simpson Desert, Northern Territory, Australia, 1. geomorphology and grain size relationships. *Sedimentology* 16, 5-54.

Muhs, D.R., 2017. Evaluation of simple geochemical indicators of aeolian sand provenance: Late Quaternary dune fields of North America revisited. *Quaternary Science Reviews* 171, 260-296.

References added as suggested.

Reviewer #2

Minor issues:

1. In a normal paper in Geomorphology, the section of introduction should be short. The different opinions or ideas would be discussed in the section of Discussion. Thus the text from Line 47 to 152 should be combined or shortened.

We shorten this section by moving line 134-152 to the methods section, where we agree it clearly sits better, as suggested by both referees. However, as both reviewers suggest some additions (see below) to the introduction, and we feel that the research question needs framing to justify the methodology and sampling strategy, we retain the section on linear dune formational hypotheses.

2. Line 55-56: Referring to geophysical surveys of dunes an additional method, i.e., gravity, could be added (Yang, X., Scuderi, L., Liu, T., Paillou, P., Li, H., Dong, J., Zhu, B., Jiang, W., Jochems, A., Weissmann, G., 2011. Formation of the highest sand dunes on Earth. *Geomorphology*, 135, 108-116.).

Now added as suggested.

3. Geographical coordinates should be added to Figs. 2 and 13.

We have added these to figure 2, and also provided a link in the methods to a .kmz file giving exact sample locations. We suggest that repeating these coordinates is not needed in Figure 13 for a number of reasons: 1) It may detract from the visual impact of the figure, 2) Relational, rather than actual locational, information is more important in this figure and 3) If locational information is needed, the accompanying .kmz file can be used.

The formative mechanisms of linear (longitudinal) dunes and dunefields remain uncertain, and multiple hypotheses have been proposed. A central debate is the degree to which dunes act as along-dune sediment transport corridors, implying that dunes grow primarily by extension, or whether they are comprised of locally-derived sands moved from adjacent interdunes (the 'wind-rift' model). Sediment fingerprinting studies, with origins in fluvial science, have been shown to offer the possibility to trace the provenance of aeolian sands, and thus elucidate transport pathways.

Two models (a Monte Carlo framework and a Generalized Likelihood Uncertainty Estimate framework) are used here to provide quantitative estimates of the sediment sources that have supplied a linear dune in the central Simpson Desert of central Australia. Four possible sources are identified that may have supplied the dune; two adjacent interdunes, one upwind low ridge of sand, and a merging upwind dune. Two sites near the dune's crest are used as the target, and provided twenty surface samples for analysis. Following geochemical assay, stepwise discriminant function analysis identified optimum elemental sediment fingerprints for a variety of possible sediment pathway configurations.

Results suggest that the sands of the dune are sourced predominantly from upwind dunes and sand sources, and that likely contributions from neighbouring dune swales are typically <20%. As such, wind-rift mechanisms of linear dune formation are not supported by these data. More complex sediment pathway configurations (i.e. other than a binary approach: interdune vs. along-dune), whilst confirming the initial findings, had reduced discriminatory power. Further separation of source pathways (e.g. identifying the relative roles of different upwind sources) was not possible with any confidence.

The findings suggest recent sediment accretion of a linear dune dominated by along-dune sand flux, and thus support an extensional component for the development of such dunes. Whilst it is noted that at a point-by-point basis this might not exclude accretion by vertical growth, as some have observed, there is no clear support for a substantive contribution to the dune sands from adjacent interdunes. Moreover, the use of contemporary sediment fingerprinting methods to question hypotheses of aeolian geomorphology suggests that such methods have great potential for addressing other terrestrial geomorphological questions where identifying sediment pathways can provide vital insight.

1 **Testing models of linear dune formation by provenance analysis with composite sediment**
2 **fingerprints**

3 Telfer, M.W.¹, Gholami, H.², Hesse, P.P.³, Fisher, A.¹, Hartley, R.¹

4 1. SOGEES, University of Plymouth, Drake Circus, Plymouth, Devon, PL4 8AA, UK.

5 2. Department of Natural Resources Engineering, University of Hormozgan, Bandar-Abbas,
6 Hormozgan, Iran.

7 3. Department of Earth and Environmental Sciences, Macquarie University, North Ryde, NSW,
8 Australia

9 **Highlights**

- 10 • Two sediment fingerprinting methods used to determine sources of linear dune sand.
11 • Models consistent in supporting along-dune sediment flux.
12 • Little evidence of wind-rift mechanisms of linear dune formation.
13 • Sediment fingerprinting methods can address questions in aeolian geomorphology.

14

15 **Key words:** Linear dunes, Dune extension, Sediment provenance, Monte Carlo simulation.

16

17

18 **Abstract**

19 The formative mechanisms of linear (longitudinal) dunes and dunefields remain uncertain, and
20 multiple hypotheses have been proposed. A central debate is the degree to which dunes act as
21 along-dune sediment transport corridors, implying that dunes grow primarily by extension, or
22 whether they are comprised of locally-derived sands moved from adjacent interdunes (the 'wind-rift'
23 model). Sediment fingerprinting studies, with origins in fluvial science, have been shown to offer the
24 possibility to trace the provenance of aeolian sands, and thus elucidate transport pathways.

25 Two models (a Monte Carlo framework and a Generalized Likelihood Uncertainty Estimate
26 framework) are used here to provide quantitative estimates of the sediment sources that have
27 supplied a linear dune in the central Simpson Desert of central Australia. Four possible sources are
28 identified that may have supplied the dune; two adjacent interdunes, one upwind low ridge of sand,
29 and a merging upwind dune. Two sites near the dune's crest are used as the target, and provided
30 twenty surface samples for analysis. Following geochemical assay, stepwise discriminant function
31 analysis identified optimum elemental sediment fingerprints for a variety of possible sediment
32 pathway configurations.

33 Results suggest that the sands of the dune are sourced predominantly from upwind dunes and sand
34 sources, and that likely contributions from neighbouring dune swales are typically <20%. As such,
35 wind-rift mechanisms of linear dune formation are not supported by these data. More complex
36 sediment pathway configurations (i.e. other than a binary approach: interdune vs. along-dune),
37 whilst confirming the initial findings, had reduced discriminatory power. Further separation of
38 source pathways (e.g. identifying the relative roles of different upwind sources) was not possible
39 with any confidence.

40 The findings suggest recent sediment accretion of a linear dune dominated by along-dune sand flux,
41 and thus support an extensional component for the development of such dunes. Whilst it is noted
42 that at a point-by-point basis this might not exclude accretion by vertical growth, as some have

43 observed, there is no clear support for a substantive contribution to the dune sands from adjacent
44 interdunes. Moreover, the use of contemporary sediment fingerprinting methods to question
45 hypotheses of aeolian geomorphology suggests that such methods have great potential for
46 addressing other terrestrial geomorphological questions where identifying sediment pathways can
47 provide vital insight.

48 **Testing models of linear dune formation by provenance analysis with composite sediment**
49 **fingerprints**

50 *1. Introduction*

51 Linear (longitudinal) dunes are probably the most abundant desert dune morphology, and yet the
52 mechanisms of formation and development of these dunes remains unclear. Multiple hypotheses,
53 probably working in conjunction, and perhaps at different temporal and spatial scales, have been
54 proposed for the formation of linear dunes. An equally diverse range of methods have been used to
55 investigate the problem, including field-based monitoring of dunes (Craddock et al., 2015), time
56 series of remotely sensed images (Lucas et al., 2015), geophysical surveys to reveal internal
57 sedimentary structures using radar (Bristow et al., 2000, Bristow et al., 2007a, Bristow et al., 2007b,
58 Hollands et al., 2006) and gravity surveys (Yang et al., 2011), chronostratigraphic surveys (Telfer,
59 2011), numerical modelling (Werner, 1995) and sediment provenance studies (Pell et al., 1999, Pell
60 et al., 2000, Pell et al., 2001).

61 A crucial, and as yet unresolved, aspect of the formation of linear dunes lies in the provenance of the
62 sands of which the dunes are formed. Amongst a diverse range of hypotheses for the formation of
63 these features, two models emerge which can be seen as end-members of a long-standing (Melton,
64 1940, Mabbutt and Sullivan, 1968) debate regarding the degree to which linear dunes are
65 extensional depositional features (Lucas et al., 2015, Telfer, 2011), perhaps serving as long-distance
66 transport corridors for wind-blown sand, or whether they primarily accumulate by sand derived
67 from adjacent interdunes (the so-called 'wind rift' model) (Wopfner and Twidale, 2001, Zhou et al.,
68 2012, Hollands et al., 2006).

69 Composite sediment 'fingerprinting' methods, originally developed for identifying the origin of
70 fluvial sediments (Collins et al., 1997, Walling et al., 1993), and since developing in sophistication
71 with Monte Carlo and/or Bayesian methodologies (Motha et al., 2003, Fox and Papanicolaou, 2008),
72 have demonstrated the ability of the methods to identify the sources of aeolian sediment. Although

73 the term 'fingerprinting' covers a diverse range of properties and methods, ranging from
74 geochemical analyses to radionuclides and magnetic properties, today most composite sediment
75 fingerprinting methods attempt to identify the optimal properties for discerning the relative
76 contributions of different sources of sediment to a target location, and use these to derive
77 quantitative estimates of contributions with robust estimates of uncertainty.

78 Gholami et al. (2017) demonstrated the potential of quantitative fingerprinting of aeolian dune
79 sands in elucidating aeolian transport pathways and revealing sediment sources, and Behrooz et al.
80 (2019) identified the provenance and pathways of aeolian dust affecting a region in eastern Iran.
81 Gholami et al. (2019a) revealed that both long ($10\text{-}10^2$ km) and short (1-10 km) transport had
82 contributed to the sands of a small erg, and highlighted the potentially complex nature of aeolian
83 transport pathways.

84 Here, quantitative composite fingerprinting methods are used to test hypotheses regarding the
85 source of sand in a linear dune in the central Simpson Desert, in central Australia. We use a sediment
86 source fingerprinting method within two different modelling frameworks including Generalized
87 Likelihood Uncertainty Estimate (GLUE) and Monte Carlo (MC) simulations to provide quantitative
88 estimates of the source of dune sands.

89 *1.1 Aims*

90 This study aims to identify local-scale source contributions to linear dunes to improve understanding
91 of their formative mechanisms. In order to do this, we address the following objectives:

92 1) Quantify contributions and uncertainties for different possible source contributions for aeolian
93 linear sand samples in the Simpson Desert, Central Australia, with two different fingerprinting
94 approaches (GLUE and MC).

95 2) Assess the performance of both MC and GLUE models by goodness of fit (GOF) in the different
96 source -sink configurations to identify the most likely sediment transport pathways.

97

98

99 *1.2 Models of linear dune formation*

100 The debate about the formative mechanisms of linear dunes is exemplified in research in the
101 Australian dunefields, where debates have sometimes been most starkly expressed, but draw from
102 evidence worldwide; observational, experimental, modelled, and based upon field and laboratory
103 analyses. Several simultaneous debates emerged. Some suggested that linear dunes did not move
104 laterally (Bourne et al., 2019, Tsoar et al., 2004, Fujioka et al., 2009), but other evidence was more
105 equivocal (Nanson et al., 1992, Rubin et al., 2008, Rubin and Hunter, 1985), and some contradictory
106 (Hesp et al., 1989), until stratigraphic evidence from geophysical surveys proved convincingly that
107 linear dunes can indeed move laterally (Bristow et al., 2000, Bristow et al., 2005, Bristow et al.,
108 2007a). Others sought to reconcile the degree to which linear dunes grew by extension (Tsoar et al.,
109 2004), or by vertical accretion of locally-derived material (Pell et al., 1999, Pell et al., 2000, Zhou et
110 al., 2012). It is worth noting that, on a point-by-point basis, all accumulation is by necessity 'vertical',
111 and only on a landform scale does the term 'vertical accretion' really have any meaning. An
112 extension of the latter argument, taken to its most extreme, views linear dunes as erosional rather
113 than depositional features, an idea which has been vigorously contested (Zhou et al., 2013, Rubin
114 and Rubin, 2013). Whilst evidence for very long-distance (inter-basin, or at least $>10^3$ km) along-
115 dune transport is lacking on grounds of geochemical provenance (Pell et al., 1997, Pell et al., 1999,
116 Pell et al., 2000), and chronostratigraphic evidence over similar scales lacks support for a purely
117 extensional mode of linear dune formation (Hollands et al., 2006), there is decisive evidence of
118 smaller scale (<10 km) elongation from geophysical (Bristow et al., 2007b), chronostratigraphic
119 (Telfer, 2011, Miller et al., 2018) and observational evidence (Lucas et al., 2015) that linear dunes do
120 develop, at least in part, by extension. Taken to its extreme, the extensional argument has been
121 applied to streaming of sand over the entire north African deserts, including across mountain ranges,

122 for 10^2 - 10^3 km (Wilson, 1971, Mainguet and Callot, 1978). It is, perhaps, telling, that some papers
123 within this debate were characterized by distinctly didactic or binary titles; “Longitudinal dunes can
124 move sideways” (Hesp et al., 1989) or “Australian desert dunes; wind rift or depositional origin?”
125 (Wopfner and Twidale, 2001).

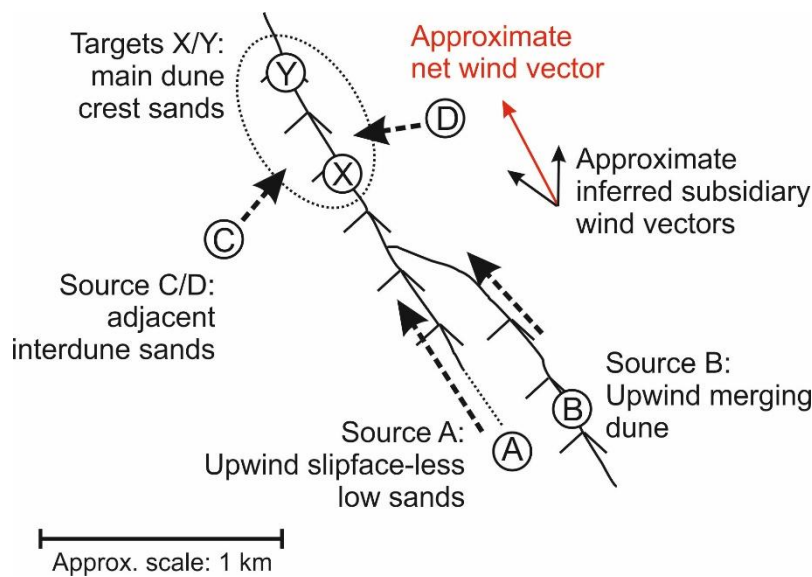
126 The concept that linear dunes may be better considered at the dunefield scale, rather than as
127 individual bedforms, was perhaps best highlighted by Werner’s classic simulations (1995), which
128 demonstrated that characteristic landscapes similar to those observed in the field could emerge
129 when forced with only large-scale forcing parameters, and that individual dune types could be
130 considered as attractors within the phase-space of a complex system. This work, followed by
131 numerous other modelling studies – though infrequently on linear dunes *per se* – suggested that
132 numerous processes may occur concurrently, and that lateral stability vs. sideways movement, or
133 vertical accretion vs. extension were not mutually exclusive conditions at the dunefield scale.
134 Moreover, new evidence emerged that long-standing theories regarding linear dune orientation may
135 not fully account for the range of alignments observed in the field, and that sediment supply also
136 plays a role in controlling dune orientation (Courrech du Pont et al., 2014). Field evidence also
137 revealed that even adjacent dunes may behave very differently in their accumulation record (Telfer
138 and Thomas, 2007, Telfer et al., 2017). This paper seeks to contribute to this discussion by applying
139 methodologies only recently applied to aeolian settings to address a specific question; at a local
140 scale, are dunes supplied with sediment more by downwind dune sources under a net time-
141 averaged wind regime, or adjacent interdunes fed by individual components of the wind regime?

142 *2. Materials and Methods*

143 *2.1 Experimental set-up*

144 To isolate the possible contributions of several different geomorphological settings, we identified a
145 dune where a) clear adjacent interdunes are present on both sides, b) the upwind termination of the
146 dune is clearly visible, where the dune ends in a low, ill-defined slipface-less sand ridge and c) where

147 a downwind-joining junction also merges laterally into the target dune. This is shown schematically
 148 in Figure 1. Samples were collected from ten locations at each site, from the top 1-5 cm of the sands.



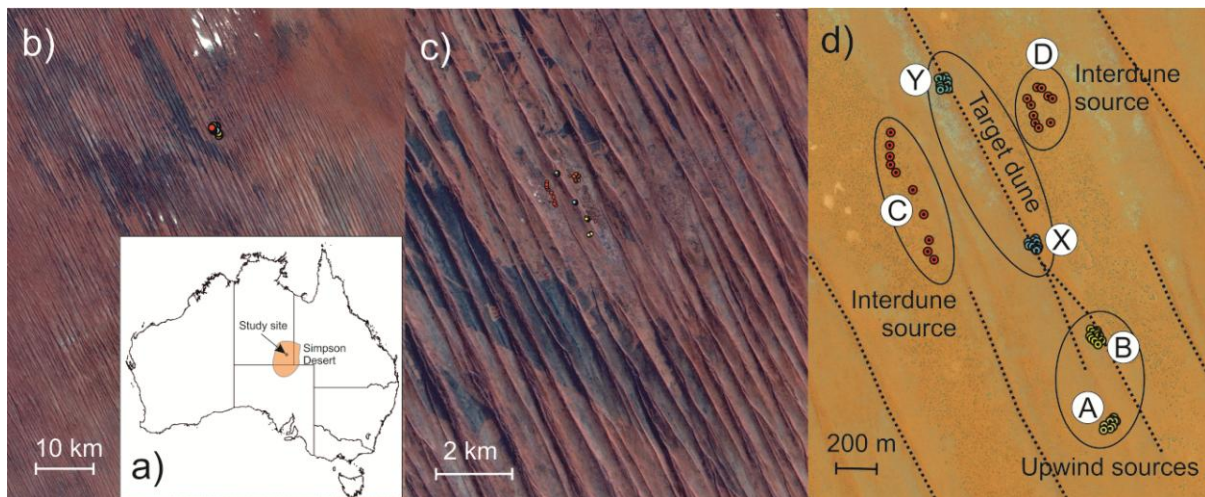
149
 150 *Figure 1. Schematic of the sampling strategy for identifying source contributions to the target dune*
 151 *crest. A and B represent upwind contributions, suggesting extensional mechanisms from the snout of*
 152 *the dune and a merging upwind dune, respectively. C and D represent adjacent interdunes. X and Y*
 153 *are the target locations on the main dune crestline.*

154 This structure facilitates the testing of different hypotheses, as different combinations of source area
 155 definitions can be considered either together, or separately. Thus it is possible to simply consider all
 156 potential upwind source samples as a single region (i.e. A+B), and all adjacent interdunes as a
 157 possible source (i.e. C+D); or to isolate individual sources (for instance, consider A and B as distinct).

158
 159 **2.2 Field location**

160 The Simpson Desert lies in the arid centre of the Australian continent (Figure 2a), and the dunefield
 161 is composed almost exclusively of linear dunes, occupying an area of around 180,000 km². Part of
 162 the continent-scale whorl of linear dunes formed under anticyclonic influence, the dunes of the
 163 Simpson are oriented approximately NNW-SSE (Figure 2b and 2c), and experience a net southerly

164 wind regime (Hesse, 2010). The misalignment of many Australian dunefields with the modern wind
165 regime has long been noted (Hesse, 2011), and whilst some young (Holocene) dunes of the
166 northwestern areas of the Simpson align with current net sand-transporting winds (Hollands et al.,
167 2006, Nanson et al., 1995), Pleistocene dunes in the southern Simpson do indeed appear out of
168 alignment (Nanson et al., 1992). The dunefield is of considerable antiquity, with luminescence dating
169 suggesting dunefield initiation prior to ~590 ka (Fujioka et al., 2009). Ages for the emplacement of
170 individual dunes suggest that some dunes have been in their current location for at least ~100 ka
171 (Nanson et al., 1992, Nanson et al., 1995), and possibly substantially more (Fujioka et al., 2009).



173 *Figure 2. The location of the dune studied, in the central Simpson Desert. a) The location of the*
174 *Simpson dunefield, in the arid centre of Australia. b) Sampling location set amongst hundreds of SSE-*
175 *NNW trending dunes. c) More detailed inspection reveals the presence of both dune terminations*
176 *and some junctions and bifurcations within the patterning. d) Local view of the study site, with main*
177 *dune crestlines highlighted with dashed lines, target dune samples (blues), possible upwind dune*
178 *crest sands (yellows) and possible adjacent interdune source sands (reds).*

179 Samples were taken from the top 1-5 cm of sand, and a .kmz file of the exact locations of samples is
180 provided along with the online version of this article.

181 2.2 Analytical Methods

182 *2.2.1 Geochemical and Sedimentological Analysis*

183 Geochemical assays were performed at the ISO9001-accredited Analytical Research Facility at the
184 University of Plymouth. Preparation involved fusion with lithium metaborate/tetraborate mixture,
185 and samples were fused at 950 °C for 20 minutes in graphite crucibles. The fused mixture was
186 dissolved in 40 mL of 10% nitric acid and then diluted to 100 mL. A further ten-fold dilution with 10%
187 nitric acid was required prior to analysis. Analysis of the samples was undertaken using a Thermo
188 Scientific iCAP 7400 ICP-OES instrument and an X Series 2 ICP-MS instrument (both Thermo
189 Scientific, UK). A total suite of 30 elements was analyzed (V, Cr, Mn, Co, Ni, Cu, Mo, Sb, Ba, Ce, Pr,
190 Nd, Sm, Eu, Gd, Tb, Dy, Ho, Er, Tm, Yb and Lu by ICP-MS, and Na, Mg, Ca, Al, Si, Fe, K and Ti by
191 ICP-OES).

192 Calibration standards were prepared by dilution of stock standards, either 10,000 or 100 mg/L and
193 were matrix matched to the samples with the appropriate amount of flux. The performance of each
194 instrument was checked against the manufacturers' specifications prior to use. A certified reference
195 material, BCR 667, and procedural blanks were prepared and analyzed in the same way as the
196 samples.

197 Particle size data was provided by laser granulometry using a Malvern Mastersizer 2000 with a
198 Hydro-G wet sample unit. Five subsamples of each sample were each analyzed five times, and mean
199 values taken. Ultrasonic dispersion @90% power was employed for 90 seconds prior to
200 measurement, and derivation of grain size fractions used Malvern's general analysis model (software
201 v5.6), with enhanced sensitivity and assuming irregular particle shape, a refractive index of 1.56 and
202 light absorption of 0.01 to 0.001.

203 *2.3 Sediment fingerprinting*

204 In this study, once an optimum fingerprint was identified for each permutation of source/target
205 sample, we used two different methods to quantify source contributions; a Monte Carlo framework

206 (Gholami et al., 2019b), and a Generalized Likelihood Uncertainty Estimate (GLUE; Beven and Binley,
207 1992, Behrooz et al., 2019) model. The use of fundamentally different procedures allows assessment
208 of the dependence of the results on the choice of methodology, as several studies have highlighted
209 potential dependence of model outputs on the choice of model employed (Palazón et al., 2015,
210 Laceby and Olley, 2015, Haddadchi et al., 2013, Haddadchi et al., 2014).

211 *2.3.1 Selection of the optimum composite fingerprints*

212 A two-stage statistical process including range test and stepwise discriminant function analysis (DFA)
213 was applied for selecting optimum composite fingerprints (Habibi et al., 2019). In the range test
214 (stage 1) (Collins et al., 2010), the maximum and minimum fingerprint values in the source and
215 sediment samples were used for identifying outliers. Tracers failing the range test were removed
216 from further analysis. In stage 2, a stepwise DFA based on the minimization of Wilk's Lambda was
217 used to select the optimum composite fingerprints (Gholami et al., 2017, Pulley and Collins, 2018).
218 Bi-plots, as a further test of the conservative behavior of the tracers included in the optimum
219 composite fingerprints, were used to assess similarities in the relationships between tracers in the
220 sediment and source samples (Habibi et al., 2019).

221 *2.3.2 Quantifying source contributions of aeolian sediment using a mixing model within a Monte* 222 *Carlo simulation framework*

223 A mixing model (Collins et al., 1997) within a Monte Carlo simulation framework (Gholami et al.,
224 2019b) was applied to quantify contributions of the potential sources in three different
225 permutations (A+B and C+D; A, B and C+D; A, B, C and D) to twenty aeolian sediment samples (X1-
226 X10 and Y1-Y10). The probability density functions (pdfs) (Collins et al., 2013) were constructed
227 based on the means and standard deviations of the optimum composite fingerprints for the
228 sediment and source samples, and these were repeatedly sampled during the Monte Carlo
229 simulations (Hughes et al., 2009). Using Latin Hypercube Sampling (LHS), 50,000 random samples

230 were drawn from the pdfs to permit Eq. (1) to be solved 50,000 times. The contributions of the two
 231 potential sources were calculated by the model with 95% confidence limits.

$$232 \quad f(X_j) = \sum_{i=1}^n \left((C_i - \sum_{j=1}^m P_j \cdot X_{j,i}) / C_i \right)^2 \quad (\text{Eq.1})$$

233 Where n is the number of fingerprint properties (here varying from 2 to 3), m is the number of
 234 sediment sources (that is, between 2 and 4 depending on experimental set-up), C_i is the mean
 235 concentration of fingerprint property (i) in the sediment sample, P_j is the relative contribution of
 236 source (j) to the sediment sample, $X_{j,i}$ is the mean concentration of fingerprint property (i) in source
 237 (j). The mixing model must satisfy two boundary constraints: each source contribution must be
 238 between 0 and 1, and all the contributions must sum to 1.

239

240 *2.3.3 Quantifying source contributions of aeolian sediment using the Generalized Likelihood* 241 *Uncertainty Estimate (GLUE) model*

242 The GLUE methodology followed Behrooz et al.'s (2019) implementation of the original
 243 methodology proposed by Beven and Binley (1992) and used the same permutations of target and
 244 source. This utilizes five steps, and is described in full in Behrooz et al. (2019), but to summarize:

245 1) Latin Hypercube Sampling (LHS) (Collins et al., 2013) is used to sample the parameter sets for
 246 200,000 iterations, based upon a uniform distribution for all parameters, due to lack of *a priori*
 247 knowledge. It is assumed all source contributions are non-negative, and sum to unity.

248 2) The Nash–Sutcliffe coefficient (ENS) is used as the likelihood function, and is defined thus:

249

$$250 \quad ENS = 1 - \frac{\sum(O_{obs} - O_{sim})^2}{\sum(O_{obs} - \hat{O}_{obs})^2} = 1 - \frac{\sigma_i^2}{\sigma_{obs}^2} \quad (\text{Eq.2})$$

251

252 where \hat{O}_{obs} is the mean value of the observed tracer concentration; O_{sim} is the simulated tracer
 253 concentration; O_{obs} is the observed tracer concentration; σ_i^2 is the error variance for the *i*th model

254 (i.e., the combination of the model and the i th parameter set) and σ_{obs}^2 is the variance of the
255 observations.

256 3) The sampled parameter sets from step 1 are fed into the mixing model (equation 2), and the
257 likelihood function is calculated for each parameter set as:

258

$$259 \quad C_{\text{Sediment}} = C_{\text{Sources}} \times P \quad (\text{Eq. 3})$$

260

261 where P is an m -dimensional column vector of sources contribution (sampled parameter sets),
262 C_{Sediment} is an n -dimensional column vector of element concentration in sediment sample, C_{Sources}
263 is an $n \times m$ -dimensional matrix representing mean tracer concentration in sources (each row
264 represents mean tracer concentration in each source).

265 4) Each parameter set is defined as either behavioural or non-behavioural types, depending on
266 whether their likelihood function exceeds a threshold value (Zhou et al., 2016). Non-behavioural
267 parameter sets were discarded.

268 5) For each parameter set defined as behavioural, likelihood weights are rescaled such that they
269 sum to one, and a cumulative distribution derived for each parameter, to enable the derivation of
270 uncertainties.

271

272 2.3.4 Assessing performance of the MC and GLUE models

273 A Goodness of Fit (GOF) test (Manjoro et al, 2016; Gholami et al., 2019b) was applied to evaluate
274 performance of the two models - MC and GLUE. Although not without critics (Palazón et al., 2015),
275 the method is widely used to give an indication of the validity of model findings (e.g. Habibi et al.,
276 2019, Zhou et al., 2016), and here we use it relatively to assess differences of the proposed source
277 configurations. Goodness of Fit, using the terms of Eq. 1, is thus defined:

$$278 \quad GOF = (1 - [SQRT \sum_{i=1}^n \left[\frac{C_i - (\sum_{j=1}^m P_j \cdot X_{ji})}{C_i} \right]^2]) / n \quad (\text{Eq. 4})$$

279

280 3. Results

281 In the first part (3.1) of the section, the basic geochemical and particle size data for the samples are
282 presented. The second section discusses the development of the statistical fingerprinting methods
283 from the geochemical data, and lastly, section 3.3 presents the outcomes of different combination of
284 source-target configurations and modelling frameworks.

285 *3.1 Geochemical and particle size results*

286 *3.1.1 Geochemical assays*

287 The results of the ICP analyses are presented in Table 1. The major species are, unsurprisingly,
288 indicative of quartz-dominated sands (indeed the Si values seem low, with even 38% Si
289 corresponding to an equivalent pure quartz concentration of 80%) with a more minor K-dominated
290 feldspar component. This is broadly inline with the few other quantitative studies of sand mineral
291 composition from central Australia, with Fitzsimmons et al. (2009) reporting 80-95% quartz and 1-
292 15% feldspar for linear dunes of the Strzelecki to the southeast.

		Na	Mg	Ca	Al	Si	Fe	K
		(ppm)	(ppm)	(ppm)	(%)	(%)	(%)	(%)
	Min	832	229	148	0.78	17.65	0.45	0.55
	Mean	1072	304	273	1.08	26.71	0.59	0.70
Sediment	Max	1934	414	408	1.45	37.83	0.8	0.90
	Min	489	313	339	0.84	16.61	0.41	0.48
	Mean	1449	645	733	1.55	29.94	0.80	0.83
Source	Max	2358	1395	2835	2.24	37.37	1.47	1.00
	Range test	P	F	F	F	F	P	P
		Ti	V	Cr	Mn	Co	Ni	Cu

		(ppm)	(ppm)	(ppm)	(ppm)	(ppb)	(ppm)	(ppm)
	Min	524	13.68	7.59	27.28	380	2.46	3.70
	Mean	769	19.56	10.58	37.09	613	4.87	5.93
Sediment	Max	1278	31.67	14.64	54.35	1168	11.78	8.68
	Min	637	14.90	7.90	29.60	407	2.70	4.32
	Mean	1122	31.55	14.57	56.19	1047	5.86	8.66
Source	Max	1697	53.50	21.70	132.70	2558	15.50	25.60
Range test		F	F	F	F	F	F	F
		Mo	Sb	Ba	Ce	Pr	Nd	Sm
		(ppb)	(ppb)	(ppb)	(ppm)	(ppm)	(ppm)	(ppb)
	Min	235	309	196	5.64	0.69	2.47	440
	Mean	496	596	251	8.89	1.05	3.75	676
Sediment	Max	1043	864	313	13.91	1.64	5.75	1042
	Min	192	87	153	6.52	0.87	2.98	558
	Mean	628	622	276	12.18	1.44	5.26	983
Source	Max	1984	1652	325	20.31	2.44	9.03	1674
Range test		P	P	P	F	F	F	F
		Eu	Gd	Tb	Dy	Ho	Er	Tm
		(ppb)	(ppb)	(ppb)	(ppb)	(ppb)	(ppb)	(ppb)
	Min	131	396	70	421	87	269	41
	Mean	185	638	110	612	129	397	66
Sediment	Max	251	985	163	933	206	672	117
	Min	128	566	84	474	97	305	48
	Mean	239	957	151	930	193	610	97
Source	Max	356	1515	237	1339	275	887	164

Range test	P	F	F	F	F	F	F
	Yb	Lu					
	(ppb)	(ppb)					
	Min	285	46				
	Mean	440	74				
Sediment	Max	729	128				
	Min	338	54				
	Mean	675	112				
Source	Max	1015	183				
Range test	F	F					

293

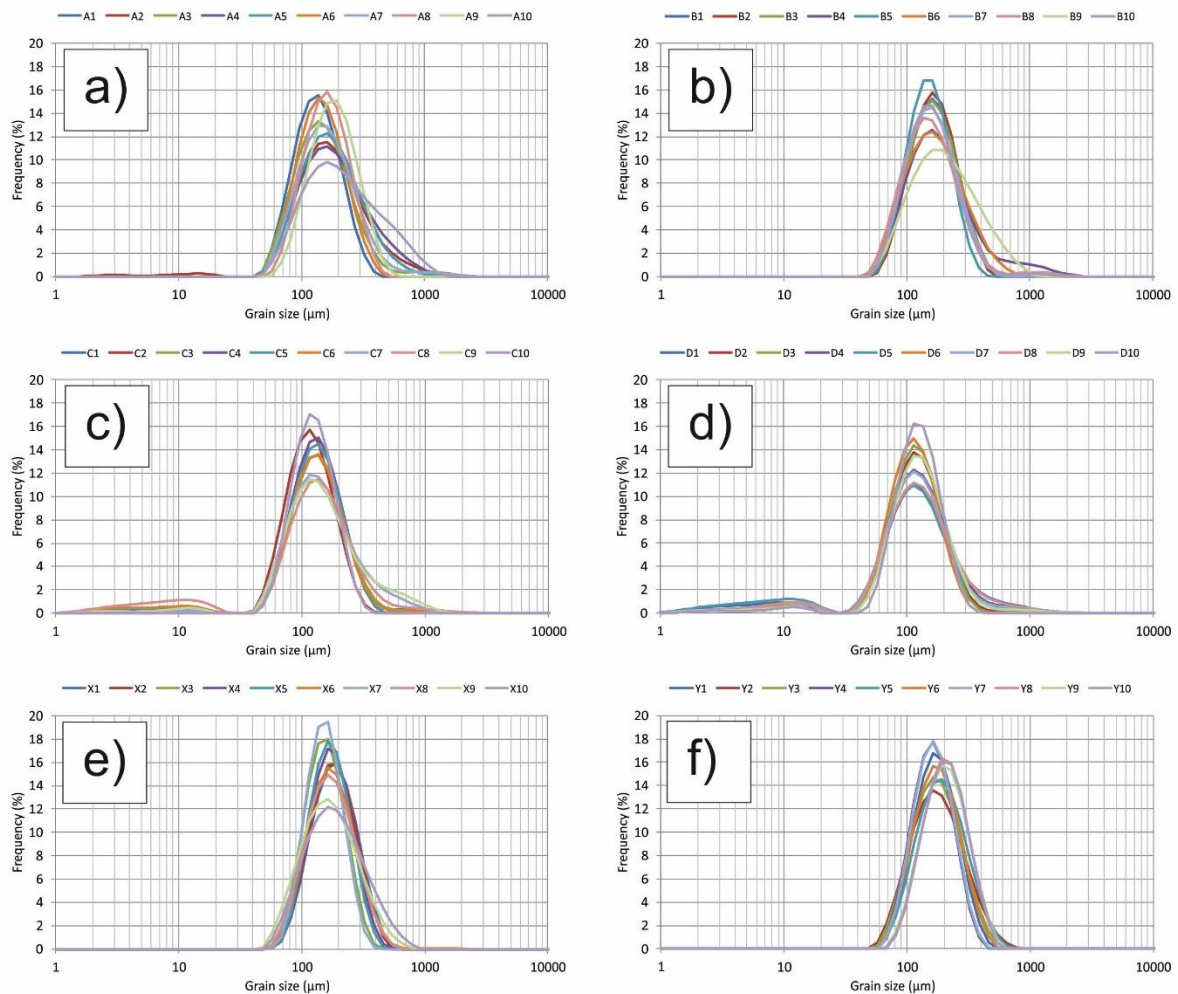
294 *Table 1: Minimum, mean and maximum concentrations of the geochemical tracers in all samples.*

295 *the source and target sediment samples. p and f indicate passing and failing the range test,*

296 *respectively; see section 3.2.1.*

297

298 *3.1.2 Physical sediment characteristics*



299

300 *Figure 3. Particle size distributions for all samples. Sand source samples a) A and b) B are dominated*
 301 *by very fine – medium sands, with a marked positive tail towards coarse sands, and whilst the*
 302 *interdune source samples c) C and d) D are also dominated by very fine – fine sands, here there is a*
 303 *negative tail in the distribution, with up to 20% silt in some samples. The target dunes e) X and f) Y*
 304 *are the best sorted, with little other than very fine – medium sand.*

305 All samples (Figure 3) are characterized by a dominance of fine sands (31.5 – 64.6%; mean 48.7%)
 306 and very fine sands (11.5 – 50.7%; mean 30.7%). In total, sands comprise 78.7 – 100% of the
 307 sediments (mean 96.0%), and silts comprise 0 – 20.4% (mean 3.9%). The interdune samples (C and D;
 308 Figure 3c and 11d) however, are typified by an increased silt component (averaging 10.2%, and up to
 309 20.4% in one sample), compared to the source and target dune sands where silts average just 0.8%
 310 and the maximum observed value is 3.6%. There is also a slight positive tail to all candidate sources

311 samples (A-D), with a minor component of coarser sands; this is in line with well-reported trends in
312 linear dunes/interdunes (e.g. Lancaster, 1982, Folk, 1971).

313

314 *3.2 Discrimination of sediment sources by range test and stepwise DFA*

315 *3.2.1 Range test*

316 Prior to applying a statistical procedure for selecting final fingerprints, a range test (Collins et al.,
317 2010; Gellis and Noe, 2013) was used to identify outliers and, therefore, significantly non-
318 conservative tracers for exclusion from further analysis. Here, the maximum and minimum tracer
319 concentrations in the source and sediment samples were used for identifying outliers (Table 1).
320 Tracers failing the range test (i.e. tracer concentrations measured for the target sediment samples
321 that fell outside the corresponding ranges of the source sample tracer concentrations) were
322 removed from further analysis (Gholami et al., 2019a, Gholami et al., 2019b, Nosrati et al., 2018).

323

324 Five tracer elements were identified as significant for the three models of sediment pathway, but
325 only one (Na) is consistent throughout. Antimony (Sb) and potassium (K) are identified as the other
326 most significant tracers for the two-source scenario, molybdenum (Mo) as the additional tracer in
327 the three-source model, and barium (Ba) in the four-source configuration. The likely sources of these
328 elements are considered in section 4.1, though for now it is worth noting that whilst some mobility
329 of soluble Na salts cannot be ruled out, antimony, with a near-equal predictive power, is very
330 insoluble in the natural environment. It is likely significant that Na and Ba together have lower
331 predictive power in the case of the four-source scenario in the later interpretation of results, as
332 indicated by the markedly lower sum of the Wilk's Lambda; the implications of this are considered in
333 section 4.1. Figure 4 shows scatterplots of the three- and four-source permutations of the stepwise
334 DFA; the two-source model yielded a single predictive discriminant function.

335

336

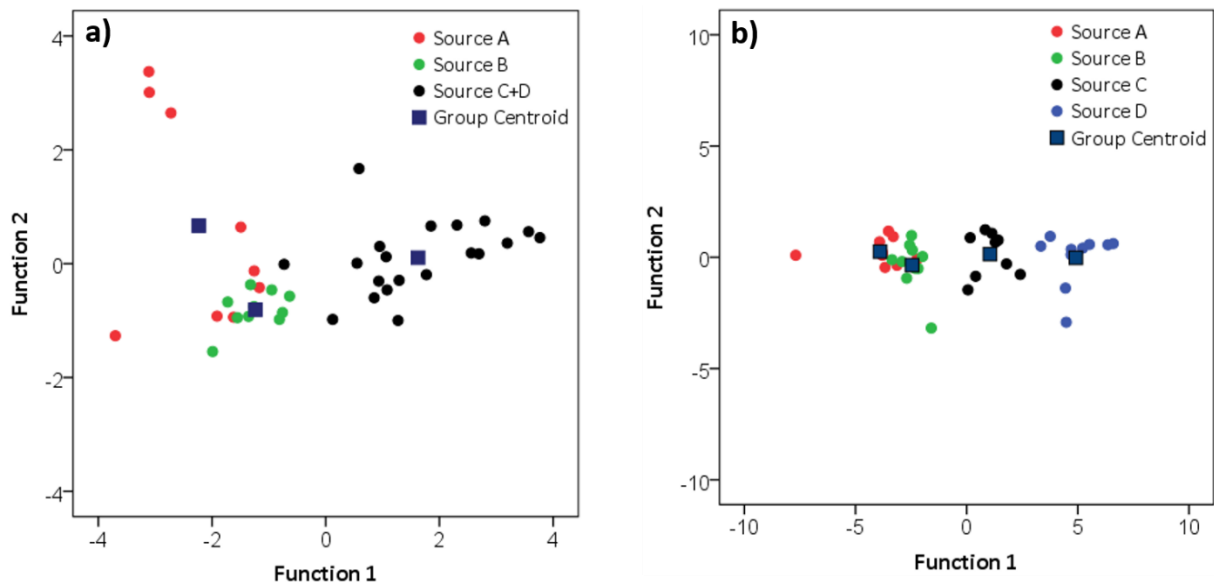
Step	Tracer selected	Wilk's Lambda	Sig
With two potential sources (A+B and C+D)			
1	Na	0.269	<0.001
2	Sb	0.230	<0.001
3	K	0.204	<0.001
With three potential sources (A, B and C+D)			
1	Na	0.262	<0.001
2	Mo	0.186	<0.001
With four potential sources (A, B, C and D)			
1	Na	0.13	<0.001
2	Ba	0.068	<0.001

337

338 *Table 2: Results of DFA for selecting optimum composite fingerprints with two (A+B and C+D),*
339 *three (A, B and C+D) and four (A, B, C and D) potential sources.*

340

341



342

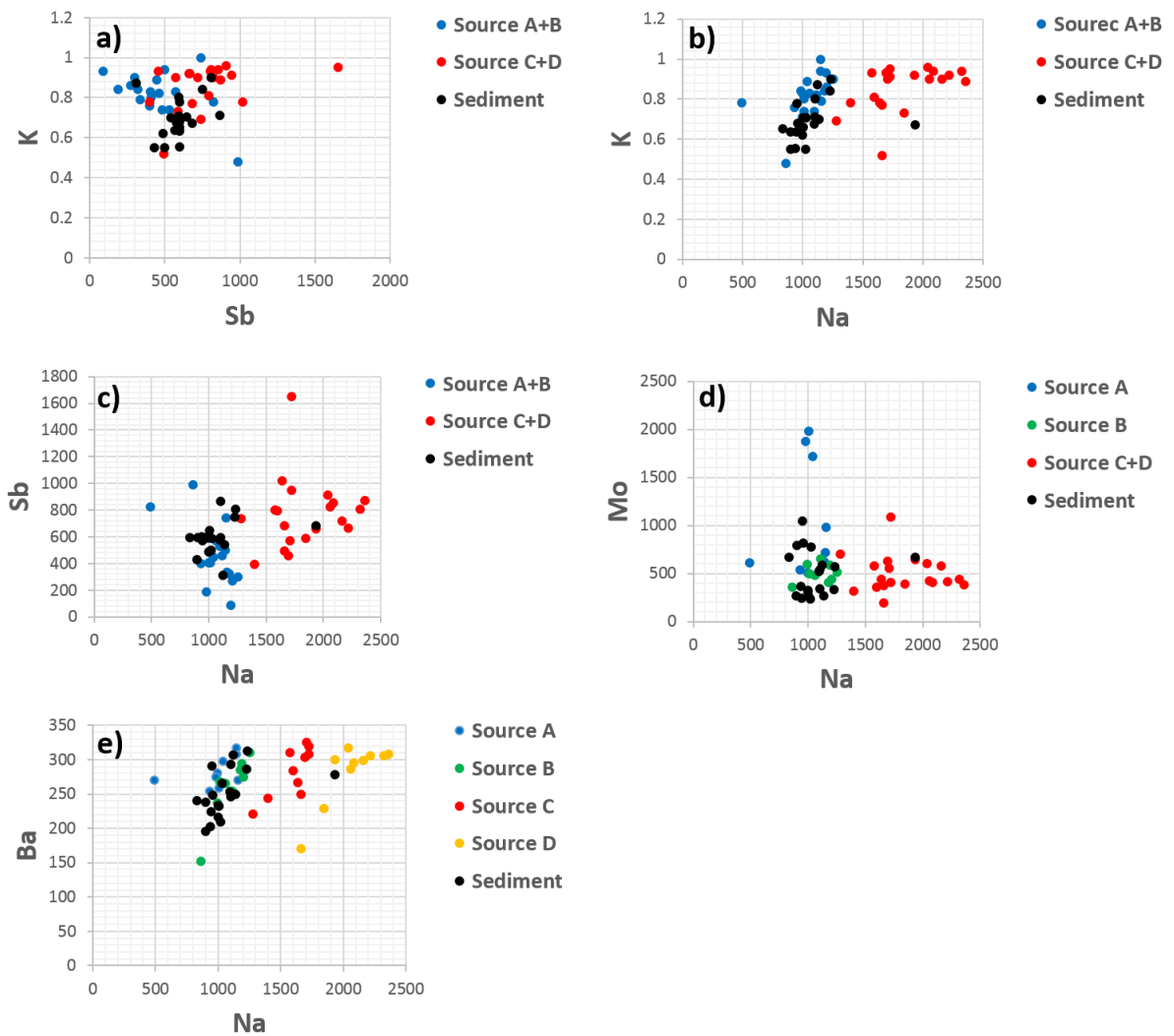
343 *Figure 4: Scatterplots were constructed from first and second functions in the stepwise DFA, a) with*
 344 *three potential sources (A, B and C+D); and b) with four potential sources (A, B, C and D). With two*
 345 *potential sources (A+B and C+D), scatterplots are not applicable because there is a single*
 346 *discrimination function. 97.4, 84.6 and 92.3% source samples were classified correctly for two, three*
 347 *and four potential sources, respectively.*

348

349 3.2.2 Conservative behaviour of optimum composite fingerprints in the sediment and source samples

350 Results from the bi-plot test are presented in Figure 5. Plots wherein the source and sediment
 351 samples do not fall in the same general space suggest non-conservative behaviour of the tracers in
 352 question.

353



354

355 *Figure 5: Bi-plots for all pairings of the geochemical tracers in the final composite signature,*
 356 *measured on the source and target sediment samples: a, b and c) with two potential sources (A+B*
 357 *and C+D), d) with three potential sources (A, B and C+D) and e) with four potential sources (A, B, C*
 358 *and D).*

359

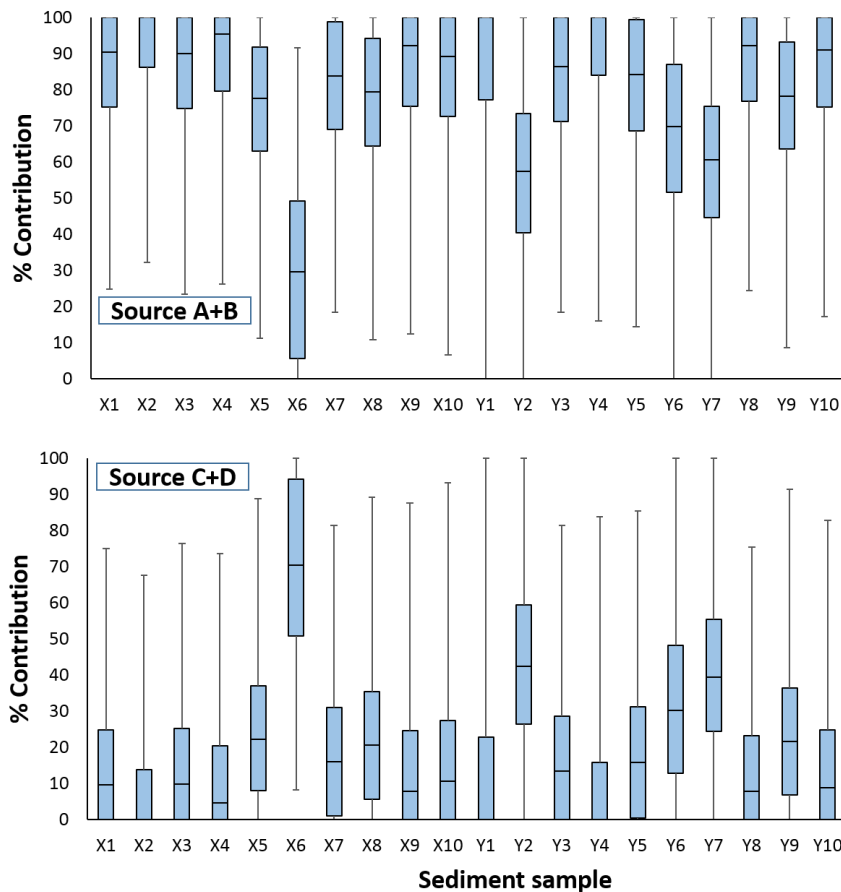
360 3.3 Source contributions from different models and various sediment pathway configurations

361 Three different source-target configurations are considered here, each with the two models
 362 proposed; Monte Carlo modelling and the GLUE framework.

363

364

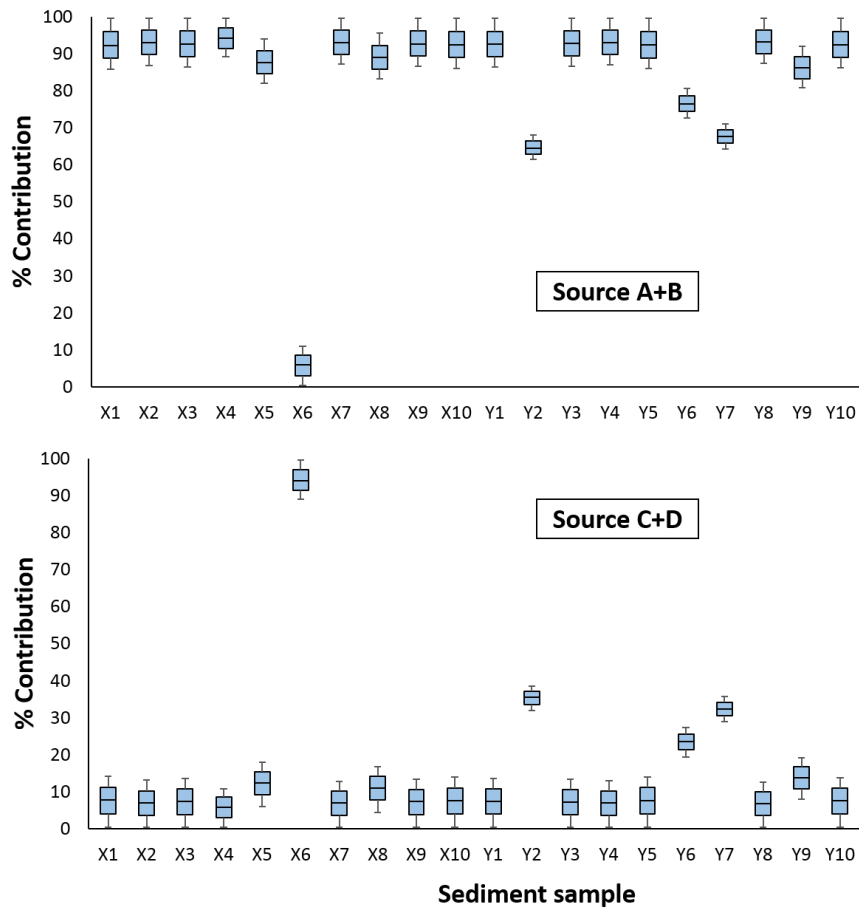
365 3.3.1 Two-source configuration: upwind and adjacent sources (A+B; C+D)



366

367 Figure 6: Monte Carlo simulation results for sand dune source contributions with 95% confidence
368 limits (with percentiles 2.5, 25, 50, 75 and 97.5). A+B and C+D indicate two potential sources for
369 aeolian sediment samples.

370 The results of the two-source configuration from both models are encouragingly consistent (Figures
371 6 and 7); both imply a system dominated by dune sands sourced from upwind locations (both the
372 upwind dune snout (A), and the merging dune (B)). By either assessment, sixteen of the twenty
373 samples are clearly dominated (>70%) by sediments with affiliation to these sources, with X6 (most
374 markedly), Y2, Y6 and Y7 as notable exceptions. Both modelling approaches are consistent in the
375 identification of which samples share greater affinity with the two possible sources. GLUE estimates
376 are typically characterized by their smaller uncertainties.

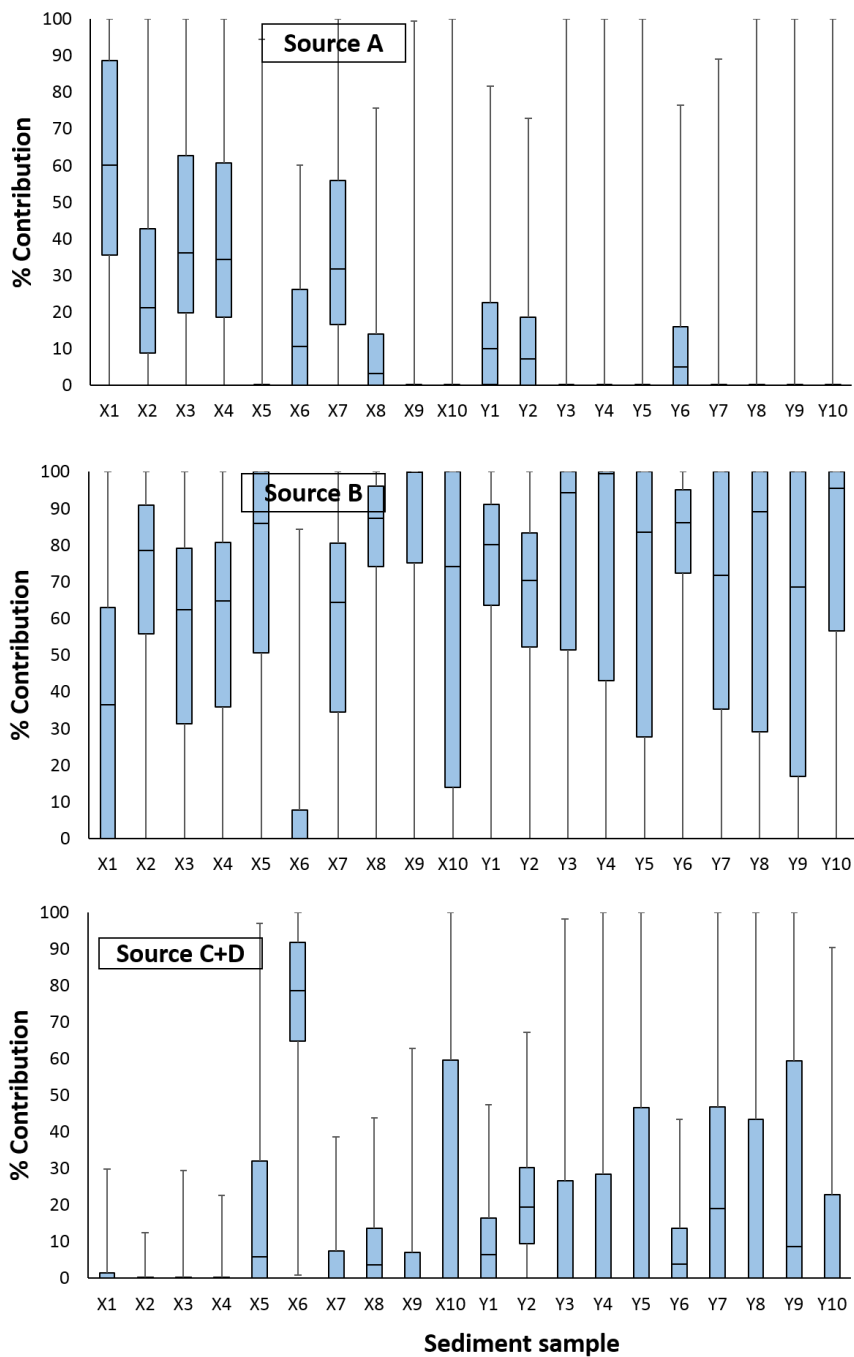


377

378 *Figure 7: GLUE results for sand dune source contributions with 95% confidence limits (with*
 379 *percentiles 2.5, 25, 50, 75 and 97.5). A+B and C+D indicate two potential sources for aeolian*
 380 *sediment samples.*

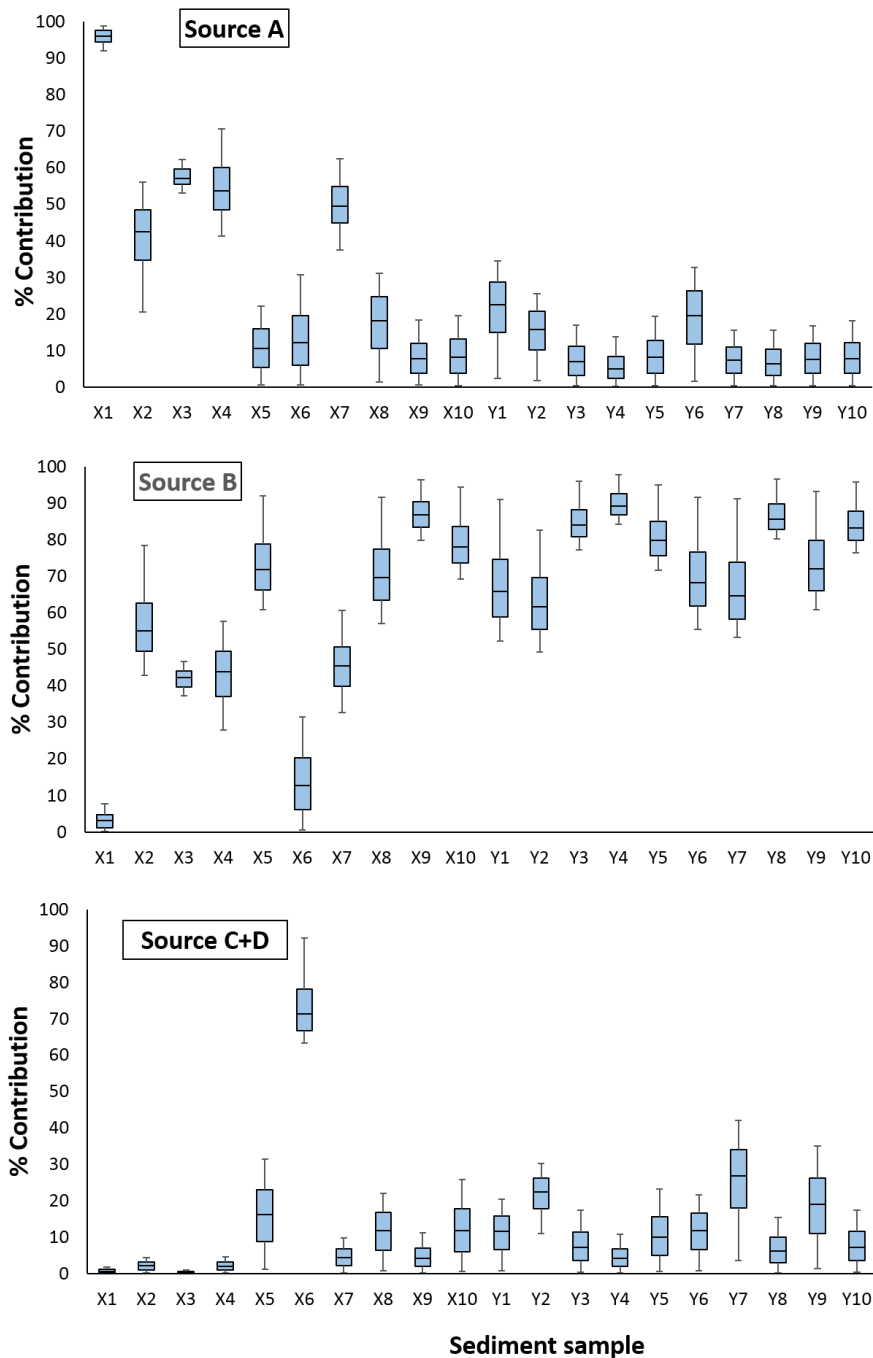
381

382



384

385 *Figure 8: Monte Carlo simulation results for sand dune source contributions with 95% confidence*
 386 *limits (with percentiles 2.5, 25, 50, 75 and 97.5). A, B and C+D indicate three potential sources for*
 387 *aeolian sediment samples.*



388

389 *Figure 9: GLUE results for sand dune source contributions with 95% confidence limits (with*
 390 *percentiles 2.5, 25, 50, 75 and 97.5). A, B and C+D indicate three potential sources for aeolian*
 391 *sediment samples.*

392 The three-source configuration (Figures 8 and 9) offers much support for the two-source scenario,
 393 but also offers further information. With both Monte Carlo and GLUE methodologies, source B – the
 394 merging dune – is seen to dominate the likely source contributions. Extreme uncertainties –

395 especially for the Monte Carlo method - are undoubtedly wider, but interquartile ranges (indicated
396 by the blue box on the box-and-whisker plots of Fig 7 and Fig 8) are generally supportive of a
397 dominant source contribution coming specifically from the merging dune (source B), beyond that
398 contributed from the immediate upwind sand source (source A). Sample X6, especially, remains a
399 clear outlier to the general trend, with greater similarity to the interdune samples.

400

401

402

403

404

405

406

407

408

409

410

411

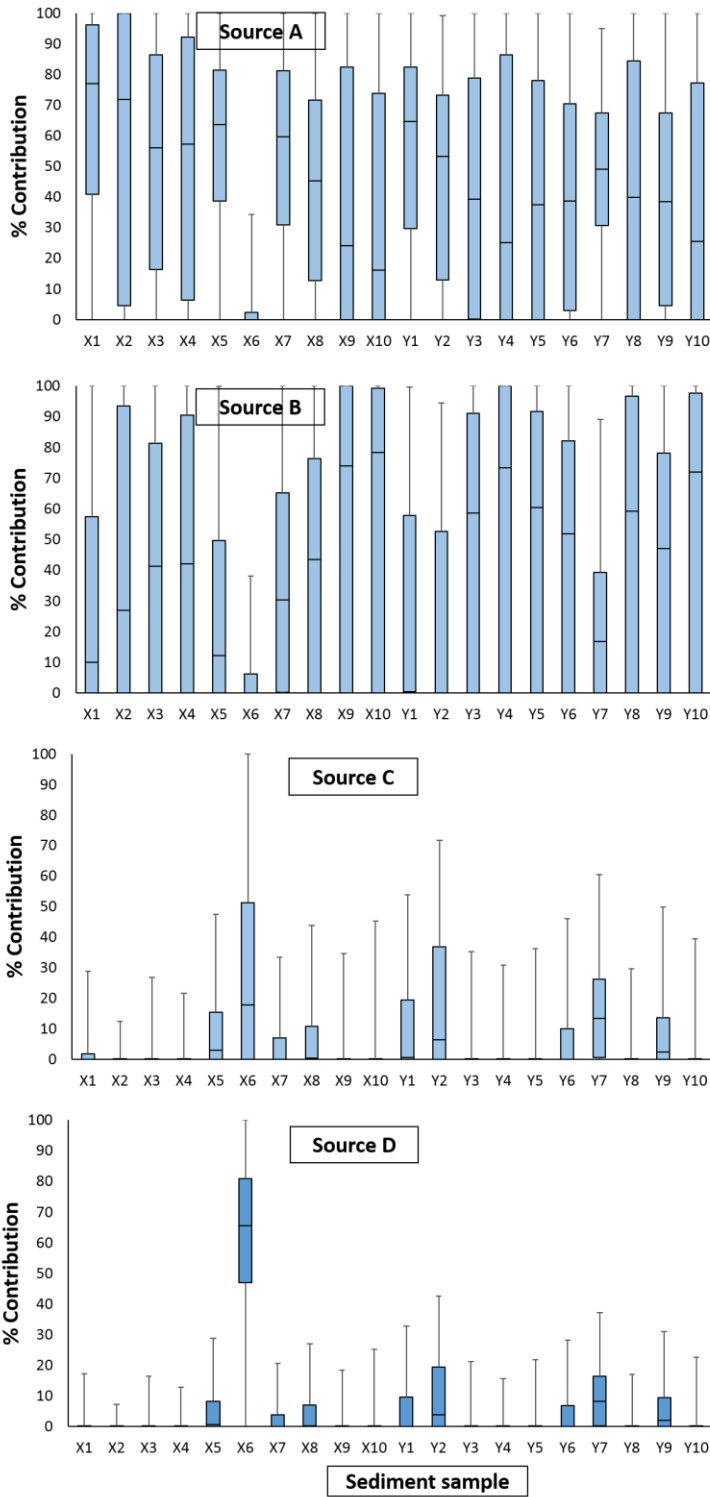
412

413

414

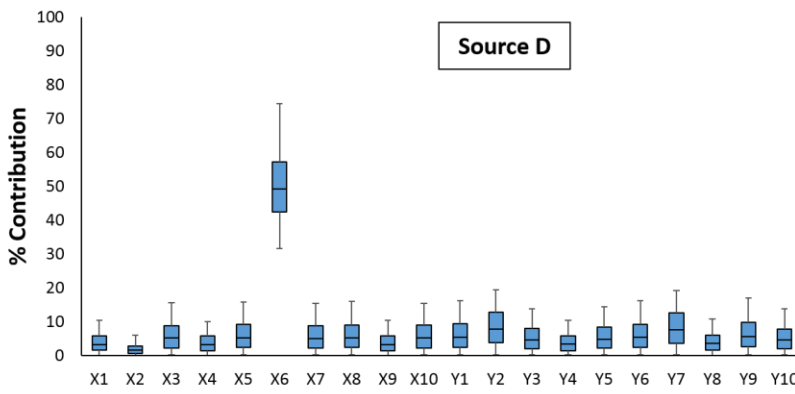
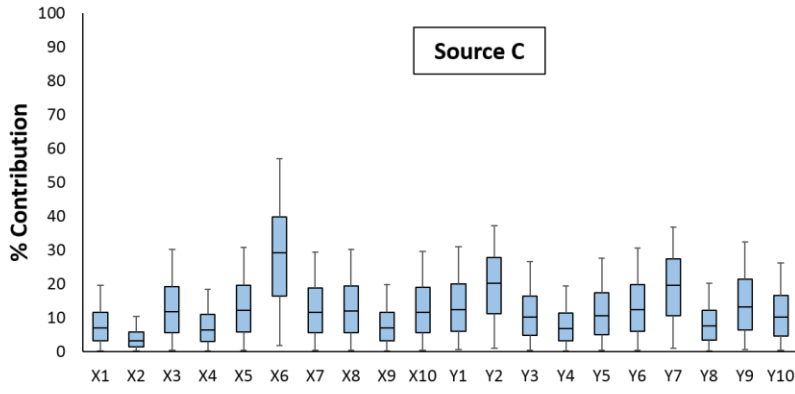
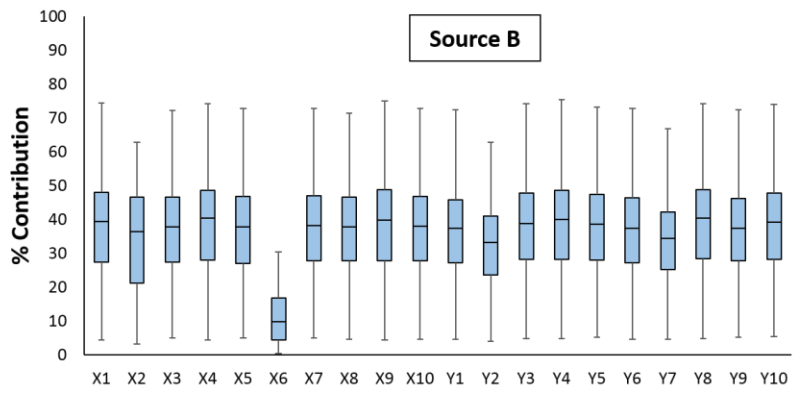
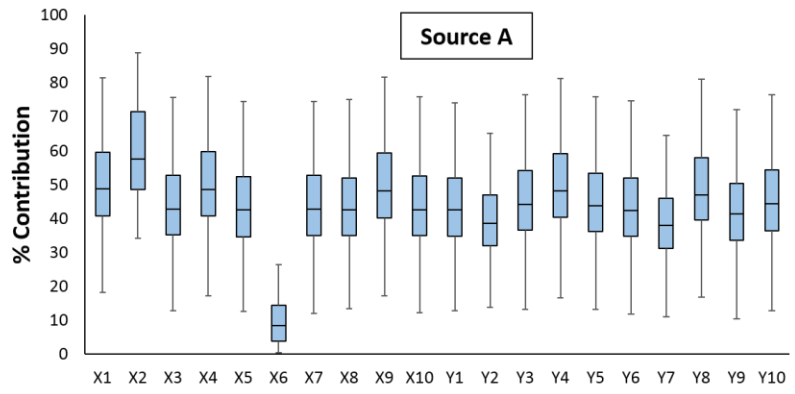
415

417 3.3.4 Four-source configuration: dune snout, merging dune and eastern and western interdune



419 *Figure 10: Monte Carlo simulation results for sand dune source contributions with 95% confidence*
420 *limits (with percentiles 2.5, 25, 50, 75 and 97.5). A, B, C and D indicate four potential sources for*
421 *aeolian sediment samples.*

422 Results from the four-case scenario are more complex, and characterized, especially in the case of
423 Monte Carlo modelling (Figure 10), by much greater uncertainties. There is still broad agreement
424 that the contribution of the upwind sources (that is, A and B) dominates that from the interdunes
425 (that is, C and D), but interquartile variance in the estimates typically exceeds 50% and, in some
426 cases, approaches 100% for the upwind sources. GLUE estimates (Figure 11) also suggest greater
427 importance of the upwind sources, and has tighter constraints on uncertainty, but it is noticeable
428 that variance is greater under this scenario than others approached with the GLUE methodology (Fig
429 7 and 9). Despite the greater uncertainties, the relative contribution of the upwind sources (the
430 immediately-upwind low sand pile, and merging dune) is apparently somewhat reversed under this
431 approach, with a greater role indicated for the immediate upwind source. Both modelling
432 approaches suggest a slightly higher input from the western interdune, compared to the eastern
433 side, with the notable exception of sample X6, with a median contribution of around 50% total from
434 the eastern interdune and just 20-30% from the west.



Sediment sample

436 *Figure 11: GLUE results for sand dune source contributions with 95% confidence limits (with*
437 *percentiles 2.5, 25, 50, 75 and 97.5). A, B, C and D indicate four potential sources for aeolian*
438 *sediment samples.*

439 *4. Discussion*

440 The performance of the models is considered first, before considering the implications of the most
441 robust findings for models of linear dune formation.

442 *4.1 Sediment fingerprinting model performance*

443 The elements identified as the most significant tracers vary from abundant mineral-forming alkali
444 metals (Na and K), to much scarcer alkaline earth metals (Ba), transitional metals (Mo) and
445 metalloids (Sb); all are relatively enriched in the source sediments relative to the target dune sands.

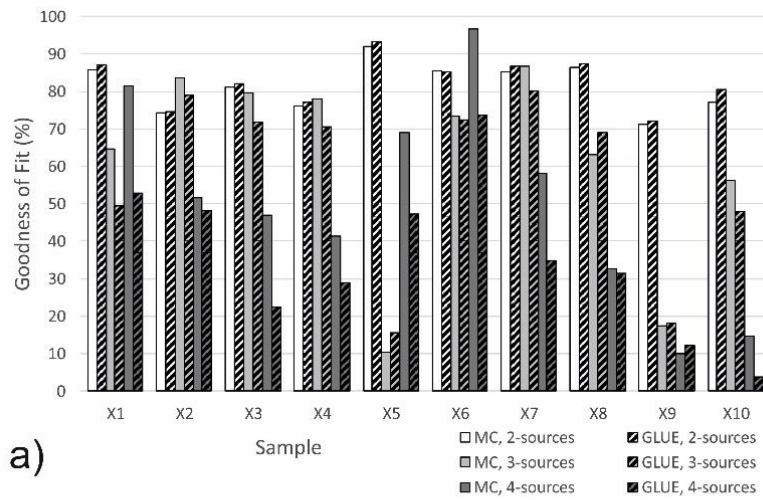
446 The alkali metals are likely associated with weathering products from feldspars and micas, and Ba
447 may substitute for K in the lattice of these minerals (Kasper-Zubillaga et al., 2007). Indeed, K/Ba ratio
448 (along with K/Rb) in aeolian K-feldspar sands was one of the indices identified by Muhs (2017) as the
449 most promising for identifying the provenance of North American dune sands. Whilst the possibility
450 of a soluble sodium component in the sands cannot be entirely discounted, most of the other tracers
451 identified are insoluble in this environment, and Muhs also note the relative chemical resistance of
452 K-feldspars (orthoclase and microcline), and likely variance in K and Ba as being attributable to
453 source geology, and not weathering. The dominant heavy minerals in the study region belong to Pell
454 *et al.*'s (2000) 'northern Simpson' population, in which haematite, epidote and muscovite are
455 abundant, and garnet, tourmaline, monazite and zircon significant. Molybdenum is most often
456 associated with Cu ores, an observation consistent with Pell et al.'s (2000) attribution of the Mount
457 Isa block, which contains substantial Cu deposits (Gregory et al., 2008), as the 'proto-source' for the
458 sands of the Simpson. Antimony is also known from the Mount Isa block, associated with lead
459 mineralization. In short, the tracers identified seem likely to reflect both primary mineralization and

460 long-distance transport of heavy minerals from proto-sources, and subsequent elemental
461 differences in sands and silts as a result of weathering.

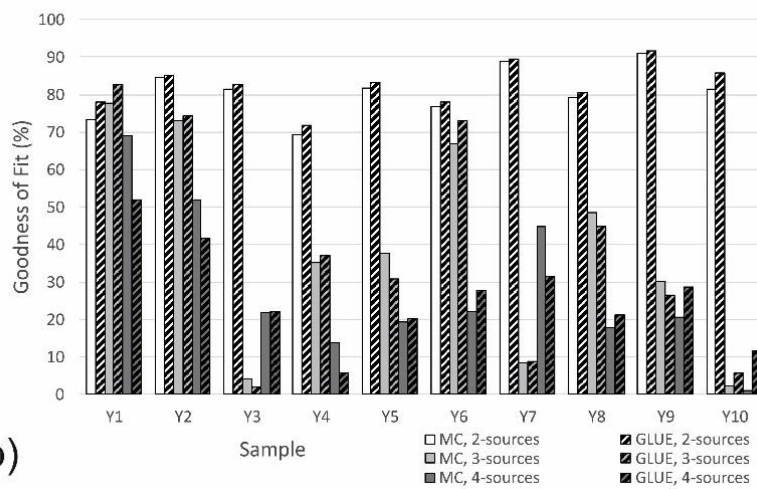
462

463 Figure 12 presents the results of the evaluation performance of the Monte Carlo simulation (MC)
464 and GLUE model by GOF for the different configurations of sources (two-, three- and four-sources).
465 Both MC and GLUE models have the highest performance associated with the simplest (two-source)
466 configuration, with GOF values for the majority of sand samples of > 80 %. In the 3-source model,
467 the GOF values for majority of the samples were 50- 80 %, and yet poorer performance for the four-
468 source model is indicated by GOF values typically < 50%. Overall, based on the GOF values (for
469 majority of samples > 80%) and scatterplot constructed stepwise DFA (97.4% source samples were
470 classified correctly), the two-sources grouping (A+B and C+D) is the best grouping for discriminating
471 sources of sand dunes in the Simpson Desert.

472



a)



b)

473

474 *Figure 12. The Goodness of Fit (GOF) values for the MC and GLUE models for 20 sand dunes samples*

475 *a) X1-X10, and b) Y1-Y10. In the majority of cases, the two-source model is seen to provide the*

476 *strongest predictive power, followed by the three-source scenario and lastly the four-source*

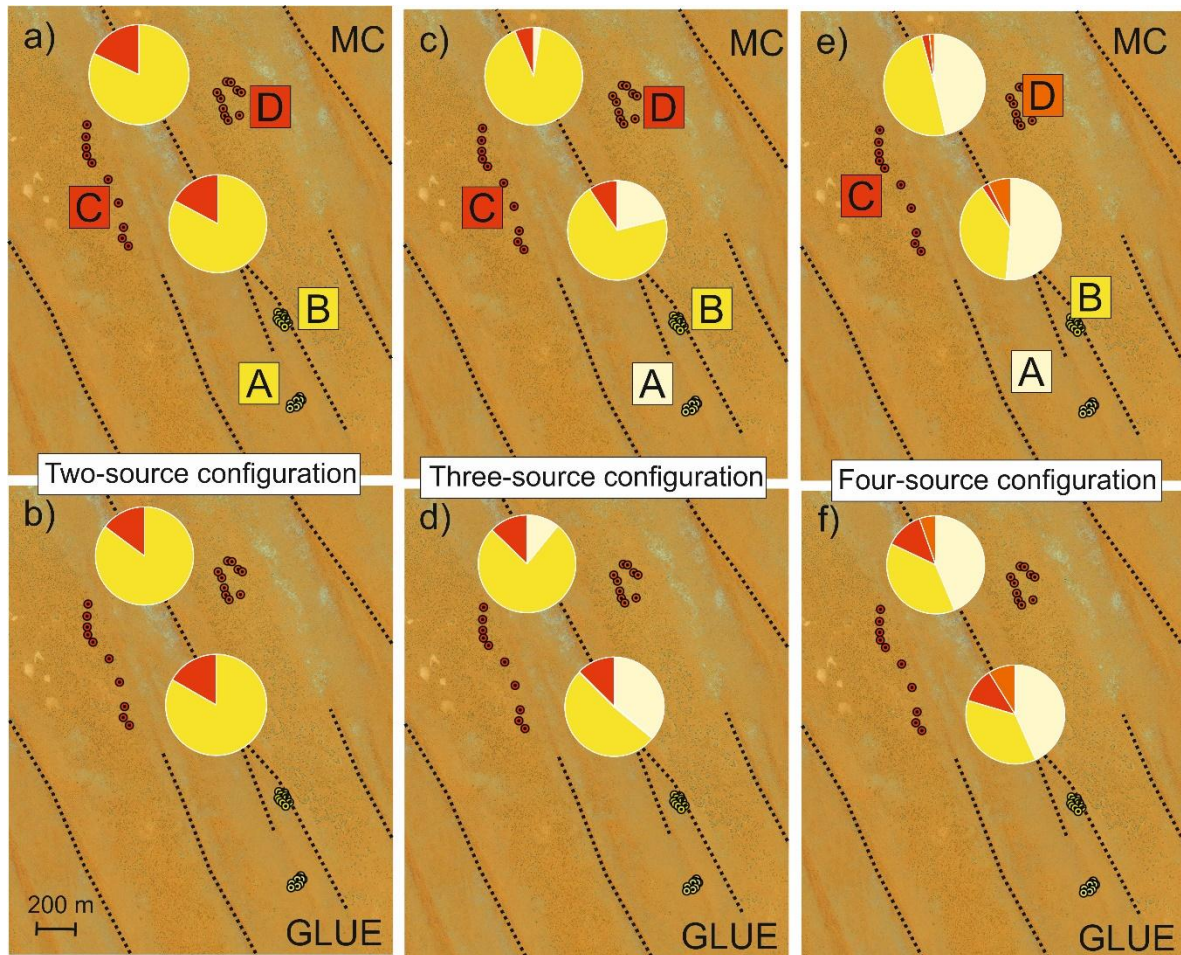
477 *configuration*

478

479 4.2 Implications for linear dune formation

480 4.2.1 Interpreting the provenance analyses

481 The results of the six provenancing assays are shown spatially in Figure 13.



482

483 *Figure 13. Spatial representation of the median estimate of source contributions under different*

484 *assumed sediment pathway configurations and using two different methodologies for the*

485 *fingerprinting. The simplest situation simply compares upwind and adjacent sources using a) Monte*

486 *Carlo and b) GLUE frameworks. c) and d) differentiate between the immediate upwind low sands (A)*

487 *and a flanking dune which merges with the target (B). e) and f) treat all four possible sources*

488 *individually. Pie charts are shaded according to the colours of the source labels in panels a), c) and e).*

489 *Under all permutations, sands from upwind sources dominate; more detailed breakdown of the*

490 *sources is less unequivocal.*

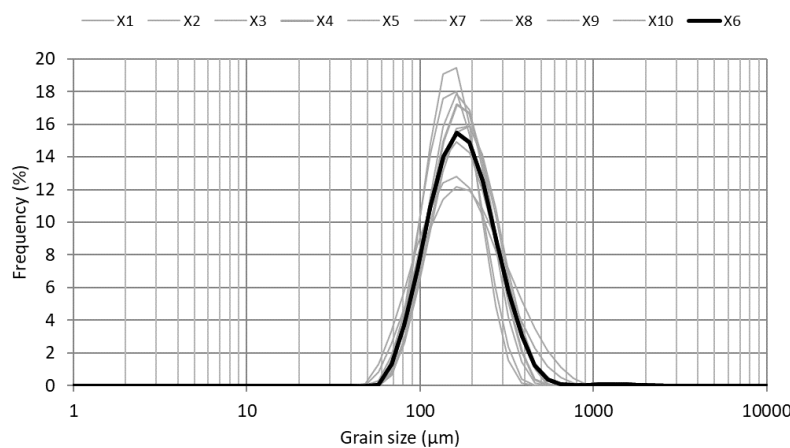
491 Results from the provenance analyses, using either methodology, and, broadly, under any of the
492 source configurations considered, suggest a dominant source component for the dune studied from
493 immediately up-wind sources; the upwind ill-defined sand ridge, and the merging dune to the
494 southwest. This is more consistent with the concept of along-dune sediment transport than wind-rift
495 models of dune formation, whereby the sands of the dune are derived from adjacent interdunes.
496 Some caveats must ride with this interpretation, under any of the suggested sediment
497 configurations, though. Firstly, this interpretation necessarily assumes that the sands – and typically
498 the interdunes are ~90% sand-sized (Figure 3) - found in the interdune today are the same as those
499 found in the interdune at the time of dune formation. Whilst no ages are available for this dune,
500 similar dunes from the Simpson are characterized by basal (i.e. emplacement) ages of 10^4 - 10^5 years
501 (Fujioka et al., 2009, Hollands et al., 2006, Nanson et al., 1992), and thus the formative timescales of
502 such landforms are long. Are the potential sources of dune sand today (i.e. interdunes vs. dunes) the
503 same as they were at the time of dune emplacement? This is, and must always be, a hypothetical
504 question; it is not possible to directly assess this. It should be noted that the sediment samples taken
505 – both source and target – are essentially surface samples, and we cannot *sensu stricto* conclude
506 that the same pathways would have been followed at the time of dune emplacement at this
507 location. The assays here address the question of recent sand transport most directly, and it is not
508 advisable to extrapolate necessarily to the timescale of tens of thousands of years.

509 Secondly, the question of similarity of the source and target samples must be addressed. It was
510 hypothesized that the most likely causes for the choice of tracers found to be the most suitable by
511 the stepwise DFA (that is, sodium, potassium and antimony for the two-source model) are most
512 likely driven by weathering of non-quartz minerals such as feldspars (which may well be found in
513 greater quantities in the finer-grained silts of the interdunes) and in resistant, heavy minerals found
514 as sand-sized grains. Given the differences observed in grain sizes, might the observed results be
515 driven not by aeolian sand transport, but by *in-situ* weathering of the interdunes? Some evidence
516 that this is not the case can be drawn from the outlying sample (X6) in the target group, which, of

517 the twenty target samples analysed, was the only one showing much clearer affinity with the
518 interdune samples than the upwind sources. If it were the case that the differences observed
519 between the possible sources are attributed largely to a size-fraction dependent cause, then it might
520 be expected that this is evident in the physical properties of sample X6 – it should be more similar in
521 texture to the interdunes, with an enhanced fine-grained component. However (Figure 14), this is
522 not evident from the physical characteristics of this sample; from this, it seems most likely that the
523 provenancing methodology is indeed identifying sediment transport-driven differences.

524

525



526

527 *Figure 14. Grain size properties for sample X6, alongside those of other samples from the target site*
528 *X. Although the provenance analysis identified X6 as being an outlying sample, and more likely*
529 *derived from the adjacent interdunes, it is physically indistinguishable from the well-sorted sands of*
530 *the other samples.*

531 4.2.2. Differing source configurations

532 The dominance of upwind sources is clear across all methods, and all source configurations tested
533 (Figure 13). Further interpreting the three- and four-source configurations, however, is harder, and
534 much more equivocal. This is likely due in part to the weaker performance of both models under

535 these configurations (Table 2 and Fig 12). Both MC and GLUE models, under the three-source
536 configuration, do suggest some additional information. The contribution from the merging dune for
537 both target sites is markedly greater than that of the immediate-upwind low sand ridge for both
538 target sites (X and Y), and both models are in agreement that this effect is more marked for the
539 northerly target site, Y (Figure 13). This could be seen as consistent with the idea of linear dunes as
540 preferential transport pathways in the landscape. In the case of the four-source model, however,
541 this result is no longer visible, and both upwind sources are attributed approximately equal
542 importance as contributions. Similarly, there is no clear differentiation between eastern and western
543 interdunes as the dominant source of the lesser lateral component of transport. Thus, whilst the
544 different configurations tested are unanimous in identifying a dominant role for the upwind sources,
545 further granularity in identifying sources is not possible from these findings.

546 *4.2.3. Results in context*

547 We interpret the results of this study as being consistent with a model favouring along-dune
548 sediment flux, and less supportive of 'wind-rift' models whereby dune sands are derived from
549 adjacent interdunes, and accretion is primarily vertical. How, then, can these findings be reconciled
550 with the findings of others (e.g. Craddock et al., 2015, Hollands et al., 2006) who have supported the
551 wind-rift/vertical accretion model? It is worth considering the very different methodologies that
552 have been employed to address the questions surrounding linear dune extension/wind-rift
553 formation. Craddock et al. (2015), for instance, used decadal-scale (8-year) field observation of
554 erosion pins, and differential GPS surveying. Others have used chronostratigraphies (e.g. Hollands et
555 al., 2006, Telfer, 2011) or stratigraphies derived from geophysical surveying (e.g. Bristow et al.,
556 2007b). Previous provenance studies have used geochemical and geochronological methods to
557 assess the role of long-distance sediment transport (e.g. Pell et al., 1997, Pell et al., 2000). Inherent
558 in these different methodologies are a vast range of timescales (from 10^0 years for field study – 10^9
559 years in the case of zircon U-Pb provenance analyses), and spatial scales (from 10^{-2} m scale accretion

560 in the case of field survey, to 10^3 - 10^4 m scale for some stratigraphic studies). The challenges in
561 reconciling such data are self-evident, and part of a wider narrative within the aeolian community
562 that has sometimes questioned the instructiveness of reductionist approaches (Livingstone et al.,
563 2007). A useful exercise may, thus, be to look for similarities, not difference, in the findings of this
564 study and the most recent study with apparently contradictory findings in this region; that of
565 Craddock et al. (2015).

566 Firstly, both studies seek to address the changes that have affected linear dunes of the Simpson
567 desert in the recent past – in the case of Craddock et al. (2015), over an eight-year period of
568 observation, and here by focusing on surficial sediment. Although it is not possible to directly assess
569 the timeframe of observation here, late Holocene ages are recorded at depths of ~1 m in the Tirari
570 and northern Strzelecki desert (Fitzsimmons et al., 2007, Telfer et al., 2017), as well as the western
571 Simpson (Nanson et al., 1995). For samples collected within the top 5 cm of the dune, it seems
572 reasonable to infer that timescales of > 100 years are likely for the sands in this study. Both studies
573 observe spatial scales on the order of 10^2 - 10^3 m, but, perhaps significantly, the dune chosen to for
574 study by Craddock et al. (2015) is located at a downwind termination, whereas this study focuses on
575 an upwind dune termination. Craddock et al. (2015) observed ~10 cm – 1 m of net accumulation on
576 most stakes, with some showing periodic exhumation towards the lower end of this range, but did
577 not see evidence of dune extension during this time in the form of progradation of the dune snout;
578 this was interpreted as dune growth by vertical accretion, which, over the timescale under
579 consideration, is clearly the case. Craddock et al. (2015) note that their findings are not necessarily
580 at odds with the millennial-scale chronostratigraphies of Telfer (2011), which were interpreted as
581 showing evidence both for elongation, and dune mobility without concurrent lengthening;
582 conclusions echoing those of Bristow et al.'s (2007b) geophysical surveys, which suggested that both
583 lengthening and vertical landform growth were possible at different times/places. Miller et al.
584 (2018), working on a linear dune whose origin is clearly tied to the adjacent Wolfe Creek meteor
585 impact crater by the deflection that the crater has imparted on the dune planform, were able to

586 estimate a minimum extension rate of ~ 3 km over ~ 120 ka, or of the order of 35 m ka^{-1} ; it is
587 unsurprising that studies working at observational timescales of ~ 10 years may not observe dune
588 extension.

589 The interdune areas surveyed by Craddock et al. (2015) experienced both net accumulation and
590 deflation of a few cm, with no clear spatial patterning. As such, there is no specific evidence here for
591 the source of the sand which, over their decadal-scale survey, contributed to vertical landform
592 growth; a condition which seems necessary for the wholesale adoption of the wind-rift model.
593 Whilst the work of Pell and colleagues on numerous Australian dunefields provides convincing
594 evidence for a lack of continental-scale aeolian sand transport fluxes (Pell et al., 1999, Pell et al.,
595 2000, Pell et al., 2001), there is again no mutual exclusivity with the findings of these studies, and
596 those suggested here. Pell et al. (1999, 2000, 2001) were considering the ultimate 'proto-source' of
597 the heavy mineral assemblages of dunes, and as such, constrained by U-Pb zircon dating, considering
598 timescales of 10^8 - 10^9 years. As there is evidence (Fujioka et al., 2009) that the Simpson dunes likely
599 have an early Pleistocene initiation age, such conclusions, whilst relevant to the degree to which
600 continental-scale wind transport has occurred, does not necessarily support the dunes sands as
601 being locally-derived over scales of $10^0 - 10^1$ km, as has sometimes been inferred (Hollands et al.,
602 2006). Here, we demonstrate evidence that the sands near the upwind snout of a linear dune are
603 predominantly derived, not from the adjacent interdunes as required by a pure wind-rift model, but
604 by downwind sediment transport, either from upwind interdune sediment sources, or by sediment
605 flux along a merging dune. Given local spatial differences in dune accumulation histories over even
606 the most local of scales (Telfer et al., 2017), we note that this does not preclude net vertical
607 accumulation of dunes occurring at certain places and times, or even that such sediment might not
608 periodically come from interdune sources.

609 In summary, there is now sufficient evidence from diverse sources that linear dunes can, at different
610 times and places, grow by extension and predominantly vertical growth at landform-scale; that they

611 can migrate laterally, and yet often do remain in the same place for 10^4 - 10^5 years; and that whilst we
612 cannot rule out predominantly lateral accretion of sediment at times, that they act as downwind
613 corridors of sediment flux, resulting in dunes which, at times, clearly grow by extension. Whilst such
614 statements may seem paradoxical, there is no reason that they cannot all be true, given sufficient
615 time and spatial timeframes, which both seem generously available for the formation of linear
616 dunefields.

617 *5. Conclusions*

618 We demonstrate here that sediment fingerprinting studies have the potential to elucidate transport
619 pathways at a scale relevant to understanding landform formation. Two different sediment
620 fingerprinting modeling frameworks (a Monte Carlo approach, and the GLUE methodology) provide
621 consistent estimates that the upwind sources, including a low sand ridge, and a merging dune, are
622 the most significant contributions for the sands of a linear dune in the central Simpson Desert,
623 compared to the adjacent interdunes. Both frameworks performed with greater success when
624 considering simpler configurations of possible sources, and metrics of model performance
625 (Goodness of Fit) suggest a high degree of confidence in the findings. The data imply greater
626 importance for along-dune sediment flux than deflation from the surrounding dune swales, and thus
627 do not provide supporting evidence for a pure 'wind-rift' model of dune formation. It is noted that as
628 such this does not preclude the possibility of primarily vertical accretion of linear dunes, especially at
629 a point-by-point basis, at certain points on dunes, at certain times. It does, however, provide a new
630 line of support for along-dune sand transport, which ultimately implies an extensional component to
631 linear dune development. Attempts to further dissect possible pathways by increasing the number
632 of possible pathways under investigation came only at the expense of reduced predictive power of
633 both models, and ultimately it was not possible to further isolate sources to any greater degree of
634 granularity with any reasonable degree of confidence.

635 As such, the findings suggest the potential for modern sediment provenancing studies to directly
636 address aeolian geomorphological questions of landform development. This applies beyond the
637 question of linear dune formation, and may apply to other bedforms and aeolian deposits such as
638 loess. Although not addressed here, the scope for the combination of such studies with
639 geochronological methods offer potentially valuable new means of adding long-term temporal
640 controls over studies of aeolian sediment pathways. Whilst this study deliberately targeted a 'typical'
641 linear dune in the central Simpson, it is also possible that careful locational choice (for instance, in
642 dunefields where sediment sources are characterized by more marked variability in local geology)
643 may have even more power in determining aeolian transport pathways.

644

645 *Acknowledgements*

646 This paper is dedicated to the memory of the late Russell Field, without whose logistic expertise the
647 fieldwork for this project would have never happened, and whose company made long drives and
648 long field days a positive pleasure.

649 We thank the Central Land Council and Traditional Land Owners for permission to undertake the
650 fieldwork in the Simpson Desert. Charlie Tier is thanked for assistance drafting some illustrations.

651 *References*

- 652 BEHROOZ, R. D., GHOLAMI, H., TELFER, M. W., JANSEN, J. D. & FATHABADI, A. 2019. Using GLUE to
653 pull apart the provenance of atmospheric dust. *Aeolian Research*, 37, 1-13.
- 654 BEVEN, K. & BINLEY, A. 1992. The future of distributed models: model calibration and uncertainty
655 prediction. *Hydrological processes*, 6, 279-298.
- 656 BOURNE, J. A., WOPFNER, H. & TWIDALE, C. R. 2019. Lateral stability of central Australian
657 longitudinal dunes. *Australian Geographer*, 50, 155-167.
- 658 BRISTOW, C. S., BAILEY, S. D. & LANCASTER, N. 2000. The sedimentary structure of linear sand dunes.
659 *Nature*, 406, 56-59.
- 660 BRISTOW, C. S., DULLER, G. A. T. & LANCASTER, N. 2007a. Age and dynamics of linear dunes in the
661 Namib Desert. *Geology*, 35, 555-558.
- 662 BRISTOW, C. S., JONES, B. G., NANSON, G. C., HOLLANDS, C., COLEMAN, M. & PRICE, D. M. 2007b.
663 GPR surveys of vegetated linear dune stratigraphy in central Australia: Evidence for linear
664 dune extension with vertical and lateral accretion. *Geological Society of America Special
665 Paper*, 432, 19-33.

666 BRISTOW, C. S., LANCASTER, N. & DULLER, G. A. T. 2005. Combining ground penetrating radar
667 surveys and optical dating to determine dune migration in Namibia. *Journal of the Geological*
668 *Society*, 162, 315-321.

669 COLLINS, A. L., WALLING, D. E. & LEEKS, G. J. L. 1997. Source type ascription for fluvial suspended
670 sediment based on a quantitative composite fingerprinting technique. *Catena*, 29, 1-27.

671 COLLINS, A. L., WALLING, D. E., WEBB, L. & KING, P. 2010. Apportioning catchment scale sediment
672 sources using a modified composite fingerprinting technique incorporating property
673 weightings and prior information. *Geoderma*, 155, 249-261.

674 COLLINS, A. L., ZHANG, Y. S., DUETHMANN, D., WALLING, D. E. & BLACK, K. S. 2013. Using a novel
675 tracing-tracking framework to source fine-grained sediment loss to watercourses at sub-
676 catchment scale. *Hydrological Processes*, 27, 959-974.

677 CRADDOCK, R. A., TOOTH, S., ZIMBELMAN, J. R., WILSON, S. A., MAXWELL, T. A. & KLING, C. 2015.
678 Temporal observations of a linear sand dune in the Simpson Desert, central Australia:
679 Testing models for dune formation on planetary surfaces. *Journal of Geophysical Research-*
680 *Planets*, 120, 1736-1750.

681 DU PONT, S. C., NARTEAU, C. & GAO, X. 2014. Two modes for dune orientation. *Geology*, 42, 743-
682 746.

683 FITZSIMMONS, K. E., MAGEE, J. W. & AMOS, K. J. 2009. Characterisation of aeolian sediments from
684 the Strzelecki and Tirari Deserts, Australia: Implications for reconstructing
685 palaeoenvironmental conditions. *Sedimentary Geology*, 218, 61-73.

686 FITZSIMMONS, K. E., RHODES, E. J., MAGEE, J. W. & BARROWS, T. T. 2007. The timing of linear dune
687 activity in the Strzelecki and Tirari Deserts, Australia. *Quaternary Science Reviews*, 26, 2598-
688 2616.

689 FOLK, R. L. 1971. LONGITUDINAL DUNES OF THE NORTHWESTERN EDGE OF THE SIMPSON DESERT,
690 NORTHERN TERRITORY, AUSTRALIA, 1. GEOMORPHOLOGY AND GRAIN SIZE RELATIONSHIPS.
691 *Sedimentology*, 16, 5-54.

692 FOX, J. F. & PAPANICOLAOU, A. N. 2008. An un-mixing model to study watershed erosion processes.
693 *Advances in Water Resources*, 31, 96-108.

694 FUJIOKA, T., CHAPPELL, J., FIFIELD, L. K. & RHODES, E. J. 2009. Australian desert dune fields initiated
695 with Pliocene-Pleistocene global climatic shift. *Geology*, 37, 51-54.

696 GHOLAMI, H., DOLAT KORDESTANI, M., LI, J., TELFER, M. W. & FATHABADI, A. 2019a. Diverse sources
697 of aeolian sediment revealed in an arid landscape in southeastern Iran using a modified
698 Bayesian un-mixing model. *Aeolian Research*, 41, 100547.

699 GHOLAMI, H., NAJAD, E. J. T., COLLINS, A. L. & FATHABADI, A. 2019b. Monte Carlo fingerprinting of
700 the terrestrial sources of different particle size fractions of coastal sediment deposits using
701 geochemical tracers: some lessons for the user community (vol 26, pg 13560, 2019).
702 *Environmental Science and Pollution Research*, 26, 23206-23206.

703 GHOLAMI, H., TELFER, M. W., BLAKE, W. H. & FATHABADI, A. 2017. Aeolian sediment fingerprinting
704 using a Bayesian mixing model. *Earth Surface Processes and Landforms*, 42, 2365-2376.

705 GREGORY, M. J., SCHAEFER, B. F., KEAYS, R. R. & WILDE, A. R. 2008. Rhenium–osmium systematics of
706 the Mount Isa copper orebody and the Eastern Creek Volcanics, Queensland, Australia:
707 implications for ore genesis. *Mineralium Deposita*, 43, 553.

708 HABIBI, S., GHOLAMI, H., FATHABADI, A. & JANSEN, J. D. 2019. Fingerprinting sources of reservoir
709 sediment via two modelling approaches. *Science of the Total Environment*, 663, 78-96.

710 HADDADCHI, A., OLLEY, J. & LACEBY, P. 2014. Accuracy of mixing models in predicting sediment
711 source contributions. *Science of the Total Environment*, 497, 139-152.

712 HADDADCHI, A., RYDER, D. S., EVRARD, O. & OLLEY, J. 2013. Sediment fingerprinting in fluvial
713 systems: review of tracers, sediment sources and mixing models. *International Journal of*
714 *Sediment Research*, 28, 560-578.

715 HESP, P., HYDE, R., HESP, V. & ZHENGYU, Q. 1989. Longitudinal dunes can move sideways. *Earth*
716 *Surface Processes And Landforms*, 14, 447-451.

717 HESSE, P. 2011. Sticky dunes in a wet desert: Formation, stabilisation and modification of the
718 Australian desert dunefields. *Geomorphology*, 134, 309-325.

719 HESSE, P. P. 2010. The Australian desert dunefields: formation and evolution in an old, flat, dry
720 continent. *Geological Society, London, Special Publications*, 346, 141.

721 HOLLANDS, C. B., NANSON, G. C., JONES, B. G., BRISTOW, C. S., PRICE, D. M. & PIETSCH, T. J. 2006.
722 Aeolian-fluvial interaction: evidence for Late Quaternary channel change and wind-rift linear
723 dune formation in the northwestern Simpson Desert, Australia. *Quaternary Science Reviews*,
724 25, 142-162.

725 KASPER-ZUBILLAGA, J. J., ZOLEZZI-RUÍZ, H., CARRANZA-EDWARDS, A., GIRÓN-GARCÍA, P.,
726 ORTIZ-ZAMORA, G. & PALMA, M. 2007. Sedimentological, modal analysis and geochemical
727 studies of desert and coastal dunes, Altar Desert, NW Mexico. *Earth Surface Processes and*
728 *Landforms: The Journal of the British Geomorphological Research Group*, 32, 489-508.

729 LACEBY, J. P. & OLLEY, J. 2015. An examination of geochemical modelling approaches to tracing
730 sediment sources incorporating distribution mixing and elemental correlations. *Hydrological*
731 *Processes*, 29, 1669-1685.

732 LANCASTER, N. 1982. Linear dunes. *Progress in Physical Geography: Earth and Environment*, 6, 475-
733 504.

734 LIVINGSTONE, I., WIGGS, G. F. S. & WEAVER, C. M. 2007. Geomorphology of desert sand dunes: A
735 review of recent progress. *Earth-Science Reviews*, 80, 239-257.

736 LUCAS, A., NARTEAU, C., RODRIGUEZ, S., ROZIER, O., CALLOT, Y., GARCIA, A. & DU PONT, S. C. 2015.
737 Sediment flux from the morphodynamics of elongating linear dunes. *Geology*, 43, 1027-
738 1030.

739 MABBUTT, J. A. & SULLIVAN, M. E. 1968. The formation of longitudinal dunes: evidence from the
740 Simpson Desert. *Australian Geographer*, 10, 483-487.

741 MAINGUET, M. M. & CALLOT, Y. 1978. L'Erg de Fachi-Bilma. *CNR S. Mem. et Doc. Nouv. Ser.*, 18, 1-
742 184.

743 MELTON, F. A. 1940. A tentative classification of sand dunes its application to dune history in the
744 southern High Plains. *The Journal of Geology*, 48, 113-174.

745 MILLER, G. H., MAGEE, J. W., FOGEL, M. L., WOOLLER, M. J., HESSE, P. P., SPOONER, N. A., JOHNSON,
746 B. J. & WALLIS, L. 2018. Wolfe Creek Crater: A continuous sediment fill in the Australian Arid
747 Zone records changes in monsoon strength through the Late Quaternary. *Quaternary*
748 *Science Reviews*, 199, 108-125.

749 MOTHA, J. A., WALLBRINK, P. J., HAIRSINE, P. B. & GRAYSON, R. B. 2003. Determining the sources of
750 suspended sediment in a forested catchment in southeastern Australia. *Water Resources*
751 *Research*, 39, 14.

752 MUHS, D. R. 2017. Evaluation of simple geochemical indicators of aeolian sand provenance: Late
753 Quaternary dune fields of North America revisited. *Quaternary Science Reviews*, 171, 260-
754 296.

755 NANSON, G. C., CHEN, X. Y. & PRICE, D. M. 1992. Lateral migration, thermoluminescence chronology
756 and color variation of longitudinal dunes near Birdsville in the Simpson Desert, Central
757 Australia. *Earth Surface Processes and Landforms*, 17, 807-819.

758 NANSON, G. C., CHEN, X. Y. & PRICE, D. M. 1995. Aeolian and fluvial evidence of changing climate
759 and wind patterns during the past 100 Ka in the Western Simpson Desert, Australia.
760 *Palaeogeography Palaeoclimatology Palaeoecology*, 113, 87-102.

761 NOSRATI, K., COLLINS, A. L. & MADANKAN, M. 2018. Fingerprinting sub-basin spatial sediment
762 sources using different multivariate statistical techniques and the Modified MixSIR model.
763 *Catena*, 164, 32-43.

764 PALAZÓN, L., LATORRE, B., GASPAS, L., BLAKE, W. H., SMITH, H. G. & NAVAS, A. 2015. Comparing
765 catchment sediment fingerprinting procedures using an auto-evaluation approach with
766 virtual sample mixtures. *Science of The Total Environment*, 532, 456-466.

- 767 PELL, S. D., CHIVAS, A. R. & WILLIAMS, I. S. 1999. Great Victoria Desert: development and sand
768 provenance. *Australian Journal of Earth Sciences*, 46, 289-299.
- 769 PELL, S. D., CHIVAS, A. R. & WILLIAMS, I. S. 2000. The Simpson, Strzelecki and Tirari Deserts:
770 development and sand provenance. *Sedimentary Geology*, 130, 107-130.
- 771 PELL, S. D., CHIVAS, A. R. & WILLIAMS, I. S. 2001. The Mallee Dunefield: development and sand
772 provenance. *Journal Of Arid Environments*, 48, 149-170.
- 773 PELL, S. D., WILLIAMS, I. S. & CHIVAS, A. R. 1997. The use of protolith zircon-age fingerprints in
774 determining the protosource areas for some Australian dune sands. *Sedimentary Geology*,
775 109, 233-260.
- 776 PULLEY, S. & COLLINS, A. L. 2018. Tracing catchment fine sediment sources using the new SIFT
777 (Sediment Fingerprinting Tool) open source software. *Science of the Total Environment*, 635,
778 838-858.
- 779 RUBIN, D. M. & HUNTER, R. E. 1985. Why deposits of longitudinal dunes are rarely recognized in the
780 geologic record. *Sedimentology*, 32, 147-157.
- 781 RUBIN, D. M. & RUBIN, A. M. 2013. Origin and lateral migration of linear dunes in the Qaidam Basin
782 of NW China revealed by dune sediments, internal structures, and optically stimulated
783 luminescence ages, with implications for linear dunes on Titan: Discussion. *Geological
784 Society of America Bulletin*, 125, 1943-1946.
- 785 RUBIN, D. M., TSOAR, H. & BLUMBERG, D. G. 2008. A second look at western Sinai seif dunes and
786 their lateral migration. *Geomorphology*, 93, 335-342.
- 787 TELFER, M. W. 2011. Growth by extension, and reworking, of a south-western Kalahari linear dune.
788 *Earth Surface Processes and Landforms*, 36, 1125-1135.
- 789 TELFER, M. W., HESSE, P. P., PEREZ-FERNANDEZ, M., BAILEY, R. M., BAJKAN, S. & LANCASTER, N.
790 2017. Morphodynamics, boundary conditions and pattern evolution within a vegetated
791 linear dunefield. *Geomorphology*, 290, 85-100.
- 792 TELFER, M. W. & THOMAS, D. S. G. 2007. Late Quaternary linear dune accumulation and
793 chronostratigraphy of the southwestern Kalahari: implications for aeolian palaeoclimatic
794 reconstructions and predictions of future dynamics. *Quaternary Science Reviews*, 26, 2617-
795 2630.
- 796 TSOAR, H., BLUMBERG, D. G. & STOLER, Y. 2004. Elongation and migration of sand dunes.
797 *Geomorphology*, 57, 293-302.
- 798 WALLING, D. E., WOODWARD, J. C. & NICHOLAS, A. P. 1993. A multi-parameter approach to
799 fingerprinting suspended-sediment sources. *IAHS publication*, 329-338.
- 800 WERNER, B. T. 1995. Eolian dunes: Computer simulations and attractor interpretations. *Geology*, 23,
801 1107-1110.
- 802 WILSON, I. G. 1971. Desert Sandflow Basins and a Model for the Development of Ergs. *The
803 Geographical Journal*, 137, 180-199.
- 804 WOPFNER, H. & TWIDALE, C. R. 2001. Australian desert dunes: wind rift or depositional origin? *Aust J
805 Earth Sci*, 48, 239-244.
- 806 ZHOU, H., CHANG, W. & ZHANG, L. 2016. Sediment sources in a small agricultural catchment: A
807 composite fingerprinting approach based on the selection of potential sources.
808 *Geomorphology*, 266, 11-19.
- 809 ZHOU, J., ZHU, Y. & YUAN, C. 2012. Origin and lateral migration of linear dunes in the Qaidam Basin
810 of NW China revealed by dune sediments, internal structures, and optically stimulated
811 luminescence ages, with implications for linear dunes on Titan. *Bulletin*, 124, 1147-1154.
- 812 ZHOU, J., ZHU, Y. & YUAN, C. 2013. Origin and lateral migration of linear dunes in the Qaidam Basin
813 of NW China revealed by dune sediments, internal structures, and optically stimulated
814 luminescence ages, with implications for linear dunes on Titan: Reply. *Geological Society of
815 America Bulletin*, 125, 1947-1949.

1 **Testing models of linear dune formation by provenance analysis with composite sediment**
2 **fingerprints**

3 M.W. Telfer¹, H. Gholami², P.P. Hesse³, A. Fisher¹, R. Hartley¹

4 1. SOGEES, University of Plymouth, Drake Circus, Plymouth, Devon, PL4 8AA, UK.

5 2. Department of Natural Resources Engineering, University of Hormozgan, Bandar-Abbas,
6 Hormozgan, Iran.

7 3. Department of Earth and Environmental Sciences, Macquarie University, North Ryde, NSW,
8 Australia

9 **Highlights**

- 10 • Two sediment fingerprinting methods used to determine sources of linear dune sand.
11 • Models consistent in supporting along-dune sediment flux.
12 • Little evidence of wind-rift mechanisms of linear dune formation.
13 • Sediment fingerprinting methods can address questions in aeolian geomorphology.

14

15 **Key words:** Linear dunes, Dune extension, Sediment provenance, Monte Carlo simulation.

16

17

18 **Abstract**

19 The formative mechanisms of linear (longitudinal) dunes and dunefields remain uncertain, and
20 multiple hypotheses have been proposed. A central debate is the degree to which dunes act as
21 along-dune sediment transport corridors, implying that dunes grow primarily by extension, or
22 whether they are comprised of locally-derived sands moved from adjacent interdunes (the 'wind-rift'
23 model). Sediment fingerprinting studies, with origins in fluvial science, have been shown to offer the
24 possibility to trace the provenance of aeolian sands, and thus elucidate transport pathways.

25 Two models (a Monte Carlo framework and a Generalized Likelihood Uncertainty Estimate
26 framework) are used here to provide quantitative estimates of the sediment sources that have
27 supplied a linear dune in the central Simpson Desert of central Australia. Four possible sources are
28 identified that may have supplied the dune; two adjacent interdunes, one upwind low ridge of sand,
29 and a merging upwind dune. Two sites near the dune's crest are used as the target and provided
30 twenty surface samples for analysis. Following geochemical assay, stepwise discriminant function
31 analysis identified optimum elemental sediment fingerprints for a variety of possible sediment
32 pathway configurations.

33 Results suggest that the sands of the dune are sourced predominantly from upwind dunes and sand
34 sources, and that likely contributions from neighbouring dune swales are typically <20%. As such,
35 wind-rift mechanisms of linear dune formation are not supported by these data. More complex
36 sediment pathway configurations (i.e., other than a binary approach: interdune vs. along-dune),
37 whilst confirming the initial findings, had reduced discriminatory power. Further separation of
38 source pathways (e.g., identifying the relative roles of different upwind sources) was not possible
39 with any confidence.

40 The findings suggest recent sediment accretion of a linear dune dominated by along-dune sand flux,
41 and thus support an extensional component for the development of such dunes. Whilst it is noted
42 that at a point-by-point basis this might not exclude accretion by vertical growth, as some have

43 observed, there is no clear support for a substantive contribution to the dune sands from adjacent
44 interdunes. Moreover, the use of contemporary sediment fingerprinting methods to question
45 hypotheses of aeolian geomorphology suggests that such methods have great potential for
46 addressing other terrestrial geomorphological questions where identifying sediment pathways can
47 provide vital insight.

48 **Testing models of linear dune formation by provenance analysis with composite sediment**
49 **fingerprints**

50 *1. Introduction*

51 Linear (longitudinal) dunes are probably the most abundant desert dune morphology, and yet the
52 mechanisms of formation and development of these dunes remains unclear. Multiple hypotheses,
53 probably working in conjunction, and perhaps at different temporal and spatial scales, have been
54 proposed for the formation of linear dunes. An equally diverse range of methods have been used to
55 investigate the problem, including field-based monitoring of dunes (Craddock et al., 2015), time
56 series of remotely sensed images (Lucas et al., 2015), geophysical surveys to reveal internal
57 sedimentary structures using radar (Bristow et al., 2000, Bristow et al., 2007a, Bristow et al., 2007b,
58 Hollands et al., 2006) and gravity surveys (Yang et al., 2011), chronostratigraphic surveys (Telfer,
59 2011), numerical modelling (Werner, 1995) and sediment provenance studies (Pell et al., 1999, Pell
60 et al., 2000, Pell et al., 2001).

61 A crucial, and as yet unresolved, aspect of the formation of linear dunes lies in the provenance of the
62 sands of which the dunes are formed. Amongst a diverse range of hypotheses for the formation of
63 these features, two models emerge that can be seen as end-members of a long-standing (Melton,
64 1940, Mabbutt and Sullivan, 1968) debate regarding the degree to which linear dunes are
65 extensional depositional features (Lucas et al., 2015, Telfer, 2011), perhaps serving as long-distance
66 transport corridors for wind-blown sand, or whether they primarily accumulate by sand derived
67 from adjacent interdunes (the so-called 'wind rift' model) (Wopfner and Twidale, 2001, Zhou et al.,
68 2012, Hollands et al., 2006).

69 Composite sediment 'fingerprinting' methods, originally developed for identifying the origin of
70 fluvial sediments (Collins et al., 1997, Walling et al., 1993), and since developing in sophistication
71 with Monte Carlo and/or Bayesian methodologies (Motha et al., 2003, Fox and Papanicolaou, 2008),
72 have demonstrated the ability of the methods to identify the sources of aeolian sediment. Although

73 the term 'fingerprinting' covers a diverse range of properties and methods, ranging from
74 geochemical analyses to radionuclides and magnetic properties, today most composite sediment
75 fingerprinting methods attempt to identify the optimal properties for discerning the relative
76 contributions of different sources of sediment to a target location, and use these to derive
77 quantitative estimates of contributions with robust estimates of uncertainty.

78 Gholami et al. (2017) demonstrated the potential of quantitative fingerprinting of aeolian dune
79 sands in elucidating aeolian transport pathways and revealing sediment sources, and Behrooz et al.
80 (2019) identified the provenance and pathways of aeolian dust affecting a region in eastern Iran.
81 Gholami et al. (2019a) revealed that both long ($10\text{-}10^2$ km) and short (1-10 km) transport had
82 contributed to the sands of a small erg, and highlighted the potentially complex nature of aeolian
83 transport pathways.

84 Here, quantitative composite fingerprinting methods are used to test hypotheses regarding the
85 source of sand in a linear dune in the central Simpson Desert, in central Australia. We use a sediment
86 source fingerprinting method within two different modelling frameworks including Generalized
87 Likelihood Uncertainty Estimate (GLUE) and Monte Carlo (MC) simulations to provide quantitative
88 estimates of the source of dune sands.

89 *1.1 Aims*

90 This study aims to identify local-scale source contributions to linear dunes to improve understanding
91 of their formative mechanisms. In order to do this, we address the following objectives:

92 1) Quantify contributions and uncertainties for different possible source contributions for aeolian
93 linear sand samples in the Simpson Desert, central Australia, with two different fingerprinting
94 approaches (GLUE and MC).

95 2) Assess the performance of both MC and GLUE models by goodness of fit (GOF) in the different
96 source -sink configurations to identify the most likely sediment transport pathways.

97

98

99 *1.2 Models of linear dune formation*

100 The debate about the formative mechanisms of linear dunes is exemplified in research in the
101 Australian dunefields, where debates have sometimes been most starkly expressed, but draw from
102 evidence worldwide; observational, experimental, modelled, and based upon field and laboratory
103 analyses. Several simultaneous debates emerged. Some suggested that linear dunes did not move
104 laterally (Bourne et al., 2019, Tsoar et al., 2004, Fujioka et al., 2009), but other evidence was more
105 equivocal (Nanson et al., 1992, Rubin et al., 2008, Rubin and Hunter, 1985), and some contradictory
106 (Hesp et al., 1989), until stratigraphic evidence from geophysical surveys proved convincingly that
107 linear dunes can indeed move laterally (Bristow et al., 2000, Bristow et al., 2005, Bristow et al.,
108 2007a). Others sought to reconcile the degree to which linear dunes grew by extension (Tsoar et al.,
109 2004), or by vertical accretion of locally-derived material (Pell et al., 1999, Pell et al., 2000, Zhou et
110 al., 2012). It is worth noting that, on a point-by-point basis, all accumulation is by necessity 'vertical',
111 and only on a landform scale does the term 'vertical accretion' really have any meaning. An
112 extension of the latter argument, taken to its most extreme, views linear dunes as erosional rather
113 than depositional features, an idea which has been vigorously contested (Zhou et al., 2013, Rubin
114 and Rubin, 2013). Whilst evidence for very long-distance (inter-basin, or at least $>10^3$ km) along-
115 dune transport is lacking on grounds of geochemical provenance (Pell et al., 1997, Pell et al., 1999,
116 Pell et al., 2000), and chronostratigraphic evidence over similar scales lacks support for a purely
117 extensional mode of linear dune formation (Hollands et al., 2006), there is decisive evidence of
118 smaller scale (<10 km) elongation from geophysical (Bristow et al., 2007b), chronostratigraphic
119 (Telfer, 2011, Miller et al., 2018) and observational evidence (Lucas et al., 2015) that linear dunes do
120 develop, at least in part, by extension. Taken to its extreme, the extensional argument has been
121 applied to streaming of sand over the entire north African deserts, including across mountain ranges,

122 for 10^2 - 10^3 km (Wilson, 1971, Mainguet and Callot, 1978). It is, perhaps, telling, that some papers
123 within this debate were characterized by distinctly didactic or binary titles; “Longitudinal dunes can
124 move sideways” (Hesp et al., 1989) or “Australian desert dunes; wind rift or depositional origin?”
125 (Wopfner and Twidale, 2001).

126 The concept that linear dunes may be better considered at the dunefield scale, rather than as
127 individual bedforms, was perhaps best highlighted by Werner’s classic simulations (1995), which
128 demonstrated that characteristic landscapes similar to those observed in the field could emerge
129 when forced with only large-scale forcing parameters, and that individual dune types could be
130 considered as attractors within the phase-space of a complex system. This work, followed by
131 numerous other modelling studies – though infrequently on linear dunes *per se* – suggested that
132 numerous processes may occur concurrently, and that lateral stability vs. sideways movement, or
133 vertical accretion vs. extension were not mutually exclusive conditions at the dunefield scale.
134 Moreover, new evidence emerged that long-standing theories regarding linear dune orientation may
135 not fully account for the range of alignments observed in the field, and that sediment supply also
136 plays a role in controlling dune orientation (Courrech du Pont et al., 2014). Field evidence also
137 revealed that even adjacent dunes may behave very differently in their accumulation record (Telfer
138 and Thomas, 2007, Telfer et al., 2017). This paper seeks to contribute to this discussion by applying
139 methodologies only recently applied to aeolian settings to address a specific question: at a local
140 scale, are dunes supplied with sediment more by downwind dune sources under a net time-
141 averaged wind regime, or adjacent interdunes fed by individual components of the wind regime?

142 *2. Materials and Methods*

143 *2.1 Experimental set-up*

144 To isolate the possible contributions of several different geomorphological settings, we identified a
145 dune where (a) clear adjacent interdunes are present on both sides, (b) the upwind termination of
146 the dune is clearly visible, where the dune ends in a low, ill-defined slipface-less sand ridge and (c)

147 where a downwind-joining junction also merges laterally into the target dune. This is shown
148 schematically in Fig. 1. Samples were collected from ten locations at each site, from the top 1-5 cm
149 of the sands.

150 [Approx location of Figure 1]

151 *Figure 1. Schematic of the sampling strategy for identifying source contributions to the target dune*
152 *crest. A and B represent upwind contributions, suggesting extensional mechanisms from the snout of*
153 *the dune and a merging upwind dune, respectively. C and D represent adjacent interdunes. X and Y*
154 *are the target locations on the main dune crestline.*

155 This structure facilitates the testing of different hypotheses, as different combinations of source area
156 definitions can be considered either together, or separately. Thus it is possible to simply consider all
157 potential upwind source samples as a single region (i.e., A+B), and all adjacent interdunes as a
158 possible source (i.e., C+D); or to isolate individual sources (for instance, consider A and B as distinct).

159

160 2.2 Field location

161 The Simpson Desert lies in the arid centre of the Australian continent (Fig. 2a), and the dunefield is
162 composed almost exclusively of linear dunes, occupying an area of around 180,000 km². Part of the
163 continent-scale whorl of linear dunes formed under anticyclonic influence, the dunes of the Simpson
164 are oriented approximately NNW-SSE (Fig. 2b and 2c), and experience a net southerly wind regime
165 (Hesse, 2010). The misalignment of many Australian dunefields with the modern wind regime has
166 long been noted (Hesse, 2011), and whilst some young (Holocene) dunes of the northwestern areas
167 of the Simpson align with current net sand-transporting winds (Hollands et al., 2006, Nanson et al.,
168 1995), Pleistocene dunes in the southern Simpson do indeed appear out of alignment (Nanson et al.,
169 1992). The dunefield is of considerable antiquity, with luminescence dating suggesting dunefield
170 initiation prior to ~590 ka (Fujioka et al., 2009). Ages for the emplacement of individual dunes

171 suggest that some dunes have been in their current location for at least ~100 ka (Nanson et al.,
172 1992, Nanson et al., 1995), and possibly substantially more (Fujioka et al., 2009).

173 [Approx location of Figure 2]

174

175 *Figure 2. The location of the dune studied, in the central Simpson Desert. (a) The location of the*
176 *Simpson dunefield, in the arid centre of Australia. (b) Sampling location set amongst hundreds of SSE-*
177 *NNW trending dunes. (c) More detailed inspection reveals the presence of both dune terminations*
178 *and some junctions and bifurcations within the patterning. (d) Local view of the study site, with main*
179 *dune crestlines highlighted with dashed lines, target dune samples (blues), possible upwind dune*
180 *crest sands (yellows) and possible adjacent interdune source sands (reds).*

181 Samples were taken from the top 1-5 cm of sand, and a .kmz file of the exact locations of samples is
182 provided along with the online version of this article.

183 2.2 Analytical Methods

184 2.2.1 Geochemical and Sedimentological Analysis

185 Geochemical assays were performed at the ISO9001-accredited Analytical Research Facility at the
186 University of Plymouth. Preparation involved fusion with lithium metaborate/tetraborate mixture,
187 and samples were fused at 950°C for 20 min in graphite crucibles. The fused mixture was dissolved
188 in 40 mL of 10% nitric acid and then diluted to 100 mL. A further ten-fold dilution with 10% nitric
189 acid was required prior to analysis. Analysis of the samples was undertaken using a Thermo Scientific
190 iCAP 7400 ICP-OES instrument and an X Series 2 ICP-MS instrument (both Thermo Scientific, UK). A
191 total suite of 30 elements was analyzed (V, Cr, Mn, Co, Ni, Cu, Mo, Sb, Ba, Ce, Pr, Nd, Sm, Eu, Gd, Tb,
192 Dy, Ho, Er, Tm, Yb and Lu by ICP-MS, and Na, Mg, Ca, Al, Si, Fe, K and Ti by ICP-OES).

193 Calibration standards were prepared by dilution of stock standards, either 10,000 or 100 mg/L and
194 were matrix matched to the samples with the appropriate amount of flux. The performance of each

195 instrument was checked against the manufacturers' specifications prior to use. A certified reference
196 material, BCR 667, and procedural blanks were prepared and analyzed in the same way as the
197 samples.

198 Particle size data was provided by laser granulometry using a Malvern Mastersizer 2000 with a
199 Hydro-G wet sample unit. Five subsamples of each sample were each analyzed five times, and mean
200 values taken. Ultrasonic dispersion @90% power was employed for 90 s prior to measurement, and
201 derivation of grain size fractions used Malvern's general analysis model (software v5.6), with
202 enhanced sensitivity and assuming irregular particle shape, a refractive index of 1.56 and light
203 absorption of 0.01 to 0.001.

204 *2.3 Sediment fingerprinting*

205 In this study, once an optimum fingerprint was identified for each permutation of source/target
206 sample, we used two different methods to quantify source contributions; a Monte Carlo framework
207 (Gholami et al., 2019b), and a Generalized Likelihood Uncertainty Estimate (GLUE; Beven and Binley,
208 1992, Behrooz et al., 2019) model. The use of fundamentally different procedures allows assessment
209 of the dependence of the results on the choice of methodology, as several studies have highlighted
210 potential dependence of model outputs on the choice of model employed (Palazón et al., 2015,
211 Laceby and Olley, 2015, Haddadchi et al., 2013, Haddadchi et al., 2014).

212 *2.3.1 Selection of the optimum composite fingerprints*

213 A two-stage statistical process including range test and stepwise discriminant function analysis (DFA)
214 was applied for selecting optimum composite fingerprints (Habibi et al., 2019). In the range test
215 (stage 1) (Collins et al., 2010), the maximum and minimum fingerprint values in the source and
216 sediment samples were used for identifying outliers. Tracers failing the range test were removed
217 from further analysis. In stage 2, a stepwise DFA based on the minimization of Wilk's Lambda was
218 used to select the optimum composite fingerprints (Gholami et al., 2017, Pulley and Collins, 2018).

219 Bi-plots, as a further test of the conservative behavior of the tracers included in the optimum
220 composite fingerprints, were used to assess similarities in the relationships between tracers in the
221 sediment and source samples (Habibi et al., 2019).

222 *2.3.2 Quantifying source contributions of aeolian sediment using a mixing model within a Monte* 223 *Carlo simulation framework*

224 A mixing model (Collins et al., 1997) within a Monte Carlo simulation framework (Gholami et al.,
225 2019b) was applied to quantify contributions of the potential sources in three different
226 permutations (A+B and C+D; A, B and C+D; A, B, C and D) to twenty aeolian sediment samples (X1-
227 X10 and Y1-Y10). The probability density functions (pdfs) (Collins et al., 2013) were constructed
228 based on the means and standard deviations of the optimum composite fingerprints for the
229 sediment and source samples, and these were repeatedly sampled during the Monte Carlo
230 simulations (Hughes et al., 2009). Using Latin Hypercube Sampling (LHS), 50,000 random samples
231 were drawn from the pdfs to permit Eq. (1) to be solved 50,000 times. The contributions of the two
232 potential sources were calculated by the model with 95% confidence limits. The mixing model is
233 defined as:

$$234 \quad f(X_j) = \sum_{i=1}^n \left((C_i - \sum_{j=1}^m P_j \cdot X_{j,i}) / C_i \right)^2 \quad (1)$$

235 where n is the number of fingerprint properties (here varying from 2 to 3), m is the number of
236 sediment sources (that is, between 2 and 4 depending on experimental set-up), C_i is the mean
237 concentration of fingerprint property (i) in the sediment sample, P_j is the relative contribution of
238 source (j) to the sediment sample, and $X_{j,i}$ is the mean concentration of fingerprint property (i) in
239 source (j). The mixing model must satisfy two boundary constraints: each source contribution must
240 be between 0 and 1, and all the contributions must sum to 1.

241

242 *2.3.3 Quantifying source contributions of aeolian sediment using the Generalized Likelihood* 243 *Uncertainty Estimate (GLUE) model*

244 The GLUE methodology followed Behrooz et al.'s (2019) implementation of the original
245 methodology proposed by Beven and Binley (1992) and used the same permutations of target and
246 source. This utilizes five steps, and is described in full in Behrooz et al. (2019), but to summarize:

247 1) Latin Hypercube Sampling (LHS) (Collins et al., 2013) is used to sample the parameter sets for
248 200,000 iterations, based upon a uniform distribution for all parameters, due to lack of *a priori*
249 knowledge. It is assumed all source contributions are non-negative, and sum to unity.

250 2) The Nash–Sutcliffe coefficient (ENS) is used as the likelihood function, and is defined thus:

251

$$252 \quad ENS = 1 - \frac{\sum(O_{obs} - O_{sim})}{\sum(O_{obs} - \hat{O}_{obs})} = 1 - \frac{\sigma_i^2}{\sigma_{obs}^2} \quad (2)$$

253

254 where \hat{O}_{obs} is the mean value of the observed tracer concentration, O_{sim} is the simulated tracer
255 concentration, O_{obs} is the observed tracer concentration, σ_i^2 is the error variance for the *i*th model
256 (i.e., the combination of the model and the *i*th parameter set) and σ_{obs}^2 is the variance of the
257 observations.

258 3) The sampled parameter sets from step 1 are fed into the mixing model (Eq. (2)), and the
259 likelihood function is calculated for each parameter set as:

260

$$261 \quad C_{Sediment} = C_{Sources} \times P \quad (3)$$

262

263 where P is an m-dimensional column vector of sources contribution (sampled parameter sets),
264 $C_{Sediment}$ is an n-dimensional column vector of element concentration in sediment sample and
265 $C_{Sources}$ is an n×m-dimensional matrix representing mean tracer concentration in sources (each row
266 represents mean tracer concentration in each source).

267 4) Each parameter set is defined as either behavioural or non-behavioural types, depending on
268 whether their likelihood function exceeds a threshold value (Zhou et al., 2016). Non-behavioural
269 parameter sets were discarded.

270 5) For each parameter set defined as behavioural, likelihood weights are rescaled such that they
271 sum to one, and a cumulative distribution derived for each parameter, to enable the derivation of
272 uncertainties.

273

274 *2.3.4 Assessing performance of the MC and GLUE models*

275 A Goodness of Fit (GOF) test (Manjoro et al, 2016; Gholami et al., 2019b) was applied to evaluate
276 performance of the two models - MC and GLUE. Although not without critics (Palazón et al., 2015),
277 the method is widely used to give an indication of the validity of model findings (e.g., Habibi et al.,
278 2019, Zhou et al., 2016), and here we use it relatively to assess differences of the proposed source
279 configurations. Goodness of Fit, using the terms of Eq. (1), is thus defined:

$$280 \quad GOF = (1 - [SQRT \sum_{i=1}^n [\frac{C_i - (\sum_{j=1}^m P_j \cdot X_{ji})}{C_i}]^2]) / n \quad (4)$$

281

282 3. Results

283 In Section 3.1, the basic geochemical and particle size data for the samples are presented. Section
284 3.2 discusses the development of the statistical fingerprinting methods from the geochemical data,
285 and lastly, Section 3.3 presents the outcomes of different combination of source-target
286 configurations and modelling frameworks.

287 *3.1 Geochemical and particle size results*

288 *3.1.1 Geochemical assays*

289 The results of the ICP analyses are presented in Table 1. The major species are, unsurprisingly,
 290 indicative of quartz-dominated sands (indeed the Si values seem low, with even 38% Si
 291 corresponding to an equivalent pure quartz concentration of 80%) with a more minor K-dominated
 292 feldspar component. This is broadly in line with the few other quantitative studies of sand mineral
 293 composition from central Australia, with Fitzsimmons et al. (2009) reporting 80-95% quartz and 1-
 294 15% feldspar for linear dunes of the Strzelecki to the southeast.

		Na	Mg	Ca	Al	Si	Fe	K
		(ppm)	(ppm)	(ppm)	(%)	(%)	(%)	(%)
	Min	832	229	148	0.78	17.65	0.45	0.55
	Mean	1072	304	273	1.08	26.71	0.59	0.70
Sediment	Max	1934	414	408	1.45	37.83	0.8	0.90
	Min	489	313	339	0.84	16.61	0.41	0.48
	Mean	1449	645	733	1.55	29.94	0.80	0.83
Source	Max	2358	1395	2835	2.24	37.37	1.47	1.00
Range test		P	F	F	F	F	P	P
		Ti	V	Cr	Mn	Co	Ni	Cu
		(ppm)	(ppm)	(ppm)	(ppm)	(ppb)	(ppm)	(ppm)
	Min	524	13.68	7.59	27.28	380	2.46	3.70
	Mean	769	19.56	10.58	37.09	613	4.87	5.93
Sediment	Max	1278	31.67	14.64	54.35	1168	11.78	8.68
	Min	637	14.90	7.90	29.60	407	2.70	4.32
	Mean	1122	31.55	14.57	56.19	1047	5.86	8.66
Source	Max	1697	53.50	21.70	132.70	2558	15.50	25.60
Range test		F	F	F	F	F	F	F
		Mo	Sb	Ba	Ce	Pr	Nd	Sm

		(ppb)	(ppb)	(ppb)	(ppm)	(ppm)	(ppm)	(ppb)
	Min	235	309	196	5.64	0.69	2.47	440
	Mean	496	596	251	8.89	1.05	3.75	676
Sediment	Max	1043	864	313	13.91	1.64	5.75	1042
	Min	192	87	153	6.52	0.87	2.98	558
	Mean	628	622	276	12.18	1.44	5.26	983
Source	Max	1984	1652	325	20.31	2.44	9.03	1674
Range test		P	P	P	F	F	F	F
		Eu	Gd	Tb	Dy	Ho	Er	Tm
		(ppb)	(ppb)	(ppb)	(ppb)	(ppb)	(ppb)	(ppb)
	Min	131	396	70	421	87	269	41
	Mean	185	638	110	612	129	397	66
Sediment	Max	251	985	163	933	206	672	117
	Min	128	566	84	474	97	305	48
	Mean	239	957	151	930	193	610	97
Source	Max	356	1515	237	1339	275	887	164
Range test		P	F	F	F	F	F	F
		Yb	Lu					
		(ppb)	(ppb)					
	Min	285	46					
	Mean	440	74					
Sediment	Max	729	128					
	Min	338	54					
	Mean	675	112					
Source	Max	1015	183					

Range test	F	F
------------	---	---

295

296 *Table 1: Minimum, mean and maximum concentrations of the geochemical tracers in all of the*
297 *source and target sediment samples. p and f indicate passing and failing the range test, respectively;*
298 *see Section 3.2.1.*

299

300 *3.1.2 Physical sediment characteristics*

301 [Approx location of Figure 3]

302 *Figure 3. Particle size distributions for all samples. Sand source samples (a) A and (b) B are*
303 *dominated by very fine – medium sands, with a marked positive tail towards coarse sands, and whilst*
304 *the interdune source samples (c) C and (d) D are also dominated by very fine – fine sands, here there*
305 *is a negative tail in the distribution, with up to 20% silt in some samples. The target dunes (e) X and*
306 *(f) Y are the best sorted, with little other than very fine – medium sand.*

307 All samples (Fig. 3) are characterized by a dominance of fine sands (31.5 – 64.6%; mean = 48.7%) and
308 very fine sands (11.5 – 50.7%; mean = 30.7%). In total, sands comprise 78.7 – 100% of the sediments
309 (mean = 96.0%), and silts comprise 0 – 20.4% (mean = 3.9%). The interdune samples (C and D; Figs.
310 3c and 11d), however, are typified by an increased silt component (averaging 10.2%, and up to
311 20.4% in one sample) compared to the source and target dune sands where silts average just 0.8%
312 and the maximum observed value is 3.6%. A slight positive tail exists for all candidate source
313 samples (A-D), with a minor component of coarser sands; this is in line with well-reported trends in
314 linear dunes/interdunes (e.g., Lancaster, 1982, Folk, 1971).

315

316 *3.2 Discrimination of sediment sources by range test and stepwise DFA*

317 *3.2.1 Range test*

318 Prior to applying a statistical procedure for selecting final fingerprints, a range test (Collins et al.,
319 2010; Gellis and Noe, 2013) was used to identify outliers and, therefore, significantly non-
320 conservative tracers for exclusion from further analysis. Here, the maximum and minimum tracer
321 concentrations in the source and sediment samples were used for identifying outliers (Table 1).
322 Tracers failing the range test (i.e., tracer concentrations measured for the target sediment samples
323 that fell outside the corresponding ranges of the source sample tracer concentrations) were
324 removed from further analysis (Gholami et al., 2019a, Gholami et al., 2019b, Nosrati et al., 2018).

325

326 Five tracer elements were identified as significant for the three models of sediment pathway, but
327 only one (Na) is consistent throughout. Antimony (Sb) and potassium (K) are identified as the other
328 most significant tracers for the two-source scenario, molybdenum (Mo) as the additional tracer in
329 the three-source model, and barium (Ba) in the four-source configuration. The likely sources of these
330 elements are considered in Section 4.1, though for now it is worth noting that whilst some mobility
331 of soluble Na salts cannot be ruled out, Sb, with a near-equal predictive power, is very insoluble in
332 the natural environment. It is likely significant that Na and Ba together have lower predictive power
333 in the case of the four-source scenario in the later interpretation of results, as indicated by the
334 markedly lower sum of the Wilk's Lambda; the implications of this are considered in Section 4.1. Fig.
335 4 shows scatterplots of the three- and four-source permutations of the stepwise DFA; the two-
336 source model yielded a single predictive discriminant function.

337

Step	Tracer selected	Wilk's Lambda	Sig
With two potential sources (A+B and C+D)			
1	Na	0.269	<0.001
2	Sb	0.230	<0.001
3	K	0.204	<0.001
With three potential sources (A, B and C+D)			
1	Na	0.262	<0.001
2	Mo	0.186	<0.001
With four potential sources (A, B, C and D)			
1	Na	0.13	<0.001
2	Ba	0.068	<0.001

339

340 *Table 2: Results of DFA for selecting optimum composite fingerprints with two (A+B and C+D),*
341 *three (A, B and C+D) and four (A, B, C and D) potential sources.*

342

343

344 [Approx location of Figure 1]

345 [Approx location of Figure 4]

346

347 *Figure 4: Scatterplots were constructed from first and second functions in the stepwise DFA, (a) with*
348 *three potential sources (A, B and C+D); and (b) with four potential sources (A, B, C and D). With two*
349 *potential sources (A+B and C+D), scatterplots are not applicable because there is a single*

350 *discrimination function. These functions correctly classified 97.4, 84.6 and 92.3% of source samples*
351 *for two, three and four potential sources, respectively.*

352

353 *3.2.2 Conservative behaviour of optimum composite fingerprints in the sediment and source samples*

354 Results from the bi-plot test are presented in Fig. 5. Plots wherein the source and sediment
355 samples do not fall in the same general space suggest non-conservative behaviour of the tracers in
356 question.

357

358 [Approx location of Figure 5]

359

360 *Figure 5: Bi-plots for all pairings of the geochemical tracers in the final composite signature,*
361 *measured on the source and target sediment samples: (a), (b) and (c) with two potential sources*
362 *(A+B and C+D), (d) with three potential sources (A, B and C+D) and (e) with four potential sources (A,*
363 *B, C and D).*

364

365 *3.3 Source contributions from different models and various sediment pathway configurations*

366 Three different source-target configurations are considered here, each with the two models
367 proposed; Monte Carlo modelling and the GLUE framework.

368

369 *3.3.1 Two-source configuration: upwind and adjacent sources (A+B; C+D)*

370 [Approx location of Figure 6]

371

372 *Figure 6: Monte Carlo simulation results for sand dune source contributions with 95% confidence*
373 *limits (with percentiles 2.5, 25, 50, 75 and 97.5). A+B and C+D indicate two potential sources for*
374 *aeolian sediment samples.*

375 The results of the two-source configuration from both models are encouragingly consistent (Figs. 6
376 and 7); both imply a system dominated by dune sands sourced from upwind locations (both the
377 upwind dune snout (A), and the merging dune (B)). By either assessment, 16 of the 20 samples are
378 clearly dominated (>70%) by sediments with affiliation to these sources, with X6 (most markedly),
379 Y2, Y6 and Y7 as notable exceptions. Both modelling approaches are consistent in the identification
380 of which samples share greater affinity with the two possible sources. GLUE estimates are typically
381 characterized by their smaller uncertainties.

382

383 [Approx location of Figure 7]

384

385 *Figure 7: GLUE results for sand dune source contributions with 95% confidence limits (with*
386 *percentiles 2.5, 25, 50, 75 and 97.5). A+B and C+D indicate two potential sources for aeolian*
387 *sediment samples.*

388

389 *3.3.2 Three-source configuration: dune snout, merging dune and adjacent sources (A; B; C+D)*

390 [Approx location of Figure 8]

391

392 *Figure 8: Monte Carlo simulation results for sand dune source contributions with 95% confidence*
393 *limits (with percentiles 2.5, 25, 50, 75 and 97.5). A, B and C+D indicate three potential sources for*
394 *aeolian sediment samples.*

395 [Approx location of Figure 9]

396 *Figure 9: GLUE results for sand dune source contributions with 95% confidence limits (with*
397 *percentiles 2.5, 25, 50, 75 and 97.5). A, B and C+D indicate three potential sources for aeolian*
398 *sediment samples.*

399 The three-source configuration (Figs. 8 and 9) offers much support for the two-source scenario, but
400 also offers further information. With both Monte Carlo and GLUE methodologies, source B – the
401 merging dune – is seen to dominate the likely source contributions. Extreme uncertainties –
402 especially for the Monte Carlo method - are undoubtedly wider, but interquartile ranges (indicated
403 by the blue box on the box-and-whisker plots of Figs. 7 and 8) are generally supportive of a
404 dominant source contribution coming specifically from the merging dune (source B), beyond that
405 contributed from the immediate upwind sand source (source A). Sample X6, especially, remains a
406 clear outlier to the general trend, with greater similarity to the interdune samples.

407

408 *3.3.4 Four-source configuration: dune snout, merging dune and eastern and western interdune*

409 [Approx location of Figure 10]

410

411 *Figure 10: Monte Carlo simulation results for sand dune source contributions with 95% confidence*
412 *limits (with percentiles 2.5, 25, 50, 75 and 97.5). A, B, C and D indicate four potential sources for*
413 *aeolian sediment samples.*

414 Results from the four-case scenario are more complex, and characterized, especially in the case of
415 Monte Carlo modelling (Fig. 10), by much greater uncertainties. Broad agreement remains that the
416 contribution of the upwind sources (that is, A and B) dominates that from the interdunes (that is, C
417 and D), but interquartile variance in the estimates typically exceeds 50% and, in some cases,
418 approaches 100% for the upwind sources. GLUE estimates (Fig. 11) also suggest greater importance

419 of the upwind sources, and has tighter constraints on uncertainty, but it is noticeable that variance is
420 greater under this scenario than others approached with the GLUE methodology (Figs. 7 and 9).
421 Despite the greater uncertainties, the relative contribution of the upwind sources (the immediately-
422 upwind low sand pile, and merging dune) is apparently somewhat reversed under this approach,
423 with a greater role indicated for the immediate upwind source. Both modelling approaches suggest a
424 slightly higher input from the western interdune, compared to the eastern side, with the notable
425 exception of sample X6, with a median contribution of around 50% total from the eastern interdune
426 and just 20-30% from the west.

427 [Approx location of Figure 11]

428

429 *Figure 11: GLUE results for sand dune source contributions with 95% confidence limits (with*
430 *percentiles 2.5, 25, 50, 75 and 97.5). A, B, C and D indicate four potential sources for aeolian*
431 *sediment samples.*

432 *4. Discussion*

433 The performance of the models is considered first, before considering the implications of the most
434 robust findings for models of linear dune formation.

435 *4.1 Sediment fingerprinting model performance*

436 The elements identified as the most significant tracers vary from abundant mineral-forming alkali
437 metals (Na and K), to much scarcer alkaline earth metals (Ba), transitional metals (Mo) and
438 metalloids (Sb); all are relatively enriched in the source sediments relative to the target dune sands.

439 The alkali metals are likely associated with weathering products from feldspars and micas, and Ba
440 may substitute for K in the lattice of these minerals (Kasper-Zubillaga et al., 2007). Indeed, K/Ba ratio
441 (along with K/Rb) in aeolian K-feldspar sands was one of the indices identified by Muhs (2017) as the
442 most promising for identifying the provenance of North American dune sands. Whilst the possibility

443 of a soluble sodium component in the sands cannot be entirely discounted, most of the other tracers
444 identified are insoluble in this environment, and Muhs also note the relative chemical resistance of
445 K-feldspars (orthoclase and microcline), and likely variance in K and Ba as being attributable to
446 source geology, and not weathering. The dominant heavy minerals in the study region belong to Pell
447 et al.'s (2000) 'northern Simpson' population, in which haematite, epidote and muscovite are
448 abundant, and garnet, tourmaline, monazite and zircon significant. Molybdenum is most often
449 associated with Cu ores, an observation consistent with Pell et al.'s (2000) attribution of the Mount
450 Isa block, which contains substantial Cu deposits (Gregory et al., 2008), as the 'proto-source' for the
451 sands of the Simpson. Antimony is also known from the Mount Isa block, associated with Pb
452 mineralization. In short, the tracers identified seem likely to reflect both primary mineralization and
453 long-distance transport of heavy minerals from proto-sources, and subsequent elemental
454 differences in sands and silts as a result of weathering.

455

456 Fig. 12 presents the results of the evaluation performance of the Monte Carlo simulation (MC)
457 and GLUE model by GOF for the different configurations of sources (two-, three- and four-sources).
458 Both MC and GLUE models have the highest performance associated with the simplest (two-source)
459 configuration, with GOF values for the majority of sand samples of >80 %. In the three-source model,
460 the GOF values for majority of the samples were 50-80%, and yet poorer performance for the four-
461 source model is indicated by GOF values typically <50%. Overall, based on the GOF values (for
462 majority of samples >80%) and scatterplot constructed stepwise DFA (97.4% source samples were
463 classified correctly), the two-sources grouping (A+B and C+D) is the best grouping for discriminating
464 sources of sand dunes in the Simpson Desert.

465

466 [Approx location of Figure 12]

467

468 *Figure 12. The Goodness of Fit (GOF) values for the MC and GLUE models for 20 sand dunes samples*
469 *(a) X1-X10, and (b) Y1-Y10. In the majority of cases, the two-source model is seen to provide the*
470 *strongest predictive power, followed by the three-source scenario and lastly the four-source*
471 *configuration.*

472

473 *4.2 Implications for linear dune formation*

474 *4.2.1 Interpreting the provenance analyses*

475 The results of the six provenancing assays are shown spatially in Fig. 13.

476 [Approx location of Figure 13]

477

478 *Figure 13. Spatial representation of the median estimate of source contributions under different*
479 *assumed sediment pathway configurations and using two different methodologies for the*
480 *fingerprinting. The simplest situation simply compares upwind and adjacent sources using (a) Monte*
481 *Carlo and (b) GLUE frameworks. (c) and (d) differentiate between the immediate upwind low sands*
482 *(A) and a flanking dune that merges with the target (B). (e) and (f) treat all four possible sources*
483 *individually. Pie charts are shaded according to the colours of the source labels in panels (a), (c) and*
484 *(e). Under all permutations, sands from upwind sources dominate; more detailed breakdown of the*
485 *sources is less unequivocal.*

486 Results from the provenance analyses, using either methodology, and, broadly, under any of the
487 source configurations considered, suggest a dominant source component for the dune studied from
488 immediately up-wind sources; the upwind ill-defined sand ridge, and the merging dune to the
489 southwest. These results are more consistent with the concept of along-dune sediment transport

490 than wind-rift models of dune formation, whereby the sands of the dune are derived from adjacent
491 interdunes. Some caveats must ride with this interpretation, under any of the suggested sediment
492 configurations, though. First, this interpretation necessarily assumes that the sands – and typically
493 the interdunes are ~90% sand-sized (Fig. 3) - found in the interdune today are the same as those
494 found in the interdune at the time of dune formation. Whilst no ages are available for this dune,
495 similar dunes from the Simpson are characterized by basal (i.e., emplacement) ages of 10^4 - 10^5 yr
496 (Fujioka et al., 2009, Hollands et al., 2006, Nanson et al., 1992), and thus the formative timescales of
497 such landforms are long. Are the potential sources of dune sand today (i.e., interdunes vs. dunes)
498 the same as they were at the time of dune emplacement? This is, and must always be, a hypothetical
499 question; it is not possible to directly assess this. It should be noted that the sediment samples taken
500 – both source and target – are essentially surface samples, and we cannot *sensu stricto* conclude
501 that the same pathways would have been followed at the time of dune emplacement at this
502 location. The assays here address the question of recent sand transport most directly, and it is not
503 advisable to extrapolate necessarily to the timescale of tens of thousands of years.

504 Second, the question of similarity of the source and target samples must be addressed. It was
505 hypothesized that the most likely causes for the choice of tracers found to be the most suitable by
506 the stepwise DFA (that is, Na, K and Sb for the two-source model) are most likely driven by
507 weathering of non-quartz minerals such as feldspars (which may well be found in greater quantities
508 in the finer-grained silts of the interdunes) and in resistant, heavy minerals found as sand-sized
509 grains. Given the differences observed in grain sizes, might the observed results be driven not by
510 aeolian sand transport, but by *in-situ* weathering of the interdunes? Some evidence that this is not
511 the case can be drawn from the outlying sample (X6) in the target group, which, of the twenty target
512 samples analysed, was the only one showing much clearer affinity with the interdune samples than
513 the upwind sources. If it were the case that the differences observed between the possible sources
514 are attributed largely to a size-fraction dependent cause, then it might be expected that this is
515 evident in the physical properties of sample X6 – it should be more similar in texture to the

516 interdunes, with an enhanced fine-grained component. However (Fig. 14), this is not evident from
517 the physical characteristics of this sample; from this, it seems most likely that the provenancing
518 methodology is indeed identifying sediment transport-driven differences.

519

520

521 [Approx location of Figure 14]

522

523 *Figure 14. Grain size properties for sample X6, alongside those of other samples from the target site*
524 *X. Although the provenance analysis identified X6 as being an outlying sample, and more likely*
525 *derived from the adjacent interdunes, it is physically indistinguishable from the well-sorted sands of*
526 *the other samples.*

527 4.2.2. Differing source configurations

528 The dominance of upwind sources is clear across all methods, and all source configurations tested
529 (Fig. 13). Further interpreting the three- and four-source configurations, however, is harder, and
530 much more equivocal, likely due in part to the weaker performance of both models under these
531 configurations (Table 2 and Fig 12). Both MC and GLUE models, under the three-source
532 configuration, do suggest some additional information. The contribution from the merging dune for
533 both target sites is markedly greater than that of the immediate-upwind low sand ridge for both
534 target sites (X and Y), and both models are in agreement that this effect is more marked for the
535 northerly target site, Y (Fig. 13). This observation could be seen as consistent with the idea of linear
536 dunes as preferential transport pathways in the landscape. In the case of the four-source model,
537 however, this result is no longer visible, and both upwind sources are attributed approximately
538 equal importance as contributions. Similarly, there is no clear differentiation between eastern and
539 western interdunes as the dominant source of the lesser lateral component of transport. Thus,

540 whilst the different configurations tested are unanimous in identifying a dominant role for the
541 upwind sources, further granularity in identifying sources is not possible from these findings.

542 *4.2.3. Results in context*

543 We interpret the results of this study as being consistent with a model favouring along-dune
544 sediment flux, and less supportive of 'wind-rift' models whereby dune sands are derived from
545 adjacent interdunes, and accretion is primarily vertical. How, then, can these findings be reconciled
546 with the findings of others (e.g., Craddock et al., 2015, Hollands et al., 2006) who have supported the
547 wind-rift/vertical accretion model? It is worth considering the very different methodologies that
548 have been employed to address the questions surrounding linear dune extension/wind-rift
549 formation. Craddock et al. (2015), for instance, used decadal-scale (8-yr) field observation of erosion
550 pins, and differential GPS surveying. Others have used chronostratigraphies (e.g., Hollands et al.,
551 2006, Telfer, 2011) or stratigraphies derived from geophysical surveying (e.g., Bristow et al., 2007b).
552 Previous provenance studies have used geochemical and geochronological methods to assess the
553 role of long-distance sediment transport (e.g., Pell et al., 1997, Pell et al., 2000). Inherent in these
554 different methodologies are a vast range of timescales (from 10^0 yr for field study – 10^9 yr in the case
555 of zircon U-Pb provenance analyses), and spatial scales (from 10^{-2} m scale accretion in the case of
556 field survey, to 10^3 - 10^4 m scale for some stratigraphic studies). The challenges in reconciling such
557 data are self-evident, and part of a wider narrative within the aeolian community that has
558 sometimes questioned the instructiveness of reductionist approaches (Livingstone et al., 2007). A
559 useful exercise may, thus, be to look for similarities, not differences, in the findings of this study and
560 the most recent study with apparently contradictory findings in this region; that of Craddock et al.
561 (2015).

562 First, both studies seek to address the changes that have affected linear dunes of the Simpson
563 Desert in the recent past – in the case of Craddock et al. (2015), over an eight-year period of
564 observation, and here by focusing on surficial sediment. Although it is not possible to directly assess

565 the timeframe of observation here, late Holocene ages are recorded at depths of ~1 m in the Tirari
566 and northern Strzelecki deserts (Fitzsimmons et al., 2007, Telfer et al., 2017), as well as the western
567 Simpson (Nanson et al., 1995). For samples collected within the top 5 cm of the dune, it seems
568 reasonable to infer that timescales of >100 yr are likely for the sands in this study. Both studies
569 observe spatial scales on the order of 10^2 - 10^3 m, but, perhaps significantly, the dune chosen to for
570 study by Craddock et al. (2015) is located at a downwind termination, whereas this study focuses on
571 an upwind dune termination. Craddock et al. (2015) observed ~10 cm – 1 m of net accumulation on
572 most stakes, with some showing periodic exhumation towards the lower end of this range, but did
573 not see evidence of dune extension during this time in the form of progradation of the dune snout;
574 this was interpreted as dune growth by vertical accretion, which, over the timescale under
575 consideration, is clearly the case. Craddock et al. (2015) note that their findings are not necessarily
576 at odds with the millennial-scale chronostratigraphies of Telfer (2011), which were interpreted as
577 showing evidence both for elongation and dune mobility without concurrent lengthening;
578 conclusions echoing those of Bristow et al.'s (2007b) geophysical surveys, which suggested that both
579 lengthening and vertical landform growth were possible at different times/places. Miller et al.
580 (2018), working on a linear dune whose origin is clearly tied to the adjacent Wolfe Creek meteor
581 impact crater by the deflection that the crater has imparted on the dune planform, were able to
582 estimate a minimum extension rate of ~3 km over ~ 120 ka, or of the order of 35 m ka^{-1} ; it is
583 unsurprising that studies working at observational timescales of ~10 yr may not observe dune
584 extension.

585 The interdune areas surveyed by Craddock et al. (2015) experienced both net accumulation and
586 deflation of a few centimetres, with no clear spatial patterning. As such, there is no specific evidence
587 here for the source of the sand that, over their decadal-scale survey, contributed to vertical
588 landform growth; a condition that seems necessary for the wholesale adoption of the wind-rift
589 model. Whilst the work of Pell and colleagues on numerous Australian dunefields provides
590 convincing evidence for a lack of continental-scale aeolian sand transport fluxes (Pell et al., 1999,

591 Pell et al., 2000, Pell et al., 2001), there is again no mutual exclusivity with the findings of these
592 studies, and those suggested here. Pell et al. (1999, 2000, 2001) were considering the ultimate
593 'proto-source' of the heavy mineral assemblages of dunes, and as such, constrained by U-Pb zircon
594 dating, considering timescales of 10^8 - 10^9 yr. Because of evidence (Fujioka et al., 2009) that the
595 Simpson dunes likely have an early Pleistocene initiation age, such conclusions, whilst relevant to the
596 degree to which continental-scale wind transport has occurred, do not necessarily support the dune
597 sands as being locally-derived over scales of 10^0 – 10^1 km, as has sometimes been inferred (Hollands
598 et al., 2006). Here, we demonstrate evidence that the sands near the upwind snout of a linear dune
599 are predominantly derived, not from the adjacent interdunes as required by a pure wind-rift model,
600 but by downwind sediment transport, either from upwind interdune sediment sources, or by
601 sediment flux along a merging dune. Given local spatial differences in dune accumulation histories
602 over even the most local of scales (Telfer et al., 2017), we note that this does not preclude net
603 vertical accumulation of dunes occurring at certain places and times, or even that such sediment
604 might not periodically come from interdune sources.

605 In summary, sufficient evidence now exists from diverse sources that linear dunes can, at different
606 times and places, grow by extension and predominantly vertical growth at landform-scale; that they
607 can migrate laterally, and yet often do remain in the same place for 10^4 - 10^5 yr; and that whilst we
608 cannot rule out predominantly lateral accretion of sediment at times, that they act as downwind
609 corridors of sediment flux, resulting in dunes that, at times, clearly grow by extension. Whilst such
610 statements may seem paradoxical, there is no reason that they cannot all be true, given sufficient
611 time and spatial timeframes, which both seem generously available for the formation of linear
612 dunefields.

613 *5. Conclusions*

614 We demonstrate here that sediment fingerprinting studies have the potential to elucidate transport
615 pathways at a scale relevant to understanding landform formation. Two different sediment

616 fingerprinting modeling frameworks (a Monte Carlo approach, and the GLUE methodology) provide
617 consistent estimates that the upwind sources, including a low sand ridge and a merging dune, are
618 the most significant contributions for the sands of a linear dune in the central Simpson Desert,
619 compared to the adjacent interdunes. Both frameworks performed with greater success when
620 considering simpler configurations of possible sources, and metrics of model performance
621 (Goodness of Fit) suggest a high degree of confidence in the findings. The data imply greater
622 importance for along-dune sediment flux than deflation from the surrounding dune swales, and thus
623 do not provide supporting evidence for a pure 'wind-rift' model of dune formation. We note that
624 this does not preclude the possibility of primarily vertical accretion of linear dunes, especially at a
625 point-by-point basis, at certain points and times on dunes. It does, however, provide a new line of
626 support for along-dune sand transport, which ultimately implies an extensional component to linear
627 dune development. Attempts to further dissect possible pathways by increasing the number of
628 possible pathways under investigation came only at the expense of reduced predictive power of
629 both models, and ultimately it was not possible to further isolate sources to any greater degree of
630 granularity with any reasonable degree of confidence.

631 As such, the findings suggest the potential for modern sediment provenance studies to directly
632 address aeolian geomorphological questions of landform development. This result applies beyond
633 the question of linear dune formation, and may apply to other bedforms and aeolian deposits such
634 as loess. Although not addressed here, the scope for the combination of such studies with
635 geochronological methods offer potentially valuable new means of adding long-term temporal
636 controls over studies of aeolian sediment pathways. Whilst this study deliberately targeted a 'typical'
637 linear dune in the central Simpson, it is also possible that careful locational choice (for instance, in
638 dunefields where sediment sources are characterized by more marked variability in local geology)
639 may have even more power in determining aeolian transport pathways.

640

641 *Acknowledgements*

642 This paper is dedicated to the memory of the late Russell Field, without whose logistic expertise the
643 fieldwork for this project would have never happened, and whose company made long drives and
644 long field days a positive pleasure.

645 We thank the Central Land Council and Traditional Land Owners for permission to undertake the
646 fieldwork in the Simpson Desert. Charlie Tier is thanked for assistance drafting some illustrations.

647 *References*

- 648 BEHROOZ, R. D., GHOLAMI, H., TELFER, M. W., JANSEN, J. D. & FATHABADI, A. 2019. Using GLUE to
649 pull apart the provenance of atmospheric dust. *Aeolian Research*, 37, 1-13.
- 650 BEVEN, K. & BINLEY, A. 1992. The future of distributed models: model calibration and uncertainty
651 prediction. *Hydrological processes*, 6, 279-298.
- 652 BOURNE, J. A., WOPFNER, H. & TWIDALE, C. R. 2019. Lateral stability of central Australian
653 longitudinal dunes. *Australian Geographer*, 50, 155-167.
- 654 BRISTOW, C. S., BAILEY, S. D. & LANCASTER, N. 2000. The sedimentary structure of linear sand dunes.
655 *Nature*, 406, 56-59.
- 656 BRISTOW, C. S., DULLER, G. A. T. & LANCASTER, N. 2007a. Age and dynamics of linear dunes in the
657 Namib Desert. *Geology*, 35, 555-558.
- 658 BRISTOW, C. S., JONES, B. G., NANSON, G. C., HOLLANDS, C., COLEMAN, M. & PRICE, D. M. 2007b.
659 GPR surveys of vegetated linear dune stratigraphy in central Australia: Evidence for linear
660 dune extension with vertical and lateral accretion. *Geological Society of America Special
661 Paper*, 432, 19-33.
- 662 BRISTOW, C. S., LANCASTER, N. & DULLER, G. A. T. 2005. Combining ground penetrating radar
663 surveys and optical dating to determine dune migration in Namibia. *Journal of the Geological
664 Society*, 162, 315-321.
- 665 COLLINS, A. L., WALLING, D. E. & LEEKS, G. J. L. 1997. Source type ascription for fluvial suspended
666 sediment based on a quantitative composite fingerprinting technique. *Catena*, 29, 1-27.
- 667 COLLINS, A. L., WALLING, D. E., WEBB, L. & KING, P. 2010. Apportioning catchment scale sediment
668 sources using a modified composite fingerprinting technique incorporating property
669 weightings and prior information. *Geoderma*, 155, 249-261.
- 670 COLLINS, A. L., ZHANG, Y. S., DUETHMANN, D., WALLING, D. E. & BLACK, K. S. 2013. Using a novel
671 tracing-tracking framework to source fine-grained sediment loss to watercourses at sub-
672 catchment scale. *Hydrological Processes*, 27, 959-974.
- 673 CRADDOCK, R. A., TOOTH, S., ZIMBELMAN, J. R., WILSON, S. A., MAXWELL, T. A. & KLING, C. 2015.
674 Temporal observations of a linear sand dune in the Simpson Desert, central Australia:
675 Testing models for dune formation on planetary surfaces. *Journal of Geophysical Research-
676 Planets*, 120, 1736-1750.
- 677 DU PONT, S. C., NARTEAU, C. & GAO, X. 2014. Two modes for dune orientation. *Geology*, 42, 743-
678 746.
- 679 FITZSIMMONS, K. E., MAGEE, J. W. & AMOS, K. J. 2009. Characterisation of aeolian sediments from
680 the Strzelecki and Tirari Deserts, Australia: Implications for reconstructing
681 palaeoenvironmental conditions. *Sedimentary Geology*, 218, 61-73.

- 682 FITZSIMMONS, K. E., RHODES, E. J., MAGEE, J. W. & BARROWS, T. T. 2007. The timing of linear dune
683 activity in the Strzelecki and Tirari Deserts, Australia. *Quaternary Science Reviews*, 26, 2598-
684 2616.
- 685 FOLK, R. L. 1971. LONGITUDINAL DUNES OF THE NORTHWESTERN EDGE OF THE SIMPSON DESERT,
686 NORTHERN TERRITORY, AUSTRALIA, 1. GEOMORPHOLOGY AND GRAIN SIZE RELATIONSHIPS.
687 *Sedimentology*, 16, 5-54.
- 688 FOX, J. F. & PAPANICOLAOU, A. N. 2008. An un-mixing model to study watershed erosion processes.
689 *Advances in Water Resources*, 31, 96-108.
- 690 FUJIOKA, T., CHAPPELL, J., FIFIELD, L. K. & RHODES, E. J. 2009. Australian desert dune fields initiated
691 with Pliocene-Pleistocene global climatic shift. *Geology*, 37, 51-54.
- 692 GHOLAMI, H., DOLAT KORDESTANI, M., LI, J., TELFER, M. W. & FATHABADI, A. 2019a. Diverse sources
693 of aeolian sediment revealed in an arid landscape in southeastern Iran using a modified
694 Bayesian un-mixing model. *Aeolian Research*, 41, 100547.
- 695 GHOLAMI, H., NAJAD, E. J. T., COLLINS, A. L. & FATHABADI, A. 2019b. Monte Carlo fingerprinting of
696 the terrestrial sources of different particle size fractions of coastal sediment deposits using
697 geochemical tracers: some lessons for the user community (vol 26, pg 13560, 2019).
698 *Environmental Science and Pollution Research*, 26, 23206-23206.
- 699 GHOLAMI, H., TELFER, M. W., BLAKE, W. H. & FATHABADI, A. 2017. Aeolian sediment fingerprinting
700 using a Bayesian mixing model. *Earth Surface Processes and Landforms*, 42, 2365-2376.
- 701 GREGORY, M. J., SCHAEFER, B. F., KEAYS, R. R. & WILDE, A. R. 2008. Rhenium–osmium systematics of
702 the Mount Isa copper orebody and the Eastern Creek Volcanics, Queensland, Australia:
703 implications for ore genesis. *Mineralium Deposita*, 43, 553.
- 704 HABIBI, S., GHOLAMI, H., FATHABADI, A. & JANSEN, J. D. 2019. Fingerprinting sources of reservoir
705 sediment via two modelling approaches. *Science of the Total Environment*, 663, 78-96.
- 706 HADDADCHI, A., OLLEY, J. & LACEBY, P. 2014. Accuracy of mixing models in predicting sediment
707 source contributions. *Science of the Total Environment*, 497, 139-152.
- 708 HADDADCHI, A., RYDER, D. S., EVRARD, O. & OLLEY, J. 2013. Sediment fingerprinting in fluvial
709 systems: review of tracers, sediment sources and mixing models. *International Journal of*
710 *Sediment Research*, 28, 560-578.
- 711 HESP, P., HYDE, R., HESP, V. & ZHENGYU, Q. 1989. Longitudinal dunes can move sideways. *Earth*
712 *Surface Processes And Landforms*, 14, 447-451.
- 713 HESSE, P. 2011. Sticky dunes in a wet desert: Formation, stabilisation and modification of the
714 Australian desert dunefields. *Geomorphology*, 134, 309-325.
- 715 HESSE, P. P. 2010. The Australian desert dunefields: formation and evolution in an old, flat, dry
716 continent. *Geological Society, London, Special Publications*, 346, 141.
- 717 HOLLANDS, C. B., NANSON, G. C., JONES, B. G., BRISTOW, C. S., PRICE, D. M. & PIETSCH, T. J. 2006.
718 Aeolian-fluvial interaction: evidence for Late Quaternary channel change and wind-rift linear
719 dune formation in the northwestern Simpson Desert, Australia. *Quaternary Science Reviews*,
720 25, 142-162.
- 721 KASPER-ZUBILLAGA, J. J., ZOLEZZI-RUÍZ, H., CARRANZA-EDWARDS, A., GIRÓN-GARCÍA, P.,
722 ORTIZ-ZAMORA, G. & PALMA, M. 2007. Sedimentological, modal analysis and geochemical
723 studies of desert and coastal dunes, Altar Desert, NW Mexico. *Earth Surface Processes and*
724 *Landforms: The Journal of the British Geomorphological Research Group*, 32, 489-508.
- 725 LACEBY, J. P. & OLLEY, J. 2015. An examination of geochemical modelling approaches to tracing
726 sediment sources incorporating distribution mixing and elemental correlations. *Hydrological*
727 *Processes*, 29, 1669-1685.
- 728 LANCASTER, N. 1982. Linear dunes. *Progress in Physical Geography: Earth and Environment*, 6, 475-
729 504.
- 730 LIVINGSTONE, I., WIGGS, G. F. S. & WEAVER, C. M. 2007. Geomorphology of desert sand dunes: A
731 review of recent progress. *Earth-Science Reviews*, 80, 239-257.

732 LUCAS, A., NARTEAU, C., RODRIGUEZ, S., ROZIER, O., CALLOT, Y., GARCIA, A. & DU PONT, S. C. 2015.
733 Sediment flux from the morphodynamics of elongating linear dunes. *Geology*, 43, 1027-
734 1030.

735 MABBUTT, J. A. & SULLIVAN, M. E. 1968. The formation of longitudinal dunes: evidence from the
736 Simpson Desert. *Australian Geographer*, 10, 483-487.

737 MAINGUET, M. M. & CALLOT, Y. 1978. L'Erg de Fachi-Bilma. *CNR S. Mem. et Doc, Nouv. Ser.*, 18, 1-
738 184.

739 MELTON, F. A. 1940. A tentative classification of sand dunes its application to dune history in the
740 southern High Plains. *The Journal of Geology*, 48, 113-174.

741 MILLER, G. H., MAGEE, J. W., FOGEL, M. L., WOOLLER, M. J., HESSE, P. P., SPOONER, N. A., JOHNSON,
742 B. J. & WALLIS, L. 2018. Wolfe Creek Crater: A continuous sediment fill in the Australian Arid
743 Zone records changes in monsoon strength through the Late Quaternary. *Quaternary
744 Science Reviews*, 199, 108-125.

745 MOTHA, J. A., WALLBRINK, P. J., HAIRSINE, P. B. & GRAYSON, R. B. 2003. Determining the sources of
746 suspended sediment in a forested catchment in southeastern Australia. *Water Resources
747 Research*, 39, 14.

748 MUHS, D. R. 2017. Evaluation of simple geochemical indicators of aeolian sand provenance: Late
749 Quaternary dune fields of North America revisited. *Quaternary Science Reviews*, 171, 260-
750 296.

751 NANSON, G. C., CHEN, X. Y. & PRICE, D. M. 1992. Lateral migration, thermoluminescence chronology
752 and color variation of longitudinal dunes near Birdsville in the Simpson Desert, Central
753 Australia. *Earth Surface Processes and Landforms*, 17, 807-819.

754 NANSON, G. C., CHEN, X. Y. & PRICE, D. M. 1995. Aeolian and fluvial evidence of changing climate
755 and wind patterns during the past 100 Ka in the Western Simpson Desert, Australia.
756 *Palaeogeography Palaeoclimatology Palaeoecology*, 113, 87-102.

757 NOSRATI, K., COLLINS, A. L. & MADANKAN, M. 2018. Fingerprinting sub-basin spatial sediment
758 sources using different multivariate statistical techniques and the Modified MixSIR model.
759 *Catena*, 164, 32-43.

760 PALAZÓN, L., LATORRE, B., GASPARD, L., BLAKE, W. H., SMITH, H. G. & NAVAS, A. 2015. Comparing
761 catchment sediment fingerprinting procedures using an auto-evaluation approach with
762 virtual sample mixtures. *Science of The Total Environment*, 532, 456-466.

763 PELL, S. D., CHIVAS, A. R. & WILLIAMS, I. S. 1999. Great Victoria Desert: development and sand
764 provenance. *Australian Journal of Earth Sciences*, 46, 289-299.

765 PELL, S. D., CHIVAS, A. R. & WILLIAMS, I. S. 2000. The Simpson, Strzelecki and Tirari Deserts:
766 development and sand provenance. *Sedimentary Geology*, 130, 107-130.

767 PELL, S. D., CHIVAS, A. R. & WILLIAMS, I. S. 2001. The Mallee Dunefield: development and sand
768 provenance. *Journal Of Arid Environments*, 48, 149-170.

769 PELL, S. D., WILLIAMS, I. S. & CHIVAS, A. R. 1997. The use of protolith zircon-age fingerprints in
770 determining the protosource areas for some Australian dune sands. *Sedimentary Geology*,
771 109, 233-260.

772 PULLEY, S. & COLLINS, A. L. 2018. Tracing catchment fine sediment sources using the new SIFT
773 (Sediment Fingerprinting Tool) open source software. *Science of the Total Environment*, 635,
774 838-858.

775 RUBIN, D. M. & HUNTER, R. E. 1985. Why deposits of longitudinal dunes are rarely recognized in the
776 geologic record. *Sedimentology*, 32, 147-157.

777 RUBIN, D. M. & RUBIN, A. M. 2013. Origin and lateral migration of linear dunes in the Qaidam Basin
778 of NW China revealed by dune sediments, internal structures, and optically stimulated
779 luminescence ages, with implications for linear dunes on Titan: Discussion. *Geological
780 Society of America Bulletin*, 125, 1943-1946.

781 RUBIN, D. M., TSOAR, H. & BLUMBERG, D. G. 2008. A second look at western Sinai seif dunes and
782 their lateral migration. *Geomorphology*, 93, 335-342.

783 TELFER, M. W. 2011. Growth by extension, and reworking, of a south-western Kalahari linear dune.
784 *Earth Surface Processes and Landforms*, 36, 1125-1135.

785 TELFER, M. W., HESSE, P. P., PEREZ-FERNANDEZ, M., BAILEY, R. M., BAJKAN, S. & LANCASTER, N.
786 2017. Morphodynamics, boundary conditions and pattern evolution within a vegetated
787 linear dunefield. *Geomorphology*, 290, 85-100.

788 TELFER, M. W. & THOMAS, D. S. G. 2007. Late Quaternary linear dune accumulation and
789 chronostratigraphy of the southwestern Kalahari: implications for aeolian palaeoclimatic
790 reconstructions and predictions of future dynamics. *Quaternary Science Reviews*, 26, 2617-
791 2630.

792 TSOAR, H., BLUMBERG, D. G. & STOLER, Y. 2004. Elongation and migration of sand dunes.
793 *Geomorphology*, 57, 293-302.

794 WALLING, D. E., WOODWARD, J. C. & NICHOLAS, A. P. 1993. A multi-parameter approach to
795 fingerprinting suspended-sediment sources. *IAHS publication*, 329-338.

796 WERNER, B. T. 1995. Eolian dunes: Computer simulations and attractor interpretations. *Geology*, 23,
797 1107-1110.

798 WILSON, I. G. 1971. Desert Sandflow Basins and a Model for the Development of Ergs. *The*
799 *Geographical Journal*, 137, 180-199.

800 WOPFNER, H. & TWIDALE, C. R. 2001. Australian desert dunes: wind rift or depositional origin? *Aust J*
801 *Earth Sci*, 48, 239-244.

802 ZHOU, H., CHANG, W. & ZHANG, L. 2016. Sediment sources in a small agricultural catchment: A
803 composite fingerprinting approach based on the selection of potential sources.
804 *Geomorphology*, 266, 11-19.

805 ZHOU, J., ZHU, Y. & YUAN, C. 2012. Origin and lateral migration of linear dunes in the Qaidam Basin
806 of NW China revealed by dune sediments, internal structures, and optically stimulated
807 luminescence ages, with implications for linear dunes on Titan. *Bulletin*, 124, 1147-1154.

808 ZHOU, J., ZHU, Y. & YUAN, C. 2013. Origin and lateral migration of linear dunes in the Qaidam Basin
809 of NW China revealed by dune sediments, internal structures, and optically stimulated
810 luminescence ages, with implications for linear dunes on Titan: Reply. *Geological Society of*
811 *America Bulletin*, 125, 1947-1949.

812

Figure 1 (Color)

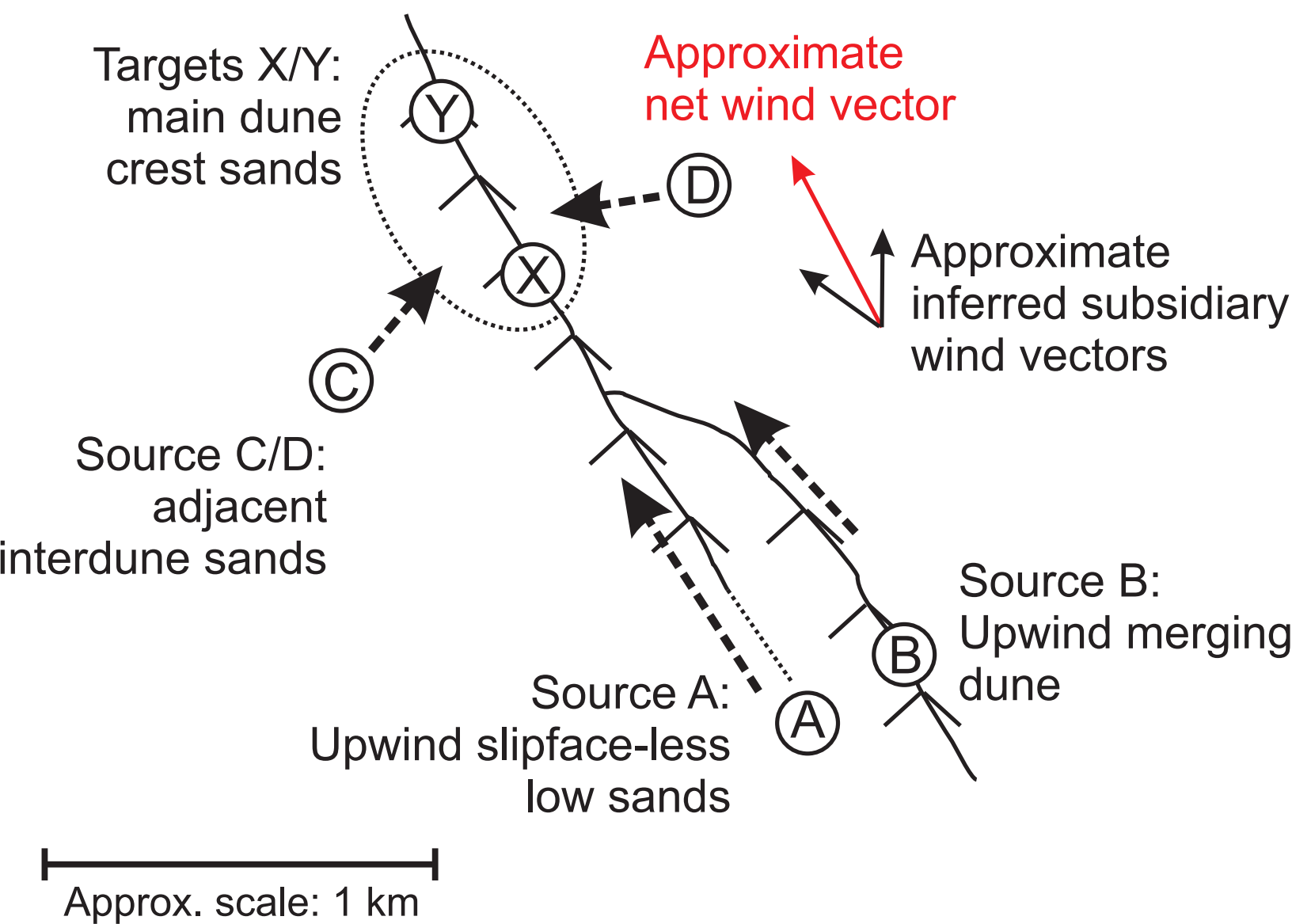


Figure 2 (Color)
[Click here to download high resolution image](#)

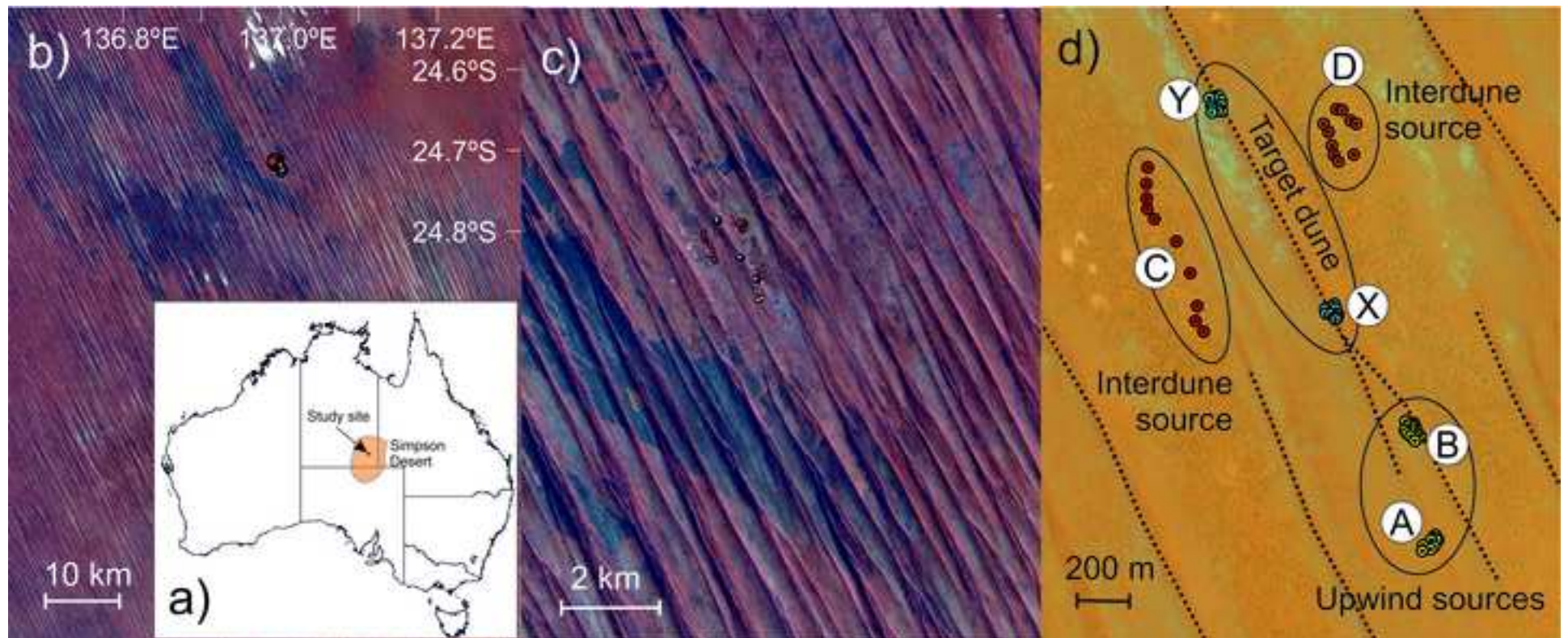


Figure 3 (Color)

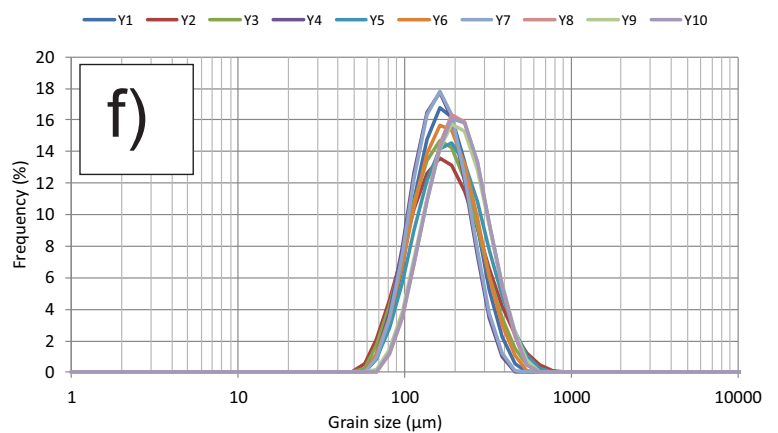
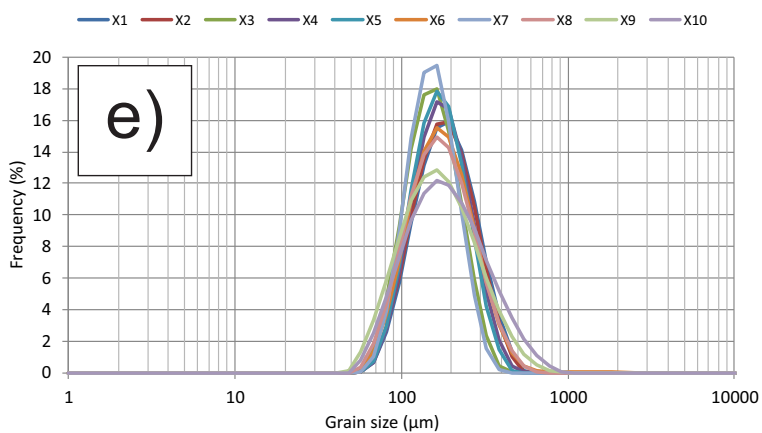
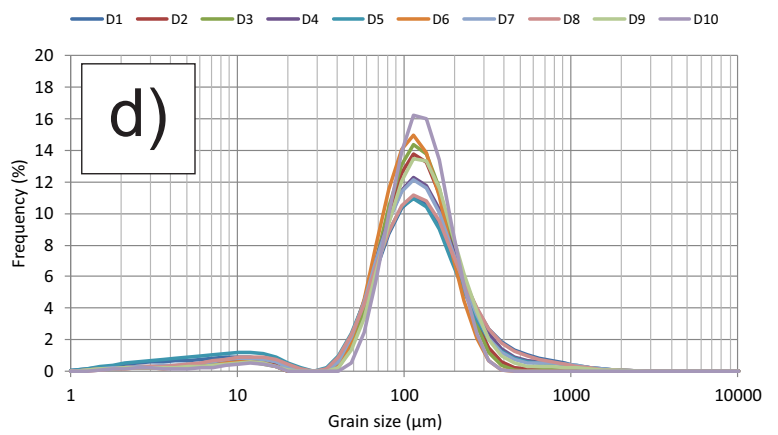
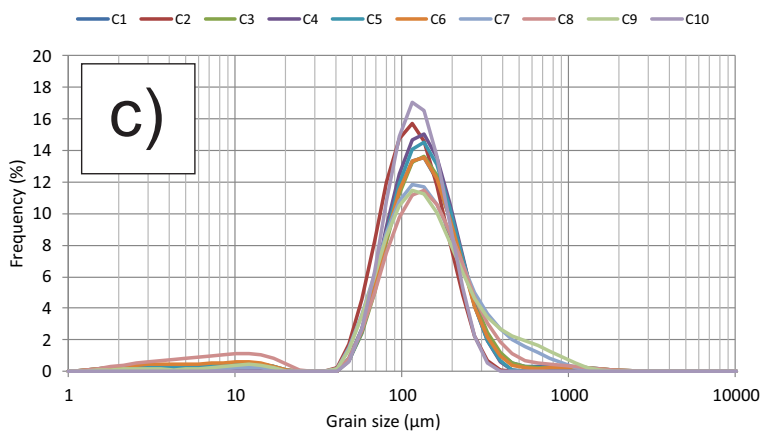
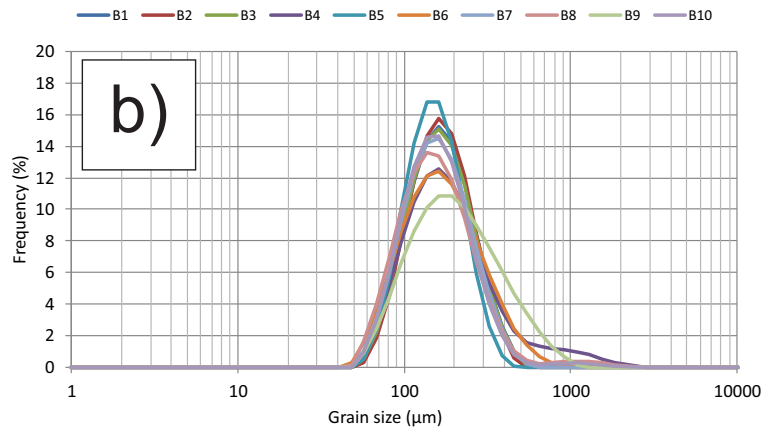
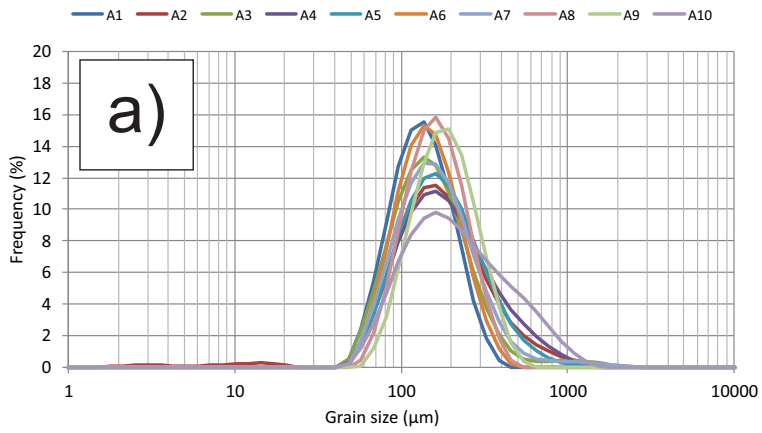


Figure 4 (Color)

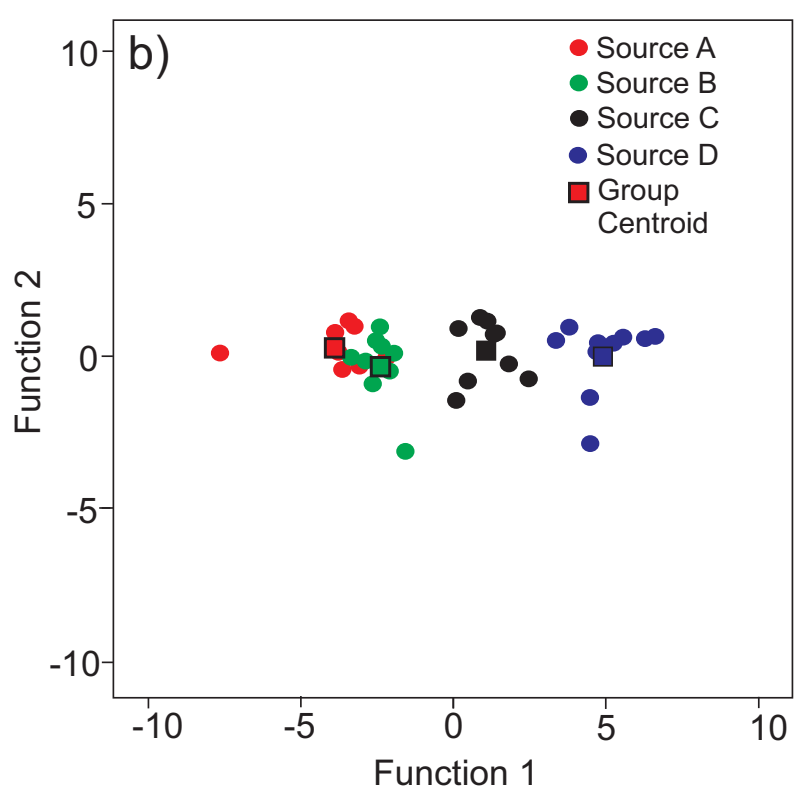
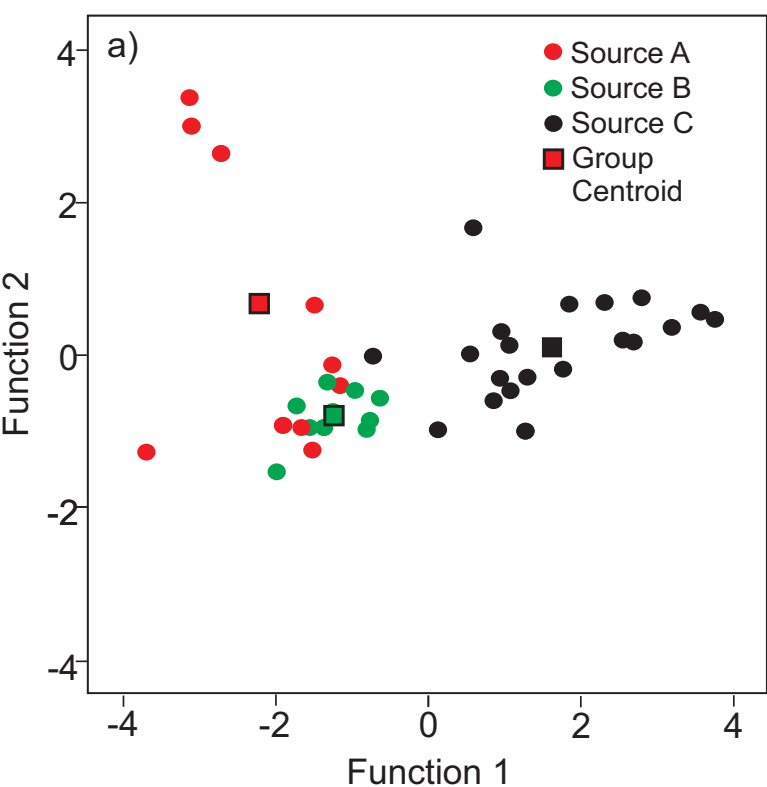


Figure 5 (Color)

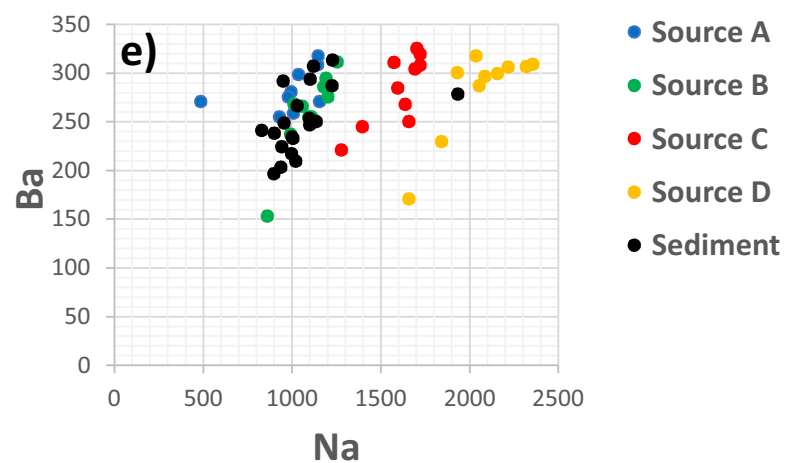
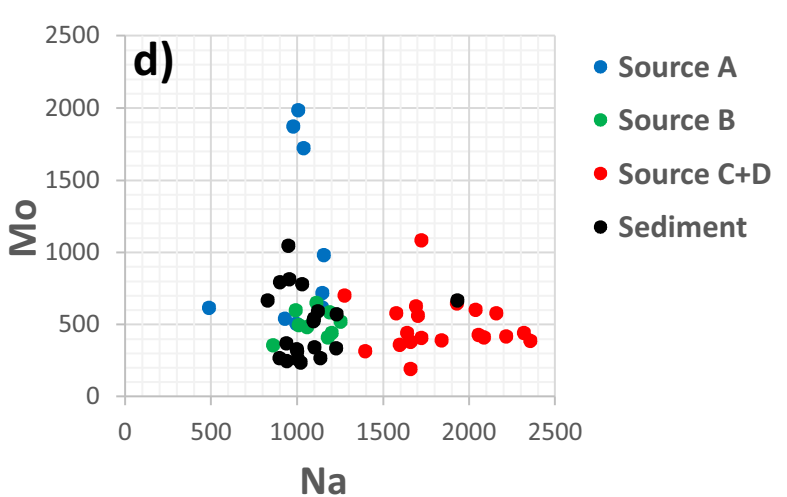
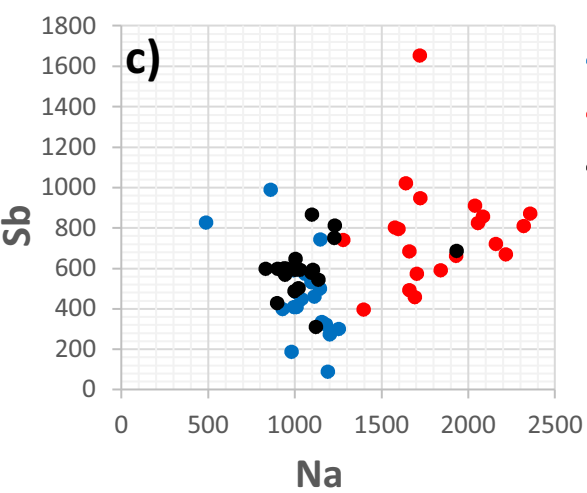
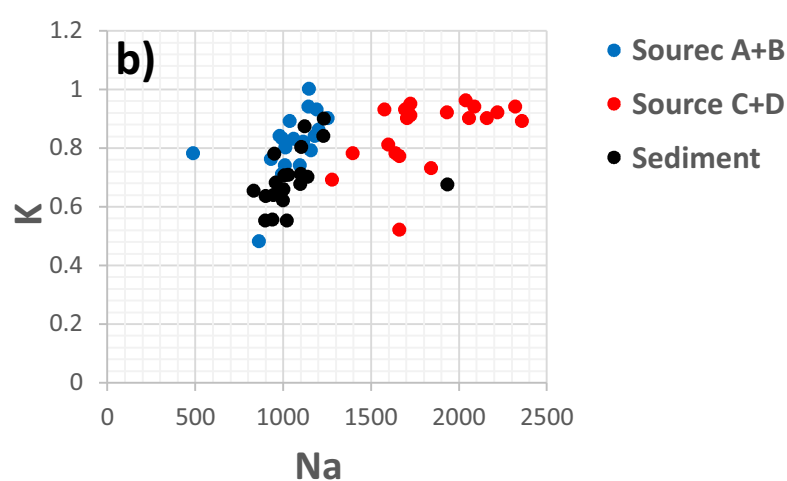
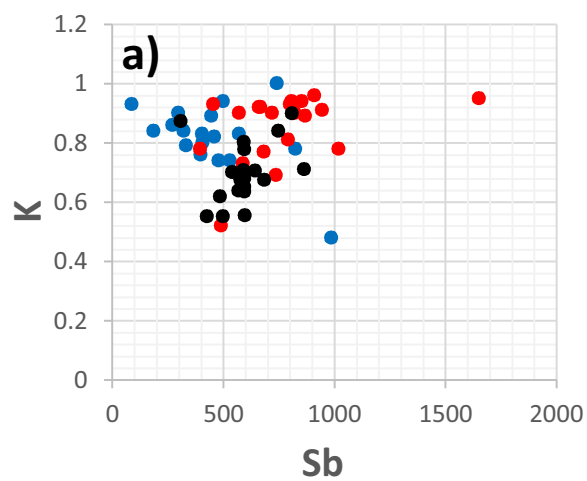


Figure 6 (Color)

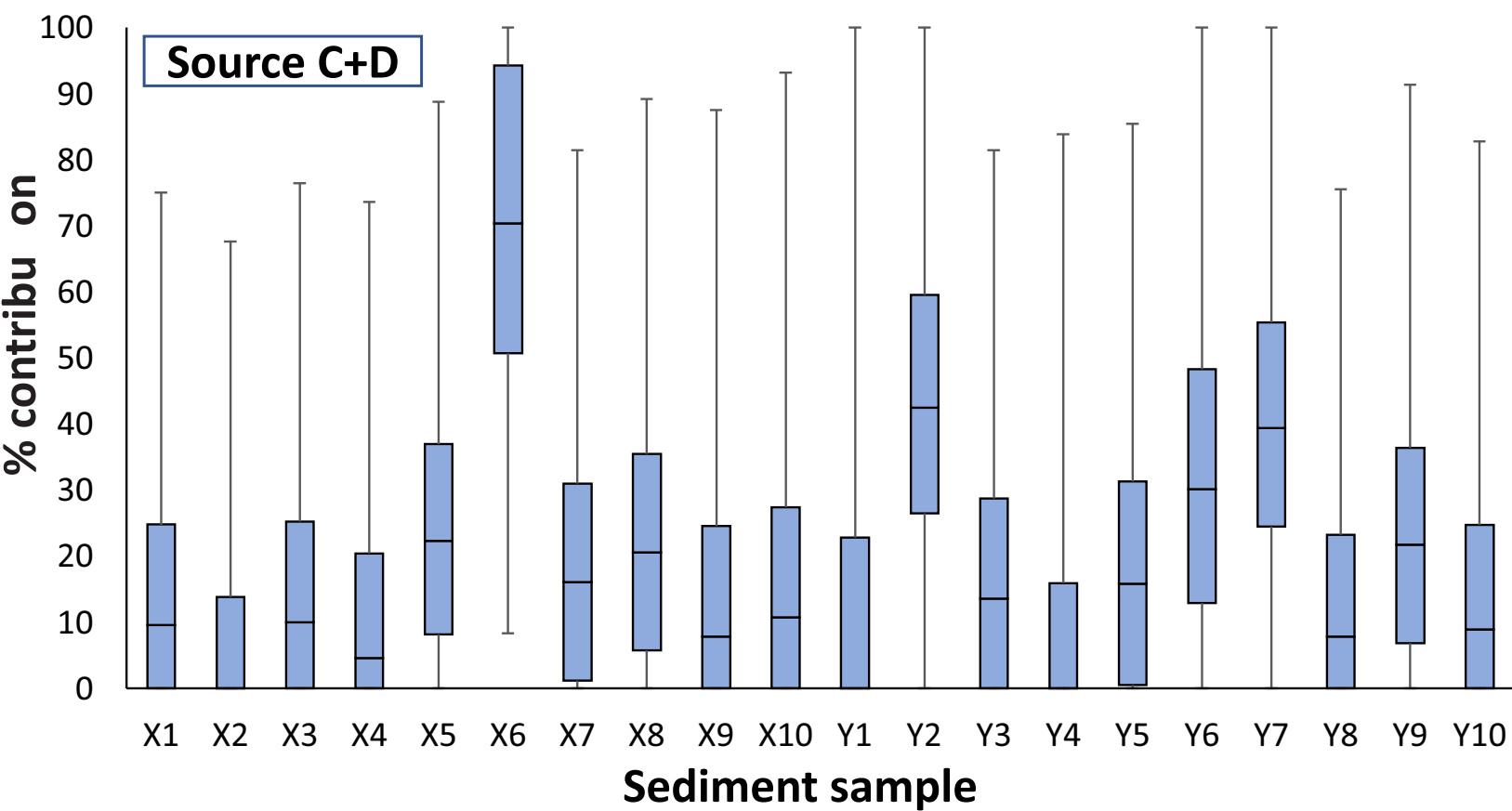
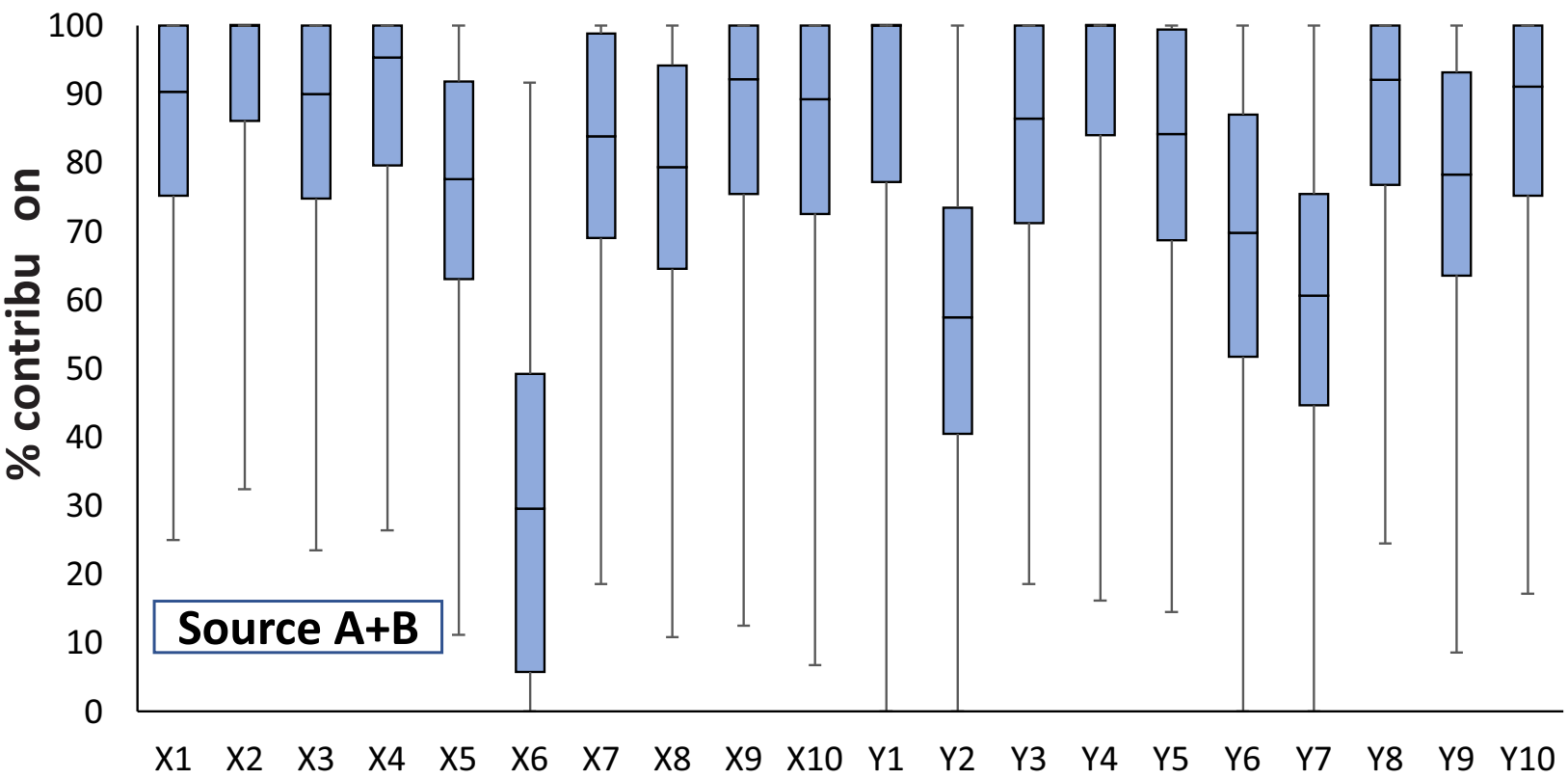


Figure 7 (Color)

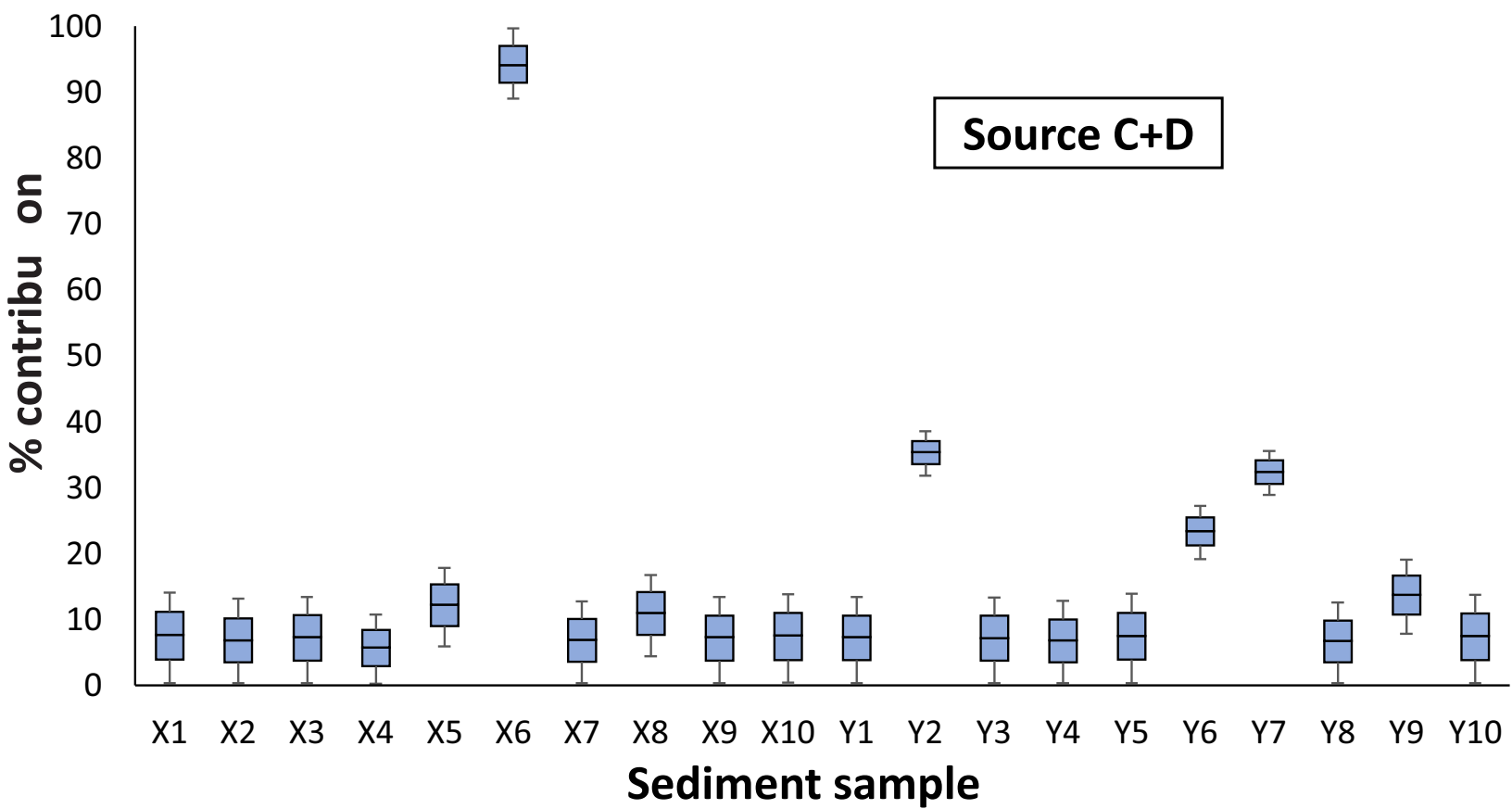
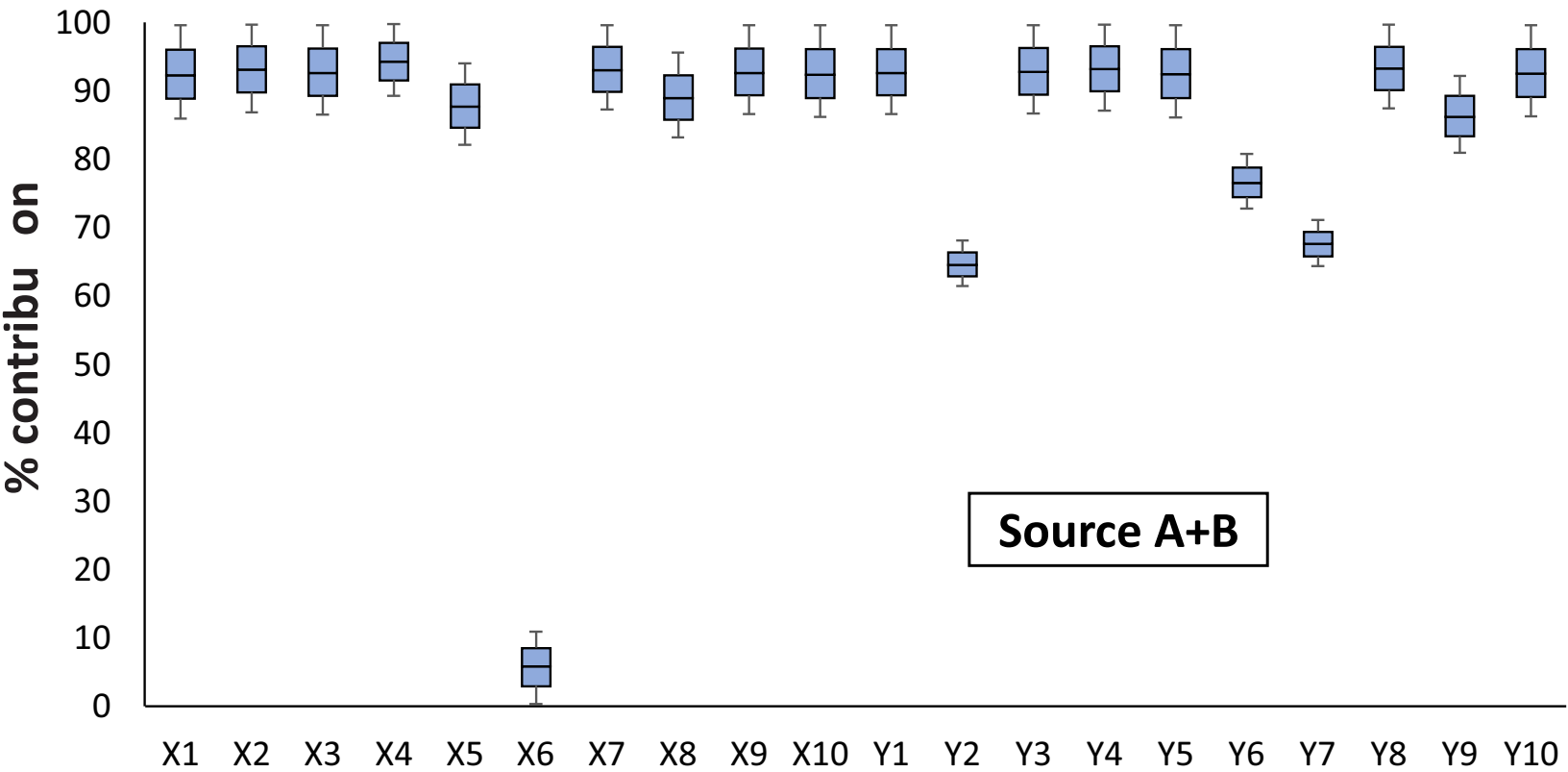
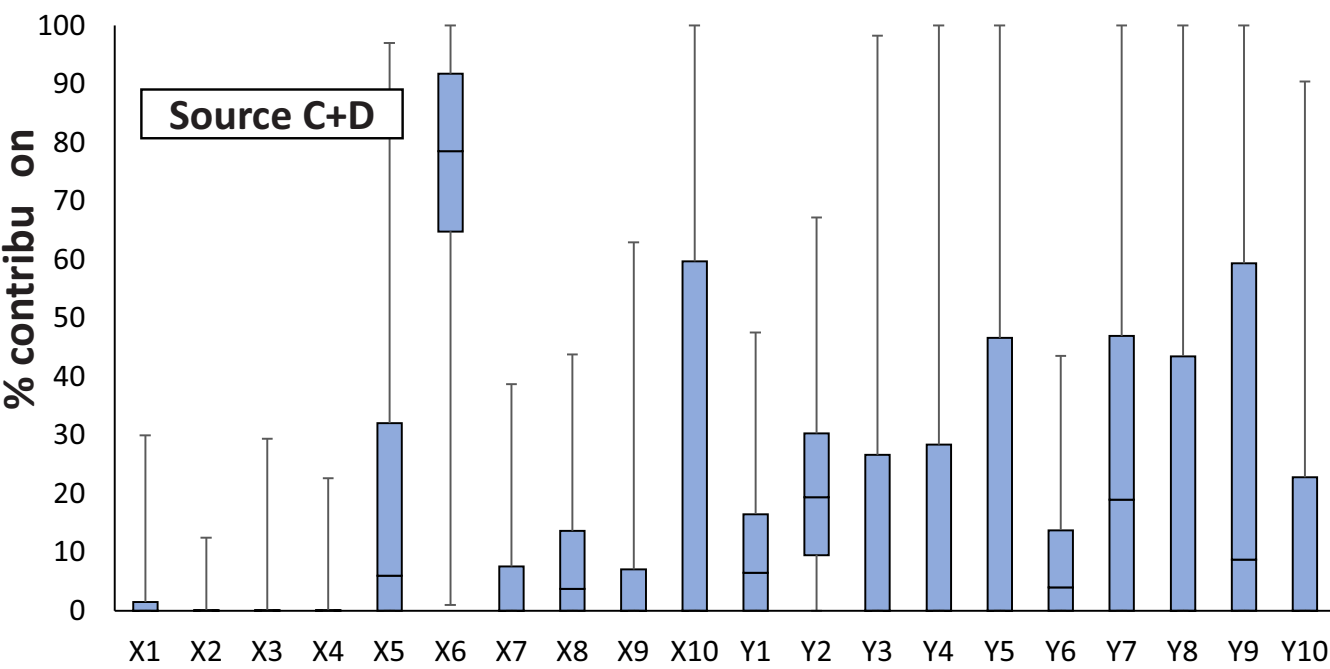
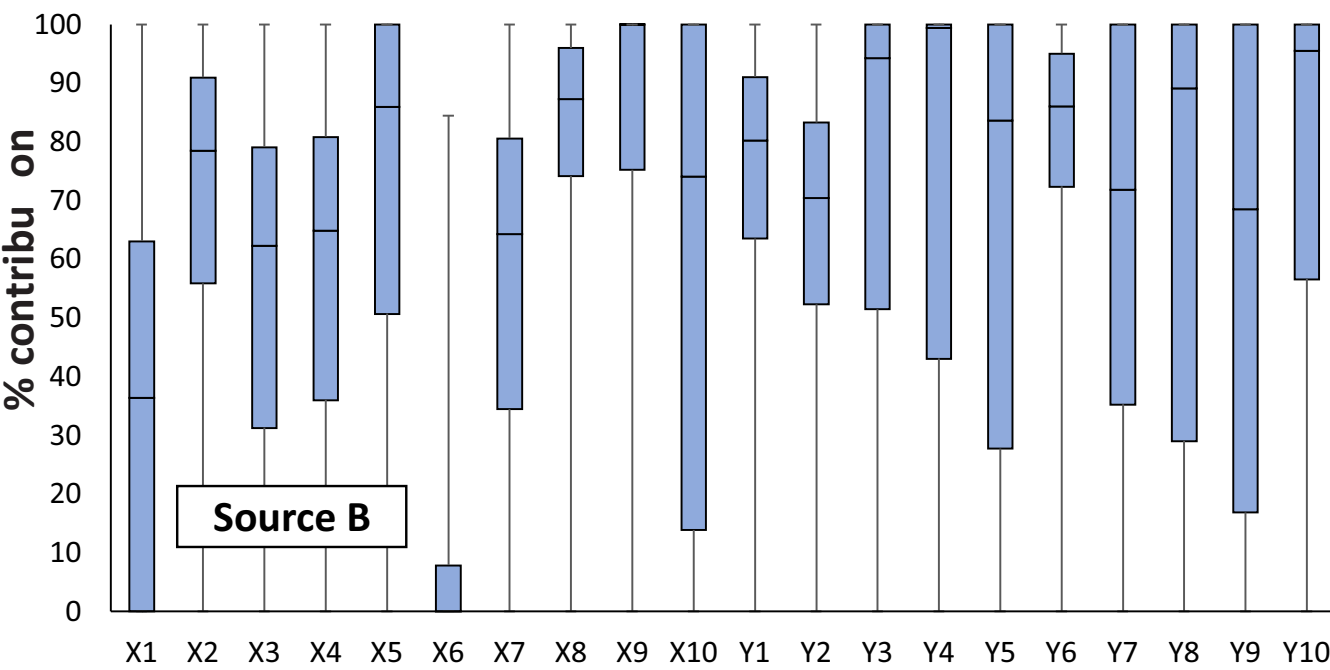
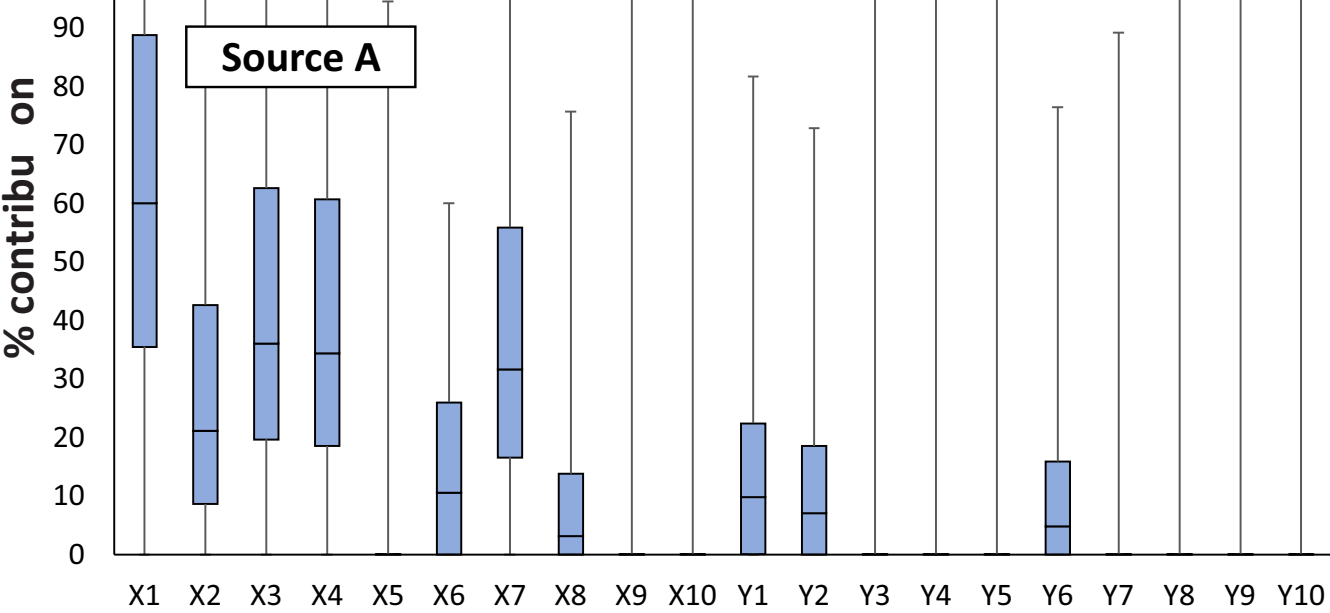
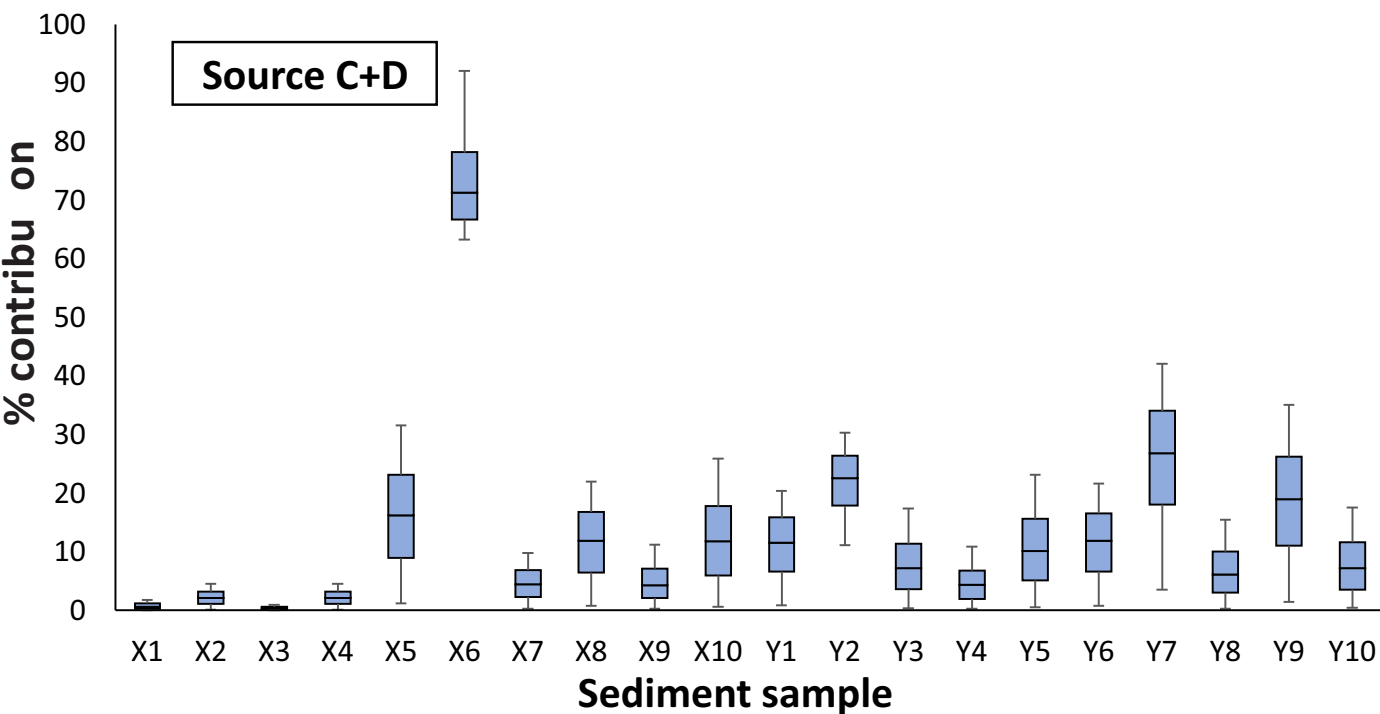
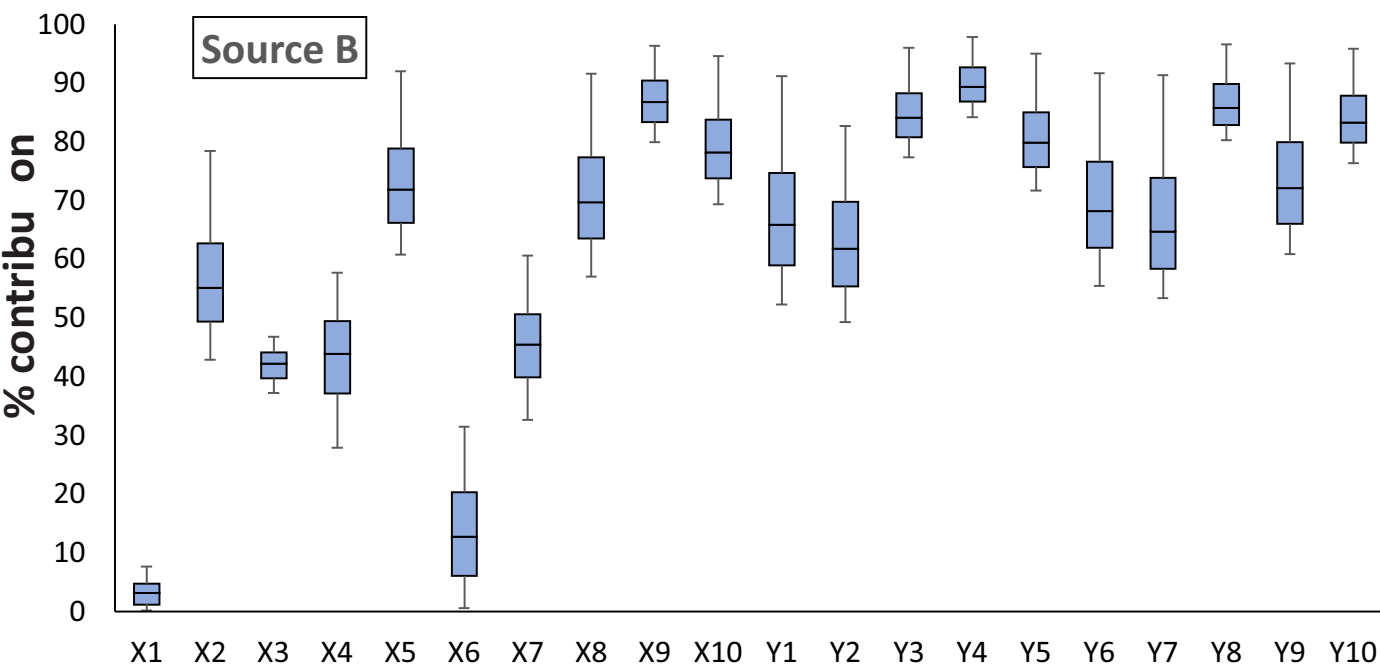
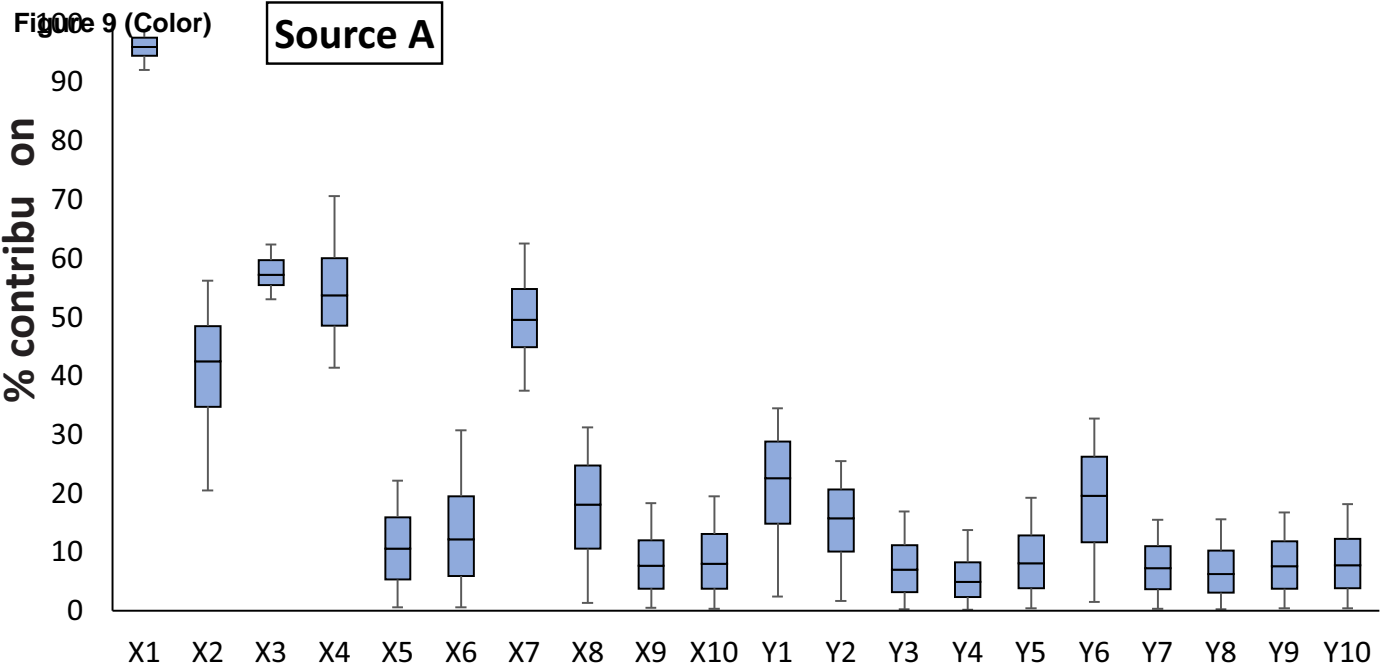


Figure 8 (Color)



Sediment sample

Figure 9 (Color)



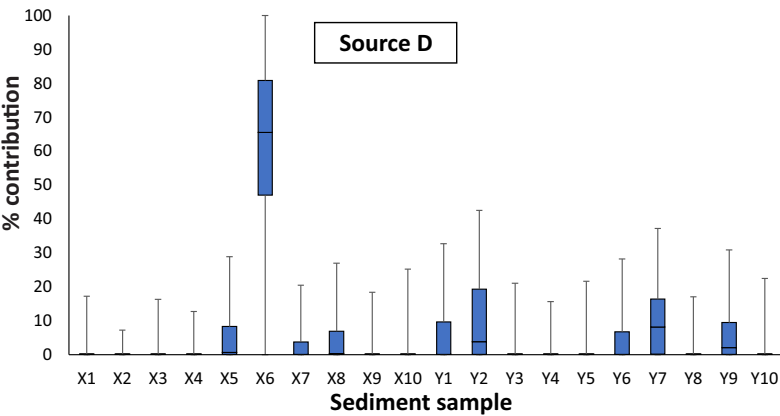
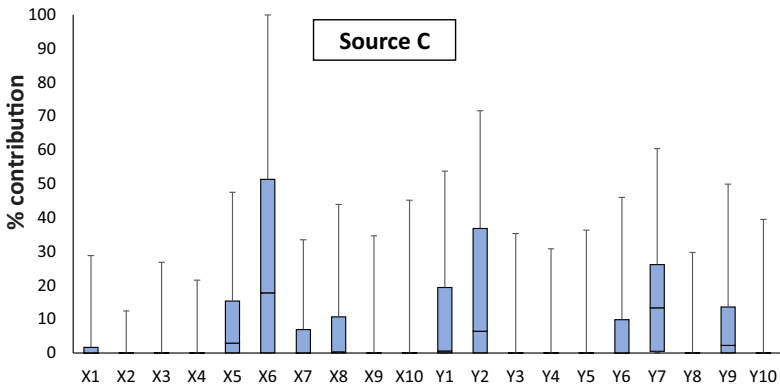
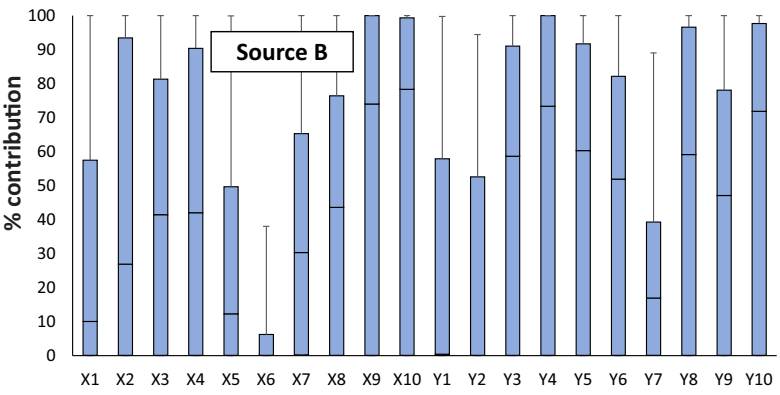
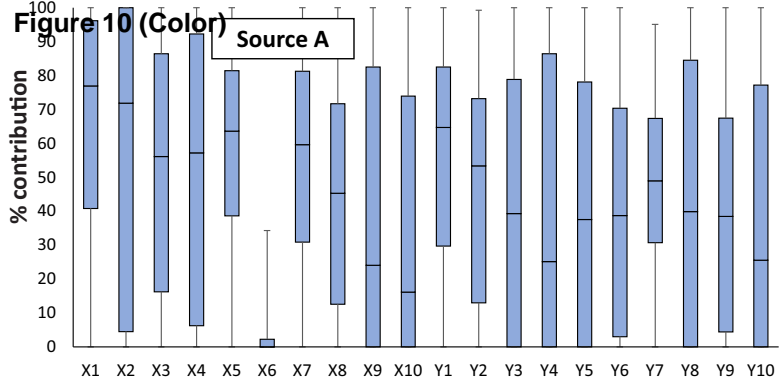
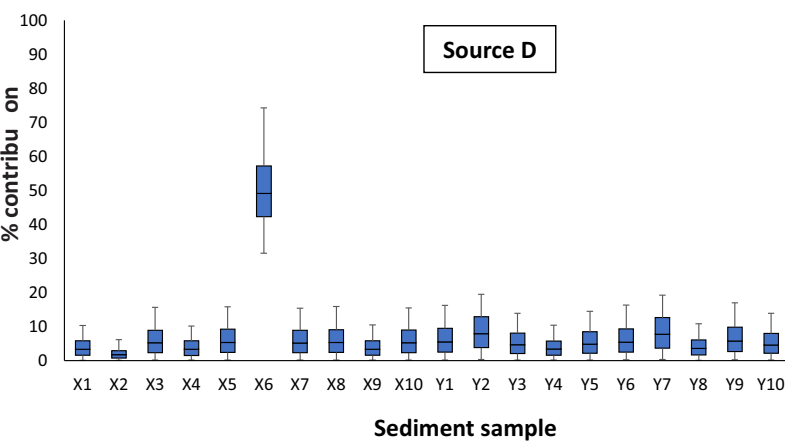
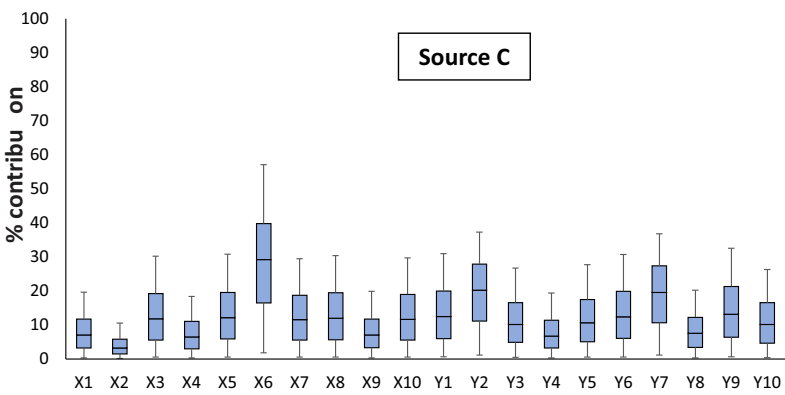
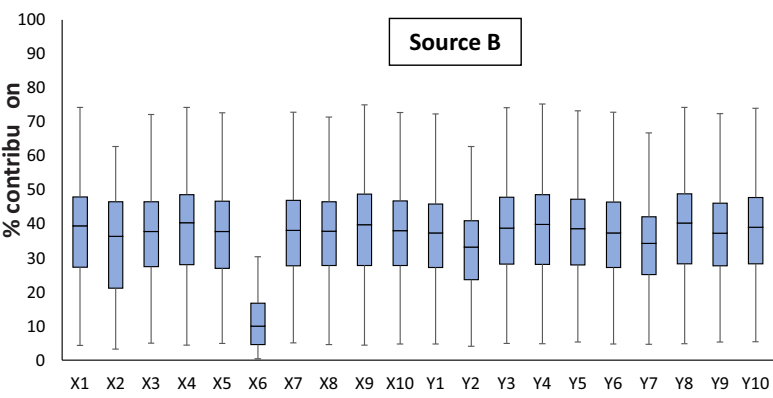
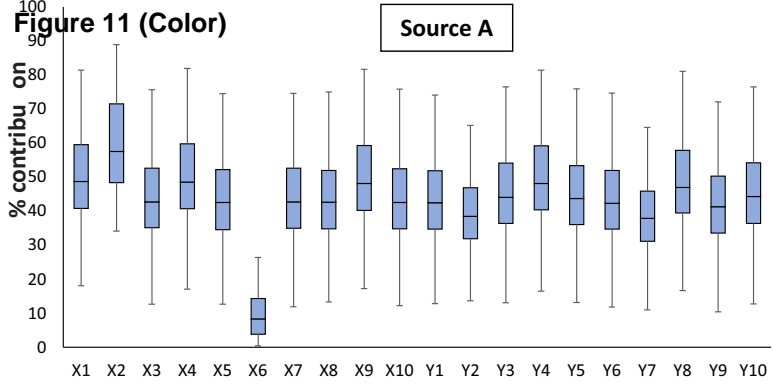


Figure 11 (Color)



Sediment sample

Figure 12 (Color)

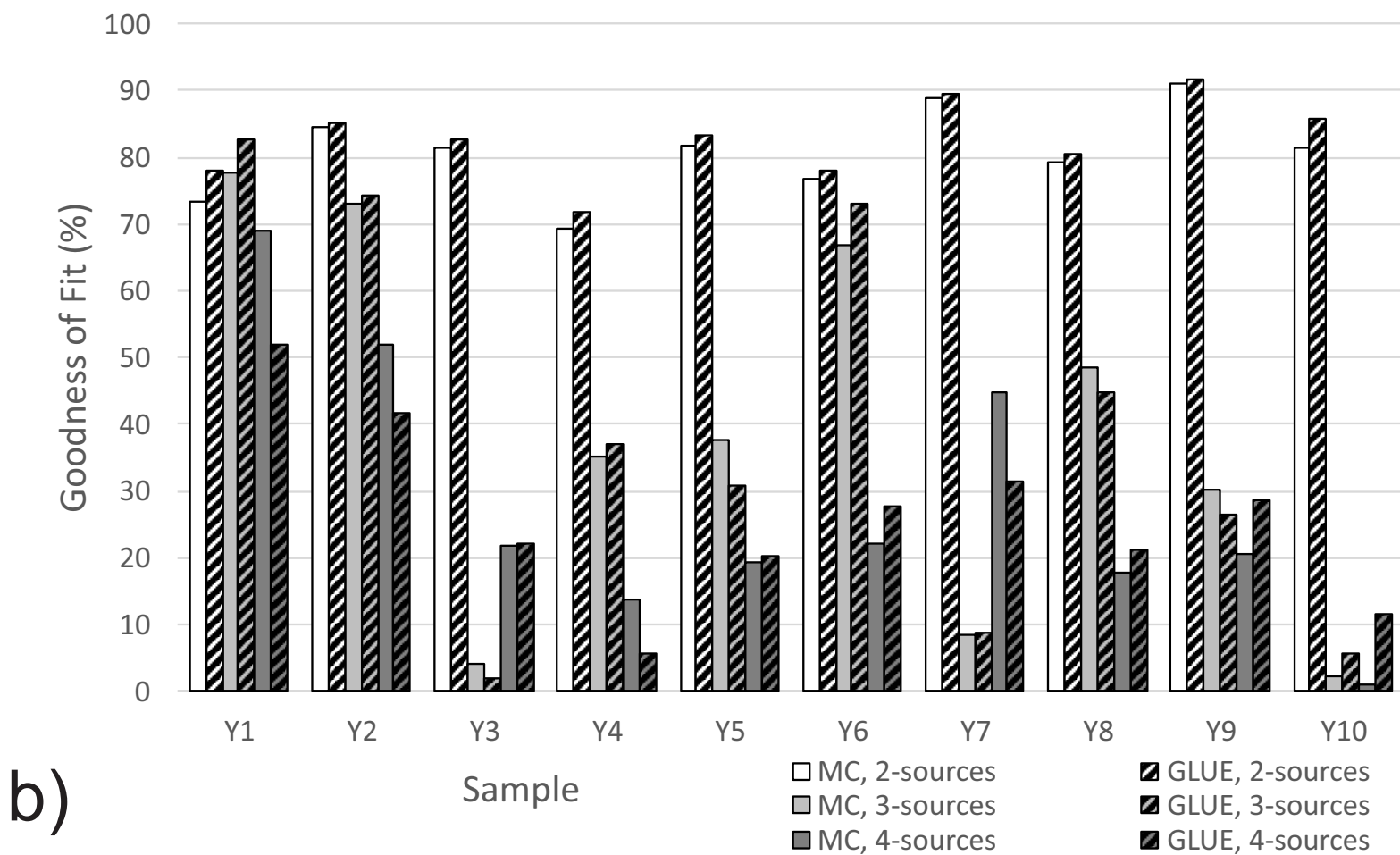
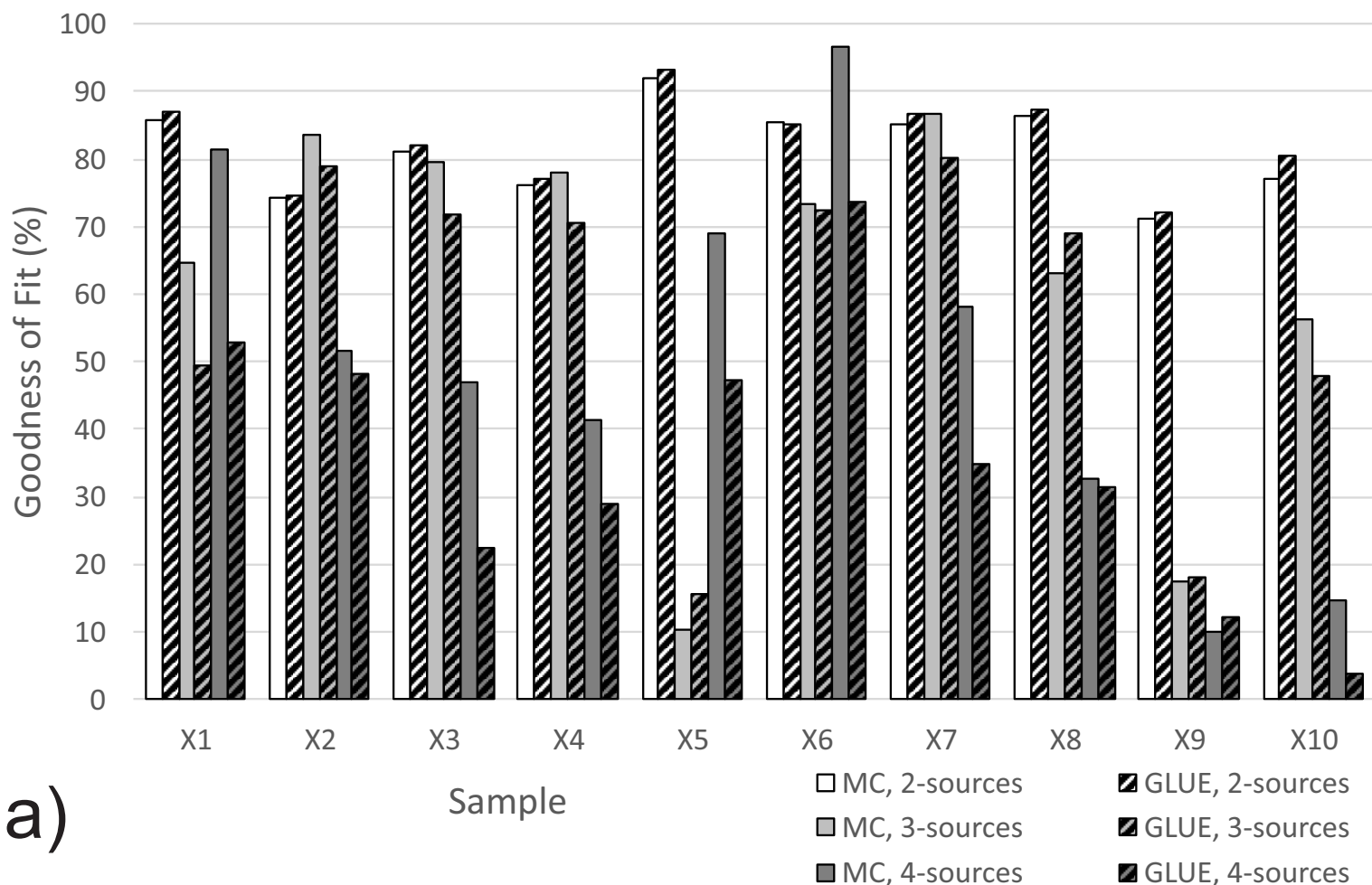


Figure 13 (Color)
[Click here to download high resolution image](#)

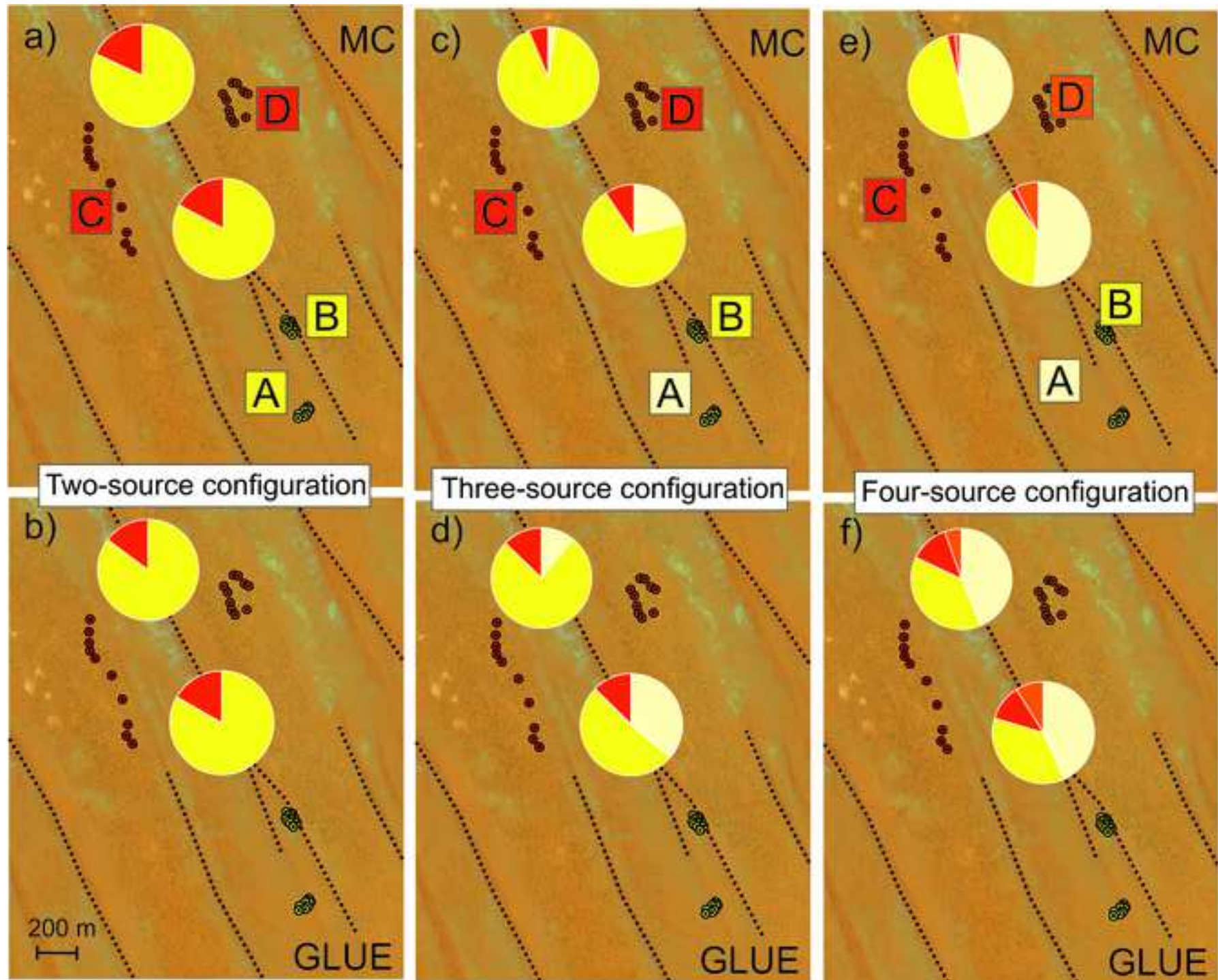


Figure 2 (Greyscale)
[Click here to download high resolution image](#)

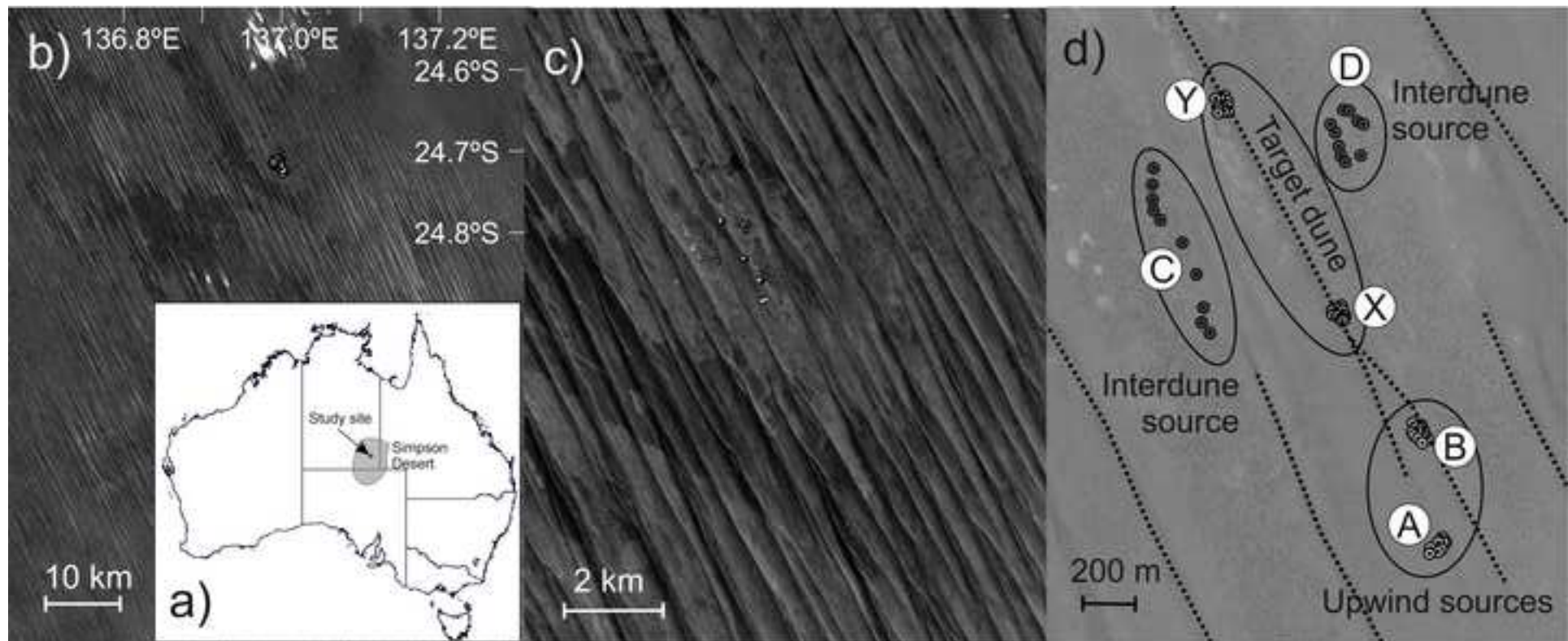
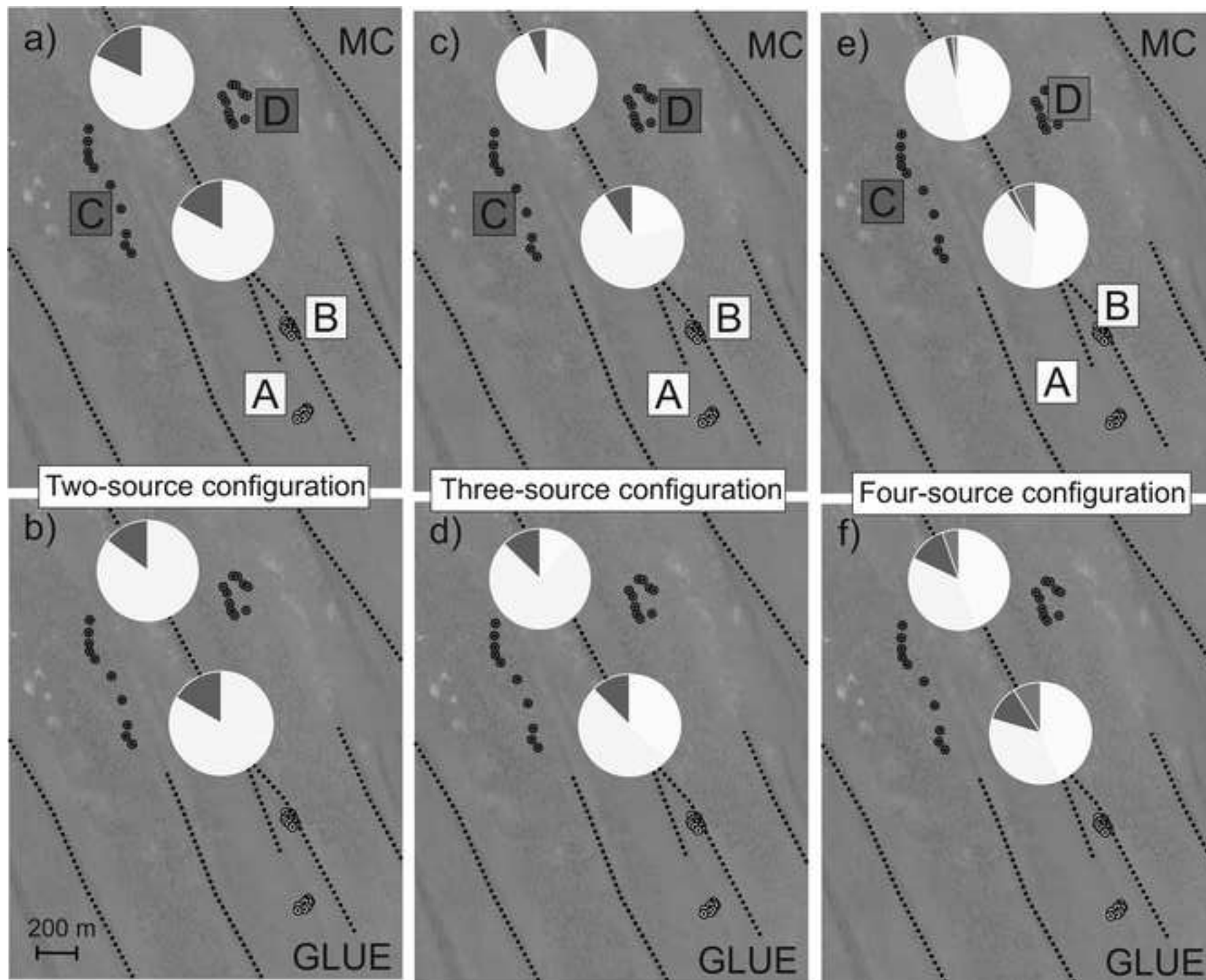


Figure 13 (Greyscale)
[Click here to download high resolution image](#)



Interactive Map file (.kml or .kmz)

[Click here to download Interactive Map file \(.kml or .kmz\): Simpson GPS.kmz](#)

Declaration of interests

The authors declare that they have no known competing financial interests or personal relationships that could have appeared to influence the work reported in this paper.

The authors declare the following financial interests/personal relationships which may be considered as potential competing interests: